# Bidirectional interactions between the gut microbiome and nervous system

Thesis by
Jessica Anne Griffiths

In Partial Fulfillment of the Requirements for
the Degree of
Doctor of Philosophy


CALIFORNIA INSTITUTE OF TECHNOLOGY
Pasadena, California

2024
(Defended January 25, 2024)

Jessica Anne Griffiths

ORCID: 0000-0002-5586-1567

# ACKNOWLEDGEMENTS

This is truly my favorite part of writing this thesis. I am overflowing with gratitude for the people that have accompanied, advised, and supported me through this journey. I could take up a thousand pages on acknowledgements, and it still wouldn't be sufficient.

Sarkis Mazmanian, thank you for everything. You have imparted the importance of storytelling, critical thinking, and being creative. You have given me the time and resources to build and try experiments no one else had tried in the lab. Through these many years, I have grown in confidence of my gut feelings and ability to figure things out, even if it may take a while.

To my committee: Viviana Gradinaru, Henry Lester, and Carlos Lois. I did not expect my PhD to become so heavily neuroscience focused. I have been so fortunate to have valuable input and feedback from all of you. Thank you.

To the Mazmanian Lab members past and present, you have been my home for the past six years. I am so grateful for the mentorship, support, and feedback on my projects every step of the way. Thank you to all the students who have allowed me to mentor them over the years, it has been one of the most rewarding experiences and opportunities for growth that I have had over the course of my PhD.

Brittany Needham, thank you for being a great mentor and becoming an even greater friend. Most of the success that I have had throughout graduate school would have been impossible without you. You have always been there to celebrate the good days and brush off the bad ones.

Wei-Li Wu, you started your own lab years ago, but you still made time to advise me in these critical last years of my PhD. Thank you for your attention and perspective, it was critical in helping me move forward.

Taren Thron, thank you for providing and maintaining the foundation of all the projects in the lab, including mine. You make your job look easy, even though I know it is not.

Yvette Garcia-Flores, I am convinced you are the best lab manager in the world. This journey would have been chaos without you. You keep the lab and all our projects moving forward. Thank you.

Catherine Oikonomou, thank you for your attention to detail and positive outlook. Your editing has improved my thesis and manuscripts, my writing skills, and how I think about my experiments.

To Bryan Yoo, thank you for being my academic brother.

To Zhuo Wang and Daniel Holschneider, thank you for being great collaborators. Your involvement in my work has helped it progress and improved it considerably.

To the Office of Laboratory Animal Resources and especially Yvonne, Kwan, Carina, Alan, Karen, Nicole, Jasmine, Gloria, Roberto, and Amy. None of this would be possible without your assistance and care.

To BBE admin, you are the cornerstone of this division. Thank you for the many things that you do.

To women in BBE (WiBBE) thank you for being such a supportive community of scientists, that have helped me in my personal and professional life.

To Kitty Cahalan and the Caltech CTLO, my participation in the visiting scientists program has often been the best part of my week. There have been times when my PhD felt pointless, but the pure wonder of science shown by the children of Madison Elementary has never failed to remind me why I decided to embark on this journey.

To my friends both near and far, you are the best. I am not sure how I have been able to befriend so many kind, loyal, and fun people with such a diverse range of interests.

Alexandros, I cannot express how happy I am that we met when we did. It is so special that we have gone through this chapter of our lives together. You have been my

companion in almost all things, and have taught me to be much more kind and patient with myself. You bring joy and lightness to my life when I need it the most.

To the Rosakis-Rosenberg-Tzefrios family, thank you for wholeheartedly welcoming me into your family. It has been such a pleasure to develop close and meaningful relationships with all of you and experience many life milestones together.

To my family, who love nature and animals. I would not be here if these interests were not shared and encouraged. Thank you for your unconditional love and support. This has been a long and confusing journey, but you have encouraged me at every step and it has made all the difference. It means so much that I can share this achievement with you.

# ABSTRACT

There is roughly one microbe for every human cell in your body. Though some are inconsequential hitchhikers, and some are potentially harmful, many perform beneficial roles. This thesis focuses on the function and interaction of resident microbes within laboratory mice, with the hope that it may translate to us as humans. Chapter (1) highlights recent findings of microbiome involvement in neurologic disorders. Each subsequent chapter presents a different interaction between the mammalian nervous system and gut microbiome. (2) Excitatory signaling in the brain is partially regulated by a genetic factor (*Shank3*), which is further modulated by environmental interactions through presence or absence of the gut microbiome. This genetic factor implicated in brain and behavior also affects gastrointestinal function and inflammation susceptibility. (3) Applying powerful genetic tools developed for the brain to the enteric nervous system reveals the impact of different enteric neuron populations on gut motility and fluid secretion as well as the immune system, pancreatic activity, and microbial populations. (4) Common opinion has shifted from the belief that microbes are primarily pathogens to viewing them as symbiotic organisms. With this paradigm shift, the artificially clean laboratory mouse microbiome has been found to stunt the immune system, and is being reevaluated. Male mice with natural “wild” microbiomes have altered behavioral and neurological profiles, which may reflect a more physiological state.

# PUBLISHED CONTENT AND CONTRIBUTIONS

Chapter I:

**Griffiths J.A.**, Mazmanian S.K. (2018) Emerging evidence linking the gut microbiome to neurologic disorders. Genome Medicine 10(1):98 [PMID: 30577867]

J.A.G. conceived the topics and wrote the bulk of the commentary.

Chapter II:

**Griffiths J. A.***, Yoo B. B.*, Thuy-Buon P., Cantu V., Weldon K., Challis C., Sweredoski M. J., Chan K. Y., Thron T. M., Sharon G., Moradian A., Humphrey G., Zhu Q., Shaffer J, Wolan D. W., Dorrestein P. C., Knight R., Gradinaru G., Mazmanian S. K. (2024). Peripheral neuronal activation shapes the microbiome and alters gut physiology. Cell Reports. (accepted in principle)

*indicates co-first author

J.A.G. designed and performed experiments and wrote the manuscript.

Chapter IV:

**Griffiths J. A.**, Wang, Z., Suryawinata, N., Tanaka, T., Simpson, P., Holschneider, D. P., Mazmanian S. K. (2024). 'Re-wilding' the microbiome of laboratory mice promotes sociability. (manuscript in preparation)

J.A.G. conceived the project, designed and performed experiments, and wrote the manuscript.

Other contributions:

Mondragón-Palomino O., Poceviciute R., Lignell A., **Griffiths J.A**., Takko H., Ismagilov R. F. (2022). Three-dimensional imaging for the quantification of spatial patterns in microbiota of the intestinal mucosa. PNAS. 19(18):e2118483119 [PMID: 35476531]

J.A.G. developed and performed experiments on probe hybridization in bacteria embedded in hydrogels.

Needham B.D., Funabashi M., Adame M.D., Wang Z, Boktor J.C., Haney J., Wu W. L., Rabut C., Ladinsky M.S., Hwang S. J., Guo Y., Zhu Q., **Griffiths J. A.**, Knight R.,Bjorkman P. J., Shapiro M. G., Geschwind D. H., Holschneider D. P., Fischbach M. A., Mazmanian S. K. (2022) A gut-derived metabolite alters brain activity and anxiety behaviour in mice. Nature 602(7898), 647-653 [PMID: 35165440]

J.A.G. developed *in vitro* techniques to test 4EP and 4EPS.

Chen X., Kumar S. R., Adams S. D., Yang D., Wang T., Wolfe D. A., Arokiaraj C. M., Ngo V., Campos L. J., **Griffiths J. A.**, Ichiki T., Mazmanian S. K., Osborne P. B., Keast J. R., Miller C. T., Fox A. S., Chiu I. M., Gradinaru V. (2022) Engineered AAVs for non-invasive gene delivery to rodent and non-human primate nervous systems. Neuron 110(14), 2242-2257 [PMID: 35643078]

J.A.G. performed experiments to characterize AAV expression in the CNS and myenteric plexus of the gut.

TABLE OF CONTENTS

## INTRODUCTION

In the past 3.7 billion years since life on Earth began, it has continued to evolve to adapt to the pressures and opportunities presented by the surrounding environment[1]. The consequences of these adaptations have led to an extraordinary diversity of life and complexity of biological systems within each life form, whether it be a single-celled organism or a multicellular organism over a quadrillion times its size[2,3]. Among the wide variety of adaptations, symbiotic relationships have evolved over and over again, suggesting it is critical to cooperate with and rely on other species to survive[4,5].

Symbiosis is a relationship between two different organisms or groups encompassing mutualism, commensalism, and parasitism[6]. There are countless fascinating examples of symbiosis in nature. Pilot fish remove parasites from the skin of sharks, and receive protection in exchange[7]. Rove beetles have evolved complex body shapes and olfactory camouflage techniques mimicking many different types of ants, fooling them into thinking they belong[8]. Amidst the wide array of symbiotic interactions, most are with microbes[9]. Corals provide shelter and sustenance that algae need for photosynthesis, and the algae provide sugars to their hosts[10]. Fungi form large networks that connect tree roots together to share resources, and fungi receive nutrients from the trees[11]. Hawaiian bobtail squid have an organ that is only colonized by *Vibrio fischeri*, which illuminate their host to hide them from predators[12].

Humans benefit from microbes in multitudes, and we provide a nutrient-rich environment in return[13,14]. All our external surfaces are colonized by microbes, collectively called the

microbiome[13]. Our gut microbiome consists of ~$10^{13}$-$10^{14}$ microbes across a tremendous diversity of species of bacteria, archaea, fungi, and viruses[13,15]. The gut microbiome educates the immune system, and enables us to combat pathogens[16]. Short chain fatty acids (SCFAs), products of bacterial fermentation, are known to mitigate inflammation[17,18]. Gut microbes can produce neurotransmitters and activate pathways in the brain through the vagus nerve[18,19]. Some microbes have enzymes that can degrade complex fibers that we cannot break down ourselves, which provide us with nutrients[13].

To ensure that the relationship with our gut microbes remains advantageous, we have developed clever ways to contain and shape the microbiome. Our gastrointestinal tract has evolved to keep microbes close, but still protect ourselves from infection. The epithelium of the gut forms tight junctions and is completely replaced every 5-7 days, in order to keep microbes within the gut[20]. Additionally, goblet cells in the epithelium excrete dense mucus that most microbes cannot penetrate[15,20]. Across the wide diversity of microbes, we possess methods to select and enrich for beneficial ones. Our immune systems can detect commensal microbes, such as *Bacteroides fragilis*, and enable effective colonization[21]. Human breast milk contains a large quantity of oligosaccharides that are indigestible by an infant, but selectively enrich for *Bifidobacterium* species[22].

Due to the wealth of studies published in the past few decades, the importance of the gut microbiome to human health is now widely accepted. It is worth noting that the importance of microbes to our welfare extends far beyond the interactions with our gut microbiomes. In fact, we wouldn't exist if it weren't for bacteria. Early photosynthesizing

microbes filled the atmosphere with oxygen and made the world into one that is hospitable for us[23]. Our mitochondria are descendants of ancient bacteria that became enveloped by a eukaryotic cell, and now provide energy for cellular function[5]. The more one investigates, the clearer it becomes how profoundly these microscopic organisms have influenced our lives. *It is a microbial world, and we are just living in it*[24].

**REFERENCES**


1. RICARDO, A. & SZOSTAK, J. W. ORIGIN OF LIFE ON EARTH. *Sci. Am.* **301**, 54–61 (2009).
2. Schluter, D. Ecology and the origin of species. *Trends Ecol. Evol.* **16**, 372–380 (2001).
3. Darwin, C. *On The Origin of Species by Means of Natural Selection, or The Preservation of Favoured Races in the Struggle for Life*. (London, UK: John Murray, 1859).
4. Dimijian, G. G. Evolving together: the biology of symbiosis, part 1. *Proc. Bayl. Univ. Med. Cent.* **13**, 217–226 (2000).
5. Margulis, L. SYMBIOSIS AND EVOLUTION. *Sci. Am.* **225**, 48–61 (1971).
6. Leung, T. & Poulin, R. PARASITISM, COMMENSALISM, AND MUTUALISM: EXPLORING THE MANY SHADES OF SYMBIOSES. *Vie Milieu - Life Environ.* **58**, 107–115 (2008).
7. Fuller, L. N. & Parsons, G. R. A Note on Associations Observed between Sharks and Teleosts. *Southeast. Nat.* **18**, 489–498 (2019).
8. Parker, J. Myrmecophily in Beetles (coleoptera): Evolutionary Patterns and Biological Mechanisms. *Myrmecol. News* 65–108 (2016).
9. McFall-Ngai, M. *et al.* Animals in a bacterial world, a new imperative for the life sciences. *Proc. Natl. Acad. Sci.* **110**, 3229–3236 (2013).
10. Frankowiak, K. *et al.* Photosymbiosis and the expansion of shallow-water corals. *Sci. Adv.* **2**, e1601122.

11. Gorzelak, M. A., Asay, A. K., Pickles, B. J. & Simard, S. W. Inter-plant communication through mycorrhizal networks mediates complex adaptive behaviour in plant communities. *AoB PLANTS* **7**, plv050 (2015).
12. Nyholm, S. V. & McFall-Ngai, M. J. A lasting symbiosis: how the Hawaiian bobtail squid finds and keeps its bioluminescent bacterial partner. *Nat. Rev. Microbiol.* **19**, 666–679 (2021).
13. Ley, R. E., Peterson, D. A. & Gordon, J. I. Ecological and evolutionary forces shaping microbial diversity in the human intestine. *Cell* **124**, 837–848 (2006).
14. Round, J. L. & Mazmanian, S. K. The gut microbiota shapes intestinal immune responses during health and disease. *Nat. Rev. Immunol.* **9**, 313–323 (2009).
15. Donaldson, G. P., Lee, S. M. & Mazmanian, S. K. Gut biogeography of the bacterial microbiota. *Nat. Rev. Microbiol.* **14**, 20–32 (2016).
16. Mazmanian, S. K. & Lee, Y. K. Interplay between Intestinal Microbiota and Host Immune System. *jbv* **44**, 1–9 (2014).
17. Vinolo, M. A. R. *et al.* Suppressive effect of short-chain fatty acids on production of proinflammatory mediators by neutrophils. *J. Nutr. Biochem.* **22**, 849–855 (2011).
18. Cryan, J. F. *et al.* The Microbiota-Gut-Brain Axis. *Physiol. Rev.* **99**, 1877–2013 (2019).
19. Barandouzi, Z. A. *et al.* Associations of neurotransmitters and the gut microbiome with emotional distress in mixed type of irritable bowel syndrome. *Sci. Rep.* **12**, 1648 (2022).
20. Odenwald, M. A. & Turner, J. R. The intestinal epithelial barrier: a therapeutic target? *Nat. Rev. Gastroenterol. Hepatol.* **14**, 9–21 (2017).

21. Donaldson, G. P. *et al.* Gut microbiota utilize immunoglobulin A for mucosal colonization. *Science* **360**, 795–800 (2018).

22. Bakshani, C. & Crouch, L. Human milk oligosaccharides and Bifidobacterium species. *Trends Microbiol.* (2023) doi:https://doi.org/10.1016/j.tim.2023.11.015.

23. Fischer, W. W., Hemp, J. & Johnson, J. E. Evolution of Oxygenic Photosynthesis. *Annu. Rev. Earth Planet. Sci.* **44**, 647–683 (2016).

24. Martin Mark O. "It's a Microbial World; We Just Live in It": Microbial Symbionts Profiled Masterfully by Yong. *J. Microbiol. Biol. Educ.* **17**, 496–498 (2016).

*Chapter 1*

# EMERGING EVIDENCE LINKING THE GUT MICROBIOME TO NEUROLOGIC DISORDERS

Griffiths J.A., Mazmanian S.K.

This chapter was published in 2018 in *Genome Medicine* 10(1): 98. DOI: 10.1186/s13073-018-0609-3.

## PREFACE

The gut microbiome contributes to the development and function of the immune, metabolic, and nervous systems. Furthermore, commensal bacteria modulate symptoms and pathology in mouse models of neuropsychiatric and neurodevelopmental diseases. Uncovering mechanisms that are utilized by the microbiome to mediate gut–brain connections may provide novel opportunities to target therapies to the gut in order to treat neurologic disorders.

## THE GUT MICROBIOME AND BRAIN DISORDERS

Disorders of the brain such as anxiety, depression, epilepsy, and autism spectrum disorder (ASD) have been linked to the gut microbiome, largely in preclinical models [1]. Microbiome changes in humans have been cataloged in many neurologic conditions, and mouse models have revealed that gut microbes contribute to disease progression and severity of symptoms [1]. Recent work in this area reports new findings in disorders of the brain and in well-established murine models of behavior [2,3,4,5]. These studies indicate that a combination of factors, including prenatal environments, diet, and host genetics, impact the fitness of an individual's microbiome. Changes to host microbiome composition coincide with neurologic changes affecting behavior, neurotransmitter levels, stress response, and gene expression in the brain [2,3,4,5]. These findings highlight a growing appreciation that gut bacteria may contribute to neuropsychiatric disorders, and potentially reveal attractive targets for translational studies in humans.

## EARLY-LIFE INFLUENCES

Upon birth, the sterile gut of a newborn is colonized by microbiota, which are required for normal adolescent brain and immune system development [6]. These early colonizers are instrumental during development in educating the immune system, metabolizing nutrients, and influencing complex behaviors. One example of the impact of early colonization is illustrated by differences in cognitive scores between infants born via cesarean section and vaginally born children [6]. The lower scores of children born via cesarean section may result from differences in early gut colonization by microbes from the mother's skin (caesarean) or vagina (natural birth), respectively [6]. Infants who have

increased exposure to antibiotics have a greater risk of developing behavioral symptoms such as depression [1]. Further evidence of early-life influences comes from observations that formula feeding, which alters the microbiome, may be a risk factor for ASD [7], although considerable additional work in humans is needed to establish causality.

Prenatal stress can also affect microbiome composition after birth and is linked to increased risk of developmental disorders of the brain [2]. Stress induces distinct changes in the vaginal microbiome composition, so mothers who are under stress may transmit an imbalanced bacterial community to their offspring [2]. Stress responses can be measured by activation of the hypothalamic-pituitary-adrenal (HPA) axis, which is one of the major routes of communication between the periphery and the brain. Male mouse pups born to stress-exposed dams exhibit increased stress, indicated by elevated levels of corticosterone in the serum and altered gene expression in the hypothalamus [2]. It is difficult to determine whether this phenotype results from prenatal effects or microbial colonization at birth. Jašarević et al. [2] showed that colonization of mice with untreated, control vaginal microbiota normalized, albeit partially, features such as body weight and corticosterone levels following acute stress in male offspring. The fact that these negative effects could not be reversed fully suggests that stress also affects the mouse pups before birth (i.e., prior to microbiome exposure). This idea is supported by transcriptomic data from the murine fetal intestine that reveals differential expression of genes implicated in innate immunity and inflammation based on prenatal stress-exposure in males [2]. Therefore, it is likely that environmental risk factors, such as prenatal stress, alter the

intestinal niche of the fetus before microbes even colonize the gut and could select against beneficial microbes.

In theory, reduced prenatal stress should promote microbiome health and normal immune system development. When early-life perturbations such as cesarean section or treatment with antibiotics contribute to symptoms, colonizing newborns with missing or depleted microbes or with a complex microbiome from a verified healthy donor may provide benefits [8].

**DIET-INDUCED CHANGES**

Although the initial colonization of the gut plays a critical role in shaping the microbiome, diet has a significant impact on microbial composition throughout life [1, 3]. A high-fat diet (HFD) can result in obesity by inducing gut dysbiosis [3]. Although obesity and diabetes are not traditionally considered neurologic disorders, they often co-occur with anxiety and depression [3].

Diet-induced obesity (DIO) mice fed an HFD exhibit hallmark characteristics of diabetes, including insulin resistance and hyperglycemia, and also display behaviors symptomatic of anxiety and depression [3]. *Soto et al*. [3] found that DIO mice display abnormal neurotransmitter levels including increases in brain levels of γ-aminobutyric acid (GABA) and tryptophan, a precursor of serotonin, which are associated with mood and behavior in humans. Antibiotic treatment with vancomycin and metronidazole depletes Gram-positive and Gram-negative anaerobic bacteria in the gut, respectively. Both

antibiotic treatments ameliorated the behavioral deficits and diabetes-like symptoms found in DIO mice. This evidence indicates that an HFD may enrich populations of gut microbes that play a role in the physiology of obesity and diabetes, and suggests that treatments that eliminate certain microbes may help treat both metabolic and behavioral conditions [3].

Conversely, some diets have therapeutic potential for neurologic disorders. The ketogenic diet (KD) consists of high fat content foods but minimal amounts of carbohydrates, which causes metabolism of fat instead of carbohydrates for energy. The KD has been used to treat epilepsy for a century, but the importance of the gut microbiome in mediating this effect was largely unknown [4]. *Olson et al*. [4] found that administration of the KD to a mouse model of epilepsy that uses electrical stimulation to induce seizures (6-Hz seizure mouse model) resulted in changes in the microbiome composition and made the mice more resistant to seizures. The microbiome is necessary for the beneficial effects of the diet, as antibiotic-treated and germ-free mice fed the KD do not reap the protective effects of the diet. KD-fed mice are enriched in the bacteria *Akkermansia muciniphila*, *Parabacteroides merdae*, and *Parabacteroides distasonis*, which were shown to be involved in promoting the diet's anti-seizure effects. Manipulation of the gut microbiome through the KD or colonization with *A. muciniphila* and Parabacteroides provided protective benefits against seizures by altering brain neurotransmitter levels, including GABA and glutamate in the hippocampus [4]. GABA is the major inhibitory neurotransmitter in the brain, and reduced levels are known to exacerbate seizures. Diet is

thus an effective means of manipulating neurotransmitter levels in the brain, with the resulting diet–microbiome interactions mediating the effects of seizures.

## GENETIC INTERACTIONS

Studies have begun to use DNA sequencing to investigate the impact of host genetics on the microbiome and to look at how gene–environment interactions affect neurological disease [9]. Whole-genome association studies have revealed genetic variants involved in host immunity and metabolism that may predispose individuals to gut dysbiosis [9]. Genetic mutations that are associated with neurological disorders may also alter the host intestinal niche and perturb the microbiome.

ASD is a complex neurological disorder with diverse genetic and environmental etiologies [5]. Children with ASD are at least three times more likely to experience chronic gastrointestinal symptoms than neurotypical children, suggesting that ASD physiology is linked to gut dysbiosis [10]. Accordingly, a number of studies have shown that the microbiome is altered in children with ASD compared with controls [5]. Many genetic variants associated with ASD involve synaptic transmission [5]. A mutation affecting SHANK3, a scaffolding protein in the postsynaptic density of excitatory neurons, contributes to about 2% of ASD cases in humans [5]. A mouse line with homozygous knockout of *Shank3* exhibited repetitive behaviors and abnormal social interactions, which are characteristic features of human ASD. *Tabouy et al.* [5] showed that *Shank3*$^{-/-}$ mice have reduced gut microbiome diversity, with diminished populations of certain species of bacteria, such as *Lactobacillus reuteri*, *Lactobacillus brevis*, and

*Lactobacillus ruminis*. Gut colonization with *L. reuteri* improved behavioral outcomes in male mice and increased the expression of GABA receptors in the brain [5]. This finding is consistent with the abnormal excitatory and inhibitory synaptic transmission through glutamate and GABA signaling reported in ASD [11]. It appears that enrichment of (or treatment with) specific commensal microbes may be a promising avenue for ameliorating certain behavioral disorders.

## FUTURE DIRECTIONS

At present, genetic and environmental factors (and their effect on the microbiome) are investigated separately. The effects of genetic predispositions on neurological disorders are compounded by diet choices, prescription medications, exercise, age, and life experiences, all of which shape the microbiome [2]. Studying these components individually ignores critical interactions between various factors, thus limiting our understanding of the complex mechanisms linking gut dysbiosis and neurologic conditions. Preclinical models that can rigorously control for and test genetic and environmental factors will serve as useful representations of the diverse influences that impact neurologic function, including the microbiome. Animal models provide opportunities to discover therapeutic options, such as microbiota transplants and potential dietary interventions, that can be individually tailored for distinct neuropsychiatric and neurodevelopmental disorders. Microbiome-based treatments aimed at influencing neurological responses, such as neurotransmitter release, stress responses, and neurological development, could be designed in accordance with an individual's genetic risk for a given disease. As it remains challenging to correct genetic predispositions, the

correction of altered microbiomes appears to be a more viable approach toward novel therapeutics for neurologic disorders.

**REFERENCES**


1. Sharon G, Sampson TR, Geschwind DH, Mazmanian SK. The central nervous system and the gut microbiome. Cell. 2016;167:915–932. Doi: 10.1016/j.cell.2016.10.027.
2. Jašarević E, Howard C, Morrison K, Misic A, Weinkopff T, Scott P, et al. The maternal vaginal microbiome partially mediates the effects of prenatal stress on offspring gut and hypothalamus. Nat Neurosci. 2018;21:1061–1071. Doi: 10.1038/s41593-018-0182-5.
3. Soto M, Herzog C, Pacheco JA, Fujisaka S, Bullock K, Clish CB, Kahn CR. Gut microbiota modulate neurobehavior through changes in brain insulin sensitivity and metabolism. Mol Psychiatry. 2018. 10.1038/s41380-018-0086-5.
4. Olson CA, Vuong HE, Yano JM, Liang QY, Nusbaum DJ, Hsiao EY. The gut microbiota mediates the anti-seizure effects of the ketogenic diet. Cell. 2018;173:1728–1741. Doi: 10.1016/j.cell.2018.04.027.
5. Tabouy L, Getselter D, Ziv O, Karpuj M, Tabouy T, Lukic I, et al. Dysbiosis of microbiome and probiotic treatment in a genetic model of autism spectrum disorders. Brain Behav Immun. 2018;73:310–319. Doi: 10.1016/j.bbi.2018.05.015.
6. Polidano C, Zhu A, Bornstein JC. The relation between cesarean birth and child cognitive development. Sci Rep. 2017;7:11483. Doi: 10.1038/s41598-017-10831-y.
7. Westmark CJ. Soy infant formula may be associated with autism behaviors. Autism Open Access. 2013;3:20727. Doi: 10.4172/2165-7890.1000120.

8. Dominguez-Bello MG, De Jesus-Laboy KM, Shen N, Cox LM, Amir A, Gonzalez A, et al. Partial restoration of the microbiota of cesarean-born infants via vaginal microbial transfer. Nat Med. 2016;22:250–253. Doi: 10.1038/nm.4039.
9. Hall AB, Tolonen AC, Xavier RJ. Human genetic variation and the gut microbiome in disease. Nat Rev Genet. 2017;18:690–699. Doi: 10.1038/nrg.2017.63.
10. Chaidez V, Hansen RL, Hertz-Picciotto I. Gastrointestinal problems in children with autism, developmental delays or typical development. J Autism Dev Disord. 2014;44:1117–1127. Doi: 10.1007/s10803-013-1973-x.
11. Horder J, et al. Glutamate and GABA in autism spectrum disorder—a translational magnetic resonance spectroscopy study in man and rodent models. Transl Psychiatry. 2018;8:106. Doi: 10.1038/s41398-018-0155-1.

*Chapter 2*

# PERIPHERAL NEURONAL ACTIVATION OF THE INTESTINAL TRACT SHAPES THE MICROBIOME AND ALTERS GUT PHYSIOLOGY

**Griffiths J. A.***, Yoo B. B.*, Thuy-Boun P., Cantu V., Weldon K., Challis C., Sweredoski M. J., Chan K. Y., Thron T. M., Sharon G., Moradian A., Humphrey G., Zhu Q., Shaffer J, Wolan D. W., Dorrestein P. C., Knight R., Gradinaru V., Mazmanian S. K. (2024)

*indicates co-first authors

This chapter is “accepted in principle” at *Cell Reports*

**SUMMARY**

The gastrointestinal (GI) tract is extensively innervated by both intrinsic neurons of the enteric nervous system (ENS) and extrinsic neurons of the central nervous system (CNS) and peripheral ganglia that together regulate gut motility, secretion, and immunity. The GI tract also harbors a diverse microbiome, but interactions between the ENS and the gut microbes remain poorly understood. Herein, we activated gut-associated neurons in mice to determine effects on intestinal microbial communities and their metabolites, as well as on host physiology. We used recombinant adeno-associated viral vectors with enhanced tropism for the gut, and no targeting to the brain, to chemogenetically activate either choline acetyltransferase (ChAT)-expressing or tyrosine hydroxylase (TH)-expressing neurons in the periphery. Targeted activation of discrete neuronal subtypes distinctively altered the metagenome, fecal metabolome, and mouse and microbial proteomes. The resulting datasets provide a rich resource, revealing broad and previously unknown roles for $ChAT^+$ and $TH^+$ neurons in modulating microbiome structure, and providing evidence for novel ENS functions such as shaping bile acid profiles and regulating fungal colonization of the gut. Further, ChAT+ neuronal activation upregulated transcriptional pathways for muscle cell proliferation, angiogenesis, and muscle development. Physiologically, while mice displayed increased fecal output following activation of gut-associated $ChAT^+$ and $TH^+$ neurons, only $ChAT^+$ neuronal activation resulted in increased colonic migrating motor complexes and diarrhea-like fluid secretion. These findings suggest that specific subsets of peripherally-activated ENS neurons differentially regulate the gut microbiome and GI physiology in mice.

## INTRODUCTION

Diverse cell types in the gastrointestinal (GI) tract coordinate physiology within the gut (Furness, 2006) and throughout the body (Rao and Gershon, 2016). The mammalian gut receives and transmits neuronal signals through ~100,000 extrinsic nerve fibers originating from the sympathetic, parasympathetic, and sensory nervous systems (Grundy and Brookes, 2011). The GI tract is also innervated by an extensive network of over 100 million intrinsic neurons organized into two distinct compartments within the GI tract, namely the myenteric plexus and submucosal plexus (Furness et al., 2014). The neurons of the GI tract, composing the enteric nervous system (ENS), have been implicated in processes including digestion (Schneider et al., 2019), immunity (Gabanyi et al., 2016; Muller et al., 2014), and even complex behaviors (Bravo et al., 2011) in mice. Interactions between neurons of the GI tract and other cell types highlight the diverse roles of the ENS. For example, neuronal pathways in the gut regulate nutrient sensation through intestinal enteroendocrine cells (Kaelberer et al., 2018), modulate the epithelial barrier and mucosal immunity (Jarret et al., 2020; Seillet et al., 2020; Talbot et al., 2020), and dynamically interface with the microbiome (Lai et al., 2019; Matheis et al., 2020). Exposure of the ENS to changing diet, microbiome, and xenobiotics creates inputs distinct from those in the central nervous system (CNS), i.e., the brain and spinal cord.

Choline acetyltransferase (ChAT) and tyrosine hydroxylase (TH) are the rate-limiting enzymes in acetylcholine and catecholamine biosynthesis, respectively, and are key chemical mediators of neurotransmission in the brain and the periphery. Acetylcholine is the primary excitatory neurotransmitter of the gut, and cholinergic neurons represent 60%

of the ENS, mediating intestinal propulsion and secretion (Nezami & Srinivasan, 2010; Qu et al., 2008). Several studies have established correlations between neuronal activity, abundance, and specific physiological outcomes (Furness, 2012; Hennig et al., 2015; Niesler et al., 2021). For example, age-associated reduction of $ChAT^+$ neurons in the ENS coincides with constipation and evacuation disorders (Nezami & Srinivasan, 2010; Qu et al., 2008), and clinical studies have shown that anticholinergic drugs cause constipation and cholinergic agonists can cause diarrhea (Lott & Jones, 2023; Monane et al., 1993). In a disease context, cholera toxin induces hypersecretion and sustained activation of submucosal $ChAT^+$ neurons in mice (Fung et al., 2018; Wang et al., 2022). Although less characterized, $TH^+$ neurons and dopamine signaling pathways have also been shown to affect GI motility (Shan Li et al., 2006), and $TH^+$ neuronal damage in individuals with Parkinson's disease (PD) correlates with increased constipation (Baumuratov et al., 2016; McQuade et al., 2021).

Though known to be important for motility and secretomotor function, $ChAT^+$ and $TH^+$ neurons have not yet been systematically characterized and interrogated for their roles in GI physiology (Furness, 2012; Mittal et al., 2017). One barrier to modulation of neuronal populations in the ENS is its size: 35-40 cm in mice. To circumvent the need for direct delivery of effectors, we leveraged a systemically-delivered engineered adeno-associated virus (AAV) with enhanced tropism for the ENS and other peripheral ganglia of mice (Chan et al., 2017). Importantly, this vector, AAV-PHP.S, does not transduce the CNS, allowing us to uncouple peripheral activation from brain-to-gut signaling. We find that activating gut-associated $ChAT^+$ and $TH^+$ neurons of mice with chemogenetic modulators (Wess et al., 2013) alters the transcriptional and proteomic landscape of the intestines, as well as the

gut metagenome and metabolome. Multi-'omic' analyses allow us to characterize detailed and complex host-microbial interactions, and enable prediction of neuronal influences on a number of biological processes in the gut, including providing novel insights into secondary bile acid production and control of fungal populations, among other interesting associations. In addition, we show that activation of gut-associated neurons strikingly impacts GI function, including motility and fluid secretion. Together, this work reveals differential effects of non-brain activation of $ChAT^+$ and $TH^+$ neurons in shaping the gut environment and GI physiology and generates rich datasets as a resource for further exploration (https://github.com/mazmanianlab/Griffiths_Yoo_et_al/).

## RESULTS

### Distinct spatial localization of ChAT$^+$ and TH$^+$ neurons in the ENS

Broad ENS morphology has been previously characterized using immunohistochemistry (IHC) (Furness, 2006; Qu et al., 2008; Hamnett et al., 2022). To map neurons in mice with higher resolution, we used recombinant AAVs to fluorescently label enteric neurons *in vivo*, and tissue clearing techniques to enhance visualization of intact GI tissue (Hama et al., 2015; Treweek et al., 2015; Yang et al., 2014). Imaging whole tissue, without the need for sectioning, preserves neuronal architectures over large distances and across both longitudinal and cross-sectional axes. The AAV capsid variant AAV-PHP.S is optimized for systemic delivery in mice (Deverman et al., 2016) and displays increased tropism for the peripheral nervous system (PNS), including the ENS (Chan et al., 2017). To further optimize ENS expression, we replaced the CAG promoter used in (Chan et al., 2017) with the human Synapsin 1 (hSYN1) promoter, which has been shown to restrict gene expression to neurons (Chan et al., 2017) and minimize expression in peripheral targets such as the dorsal root ganglia (DRGs) (Haenraets et al., 2017). To assess off-target effects, we compared expression of AAV-PHP.S-delivered hSYN1-mNeonGreen to that of CAG-mNeonGreen in various non-ENS tissues known to affect GI function (Figure S1). Expression from the hSYN1 construct only sparsely labeled the DRGs and jugular-nodose ganglia, and did not label neuronal projections in the vagus nerve or dorsal root, unlike the previously-used CAG construct (Figures S2A and S2B) (Chan et al., 2017). In the CNS, AAV-PHP.S-hSYN1 did not label neurons in the brain, brainstem, or spinal cord (Figure S3).

We packaged genes encoding fluorescent proteins (tdTomato or mNeonGreen) under control of the hSYN1 promoter into AAV-PHP.S, delivered them systemically, and found that 90% (±2.6% SD) of ENS cells labelled with antibodies against *P*rotein *G*ene *P*roduct 9.5 (PGP9.5), a pan-neuronal protein, co-localized with virally-labelled neurons in the small intestine (SI) and colon (Figure 1A). A single systemic injection of AAV-PHP.S-hSYN1-mNeonGreen at a dose of $10^{12}$ viral genomes (vg) was sufficient to label spatially diverse regions of the ENS, such as ganglia proximal and distal to the mesentery (Figure S4A). Viral transduction was uniform throughout the SI and colon, aside from a small (~1.5 cm) section of the medial colon that, for unknown reasons, was consistently not well transduced and was therefore excluded from further analysis (Figure S4B).

To explore the general architecture of the ENS, we transduced wild-type mice with a single i.v. injection of a pool of AAV-PHP.S packaging multiple fluorescent proteins (AAV-PHP.S-hSYN1-XFP), which broadly labelled enteric neurons in the gut and enabled us to distinguish cells by distinct colors resulting from stochastic transduction with different combinations of XFPs (Figure 1B). We quantified the number of neurons and ganglia, as well as the ganglion size (i.e., the number of neurons in each ganglion) in the myenteric and submucosal plexuses of seven regions of the SI and two regions of the colon (Figures S5A-S5F). Regions were approximately 1 cm in length and the tissue was sampled every 2-3 cm. We saw that in the SI, the numbers of neurons and ganglia generally increased toward the distal portion of the myenteric plexus, while the converse was true for the submucosal plexus (i.e., lower numbers in distal than proximal regions) (Figures S5A and S5B). Additionally, the size of the ganglia (i.e., the number of neurons per ganglion) increased in the distal region of the SI myenteric plexus, a feature not observed in the submucosal plexus

(Figure S5C). While neuronal numbers were similar in the proximal and distal regions of the colonic plexuses (Figure S5D), the number of myenteric ganglia increased (Figure S5E) while the size of each ganglion decreased in the distal colon (Figure S5F). Interestingly, submucosal neurons in the proximal colon localized to natural folds in the tissue (Figure 1B, dashed lines in lower second-from-right panel).

To visualize $ChAT^+$ and $TH^+$ neurons, we employed mouse lines in which Cre recombinase (Cre) is expressed under the control of the respective gene promoter and engineered viral constructs with the transgene in a double-floxed inverted orientation (DIO) so that the transgene is flipped and expressed in a Cre-dependent manner. After transducing ChAT-Cre or TH-Cre mice with AAV-PHP.S-hSYN1-DIO-XFP, we observed that both neuronal populations occupy spatially distinct layers of the GI tract, with $ChAT^+$ neurons primarily located in the myenteric plexus and $TH^+$ neurons more abundant in the submucosal plexus (Figure 1C). Quantifying this effect, we found more $ChAT^+$ than $TH^+$ neurons in all assayed regions of the myenteric plexus (Figure 1D), although the density of $TH^+$ myenteric neurons increased distally (Figure 1D, 10-fold increase from SI-1 vs SI-7; 2-fold increase from SI-7 vs SI-10/13/15). In the small intestine, by contrast, there were more $TH^+$ than $ChAT^+$ submucosal neurons (Figure 1E). In addition to providing these insights into ENS architecture, this approach for whole tissue imaging without the need for antibody labeling (which has limited penetration to deeper layers) should be broadly useful for profiling other neuronal and non-neuronal cell types in the gut.

**Activation of gut-associated neurons reshapes the gut microbiome**

The unique spatial organization of ChAT$^+$ and TH$^+$ neurons we observed suggests potentially distinct functions, which we decided to investigate through specific activation of each neuronal population. First, we examined the specificity of AAV-PHP.S-hSYN1 by staining gut-extrinsic PNS ganglia for TH, and found no transduction of TH$^+$ cells in the DRGs or jugular-nodose ganglia (Figures S2B and S2C). ChAT$^+$ neurons are absent in these peripheral ganglia (Figure S2C) (Jakob et al., 2021; Tavares-Ferreira et al., 2022). Prior research has shown that AAV-PHP.S-hSYN1 transduces the prevertebral sympathetic ganglia, which are known to innervate the gut (Challis et al., 2019), but these ganglia also lack ChAT$^+$ neurons (Kaestner et al., 2019). In fact, the vast majority of neurons in the prevertebral sympathetic ganglia are TH$^+$ (Browning & Travagli, 2014; Kaestner et al., 2019).Therefore, for the remainder of the manuscript, we will use the term "gut-associated" to refer to ChAT$^+$ neurons in the ENS, or TH$^+$ neurons in the ENS plus innervating prevertebral sympathetic ganglia.

For cell-specific neuronal activation, we employed a Cre-dependent genetic construct encoding an activating '*D*esigner *R*eceptor *E*xclusively *A*ctivated by *D*esigner *D*rugs' (DREADD), named hM3Dq, which is a modified neurotransmitter receptor designed to induce neuronal activation when exposed to Compound 21 (C21), a "designer drug" specific to this receptor (Thompson et al., 2018). We validated functional gene delivery and expression using intestinal explants from a ChAT-Cre mouse transduced with the activating DREADD and a construct encoding the calcium sensor GCaMP6f, observing a gradual increase in fluorescence consistent with a calcium transient following administration of C21 (Figure S5G and Video Supplement 1).

We reasoned that neuronal activation in the gut may impact the composition and community structure of the gut microbiome. Accordingly, we transduced ChAT-Cre or TH-Cre mice with either virus carrying the activating DREADD (AAV-PHP.S-hSYN1-DIO-hM3Dq-mRuby2) or a control virus expressing only the fluorescent reporter protein (AAV-PHP.S-hSYN1-DIO-mRuby2). We performed shotgun metagenomics on a longitudinal series of fecal samples collected prior to and following $ChAT^+$ or $TH^+$ neuron activation by C21 (on days 2, 6, and 10 of C21 administration), as well as contents of the terminal cecum collected on day 10 (Figure 2A). In $ChAT^+$-activated mice, Faith's phylogenetic diversity (i.e., alpha-diversity) decreased dramatically in the day 10 fecal and cecal samples (Figure 2B), with many microbial taxa less abundant (Figures 2I-2K; Figure S6; Figure S7). In contrast, $TH^+$-activated mice displayed similar phylogenetic diversity to controls throughout the experiment (Figure 2B). Using weighted UniFrac distances and principal coordinate analysis (PCoA) to determine the composition of microbial communities (i.e., beta-diversity), we observed a distinction between $ChAT^+$-activated and control animals in both feces and cecal contents, a shift that was absent in samples from $TH^+$-activated mice and controls (Figures 2C-H). Over the experimental time course, Verrucomicrobia became significantly enriched in $ChAT^+$-activated mice (Figure 2I). To explore differentially abundant bacterial taxa, we used linear discriminant analysis effect size (LEfSe) (Segata et al., 2011) and generated cladograms depicting the phylogenetic relationships of differentially abundant taxa (Figures 2J-2M). This analysis revealed that the bacterial species *Akkermansia muciniphila* drove the increase in Verrucomicrobia we observed in $ChAT^+$-activated mice (Figures 2N and 2O).

In addition to identifying microbial species, metagenomic analysis can reveal gene families and pathways that are differentially abundant in the microbiome. ChAT$^+$-activated mice, but not TH$^+$-activated mice, showed changes in beta-diversity of both gene families and pathways, with shifts evident in the cecal contents and feces collected 9 days after activation (Figures 2P-2S). The most distinguishing features were highly represented in the control group and downregulated in ChAT$^+$-activated mice and were mainly associated with bacterial processes, such as nucleotide biosynthesis and metabolism, and protein translation and transport (Figures 2P-2S; Figures S7C and S7D). This downregulation is consistent with the decrease in bacterial alpha-diversity we observed in ChAT$^+$-activated mice (Figure 2B). We conclude that neuronal activation actively reshapes the gut microbiome at community, species, and genetic levels, with considerable differences between the effects of ChAT$^+$ and TH$^+$ neurons.

**Neuronal stimulation impacts the gut metabolome**

Given the intimate and intertwined mouse and microbial co-metabolism, the changes in the microbial metagenome we observed in response to neuronal activation led us to predict that there would also be alterations in the profile of gut metabolites. We therefore performed untargeted metabolomics using liquid chromatography with tandem mass spectrometry (LC-MS/MS) to assay molecular changes in cecal contents and feces following neuronal activation in the gut. In both ChAT$^+$- and TH$^+$-activated neurons, compared to nonactivated controls (no DREADD), we observed a strong separation of metabolome profiles in cecal samples taken one hour following the last C21 injection (Figures 3A and 3B). Thus,

targeted activation of ChAT$^+$ and TH$^+$ gut associated neurons appears to strongly influence the gut metabolome.

To contextualize these data, we applied the Global Natural Products Social Molecular Networking (GNPS) tool (Wang et al., 2016), an open-access mass spectrometry repository and analysis pipeline. GNPS revealed metabolic networks of both annotated and unannotated molecules in the cecal contents of ChAT$^+$-activated and TH$^+$-activated mice (Figures 3C and 3D), allowing us to identify metabolites with differential abundance between control and activated samples. Activation of TH$^+$ neurons strongly increased metabolites whose closest spectral matches were linoelaidic acid (ID: 626), oleanolic acid methyl ester (ID: 378), and coproporphyrin I (ID: 739). Metabolites that spectrally resembled xanthine (ID: 259), genistein (ID: 846), and trans-ferulic acid (ID: 707) were decreased upon activation of TH$^+$ neurons (Table S1).

In both ChAT$^+$-activated and TH$^+$-activated mice, the molecular networks largely consisted of level 3 annotations (based on the Metabolomics Standards Initiative (MSI) (Sumner et al., 2007)) of compounds belonging to the bile acid molecular family and their conjugates, as well as unannotated analogs (Figures 3C-3D). Primary bile acids are chemicals derived from host (mouse) cholesterol biosynthesis, which are subsequently co-metabolized by gut bacteria into secondary bile acids (Aries et al., 1969; Sakai et al., 1980). Interestingly, metabolites with a closest spectral match to the primary bile acid cholic acid (IDs: 108, 114, 215, 219, 221, 224, 259) were significantly enriched in the cecum of ChAT$^+$-activated mice (Figures 3D-3F; Table S1). Additional metabolites that spectrally resemble tauro-conjugated primary bile acids, such as taurocholic acid (IDs: 234, 248) and taurohyocholic

acid (ID: 235), trended upwards. Conversely, features matching the spectra of secondary bile acids and bile acid metabolites such as ursodeoxycholic acid (ID: 13), deoxycholic acid (ID: 100), beta-hyodeoxycholic acid (IDs: 1, 143) and 12-ketodeoxycholic acid (IDs: 19, 138) were decreased in ChAT$^{+}$-activated mice (Figures 3D-3F). These data suggest that activation of ChAT$^{+}$ neurons may modulate, either directly or indirectly, primary bile acid secretion and/or metabolism to secondary bile acids, which have been implicated in a number of metabolic and immunologic functions, as discussed below.

**Neuronal subpopulations differentially shape the gut luminal proteome**

Proteins from the mouse, gut microbes, and diet converge and interact in the GI tract (Albenberg and Wu, 2014). We performed untargeted label-free proteomics by LC-MS/MS of cell-free supernatants of the cecal contents from ChAT$^{+}$-activated and TH$^{+}$-activated mice and controls collected one hour following the final C21 treatment (see Figure 2A). Consistent with the increase in cecal bile acid metabolites that we observed in ChAT$^{+}$-activated mice, we report an increased abundance of Niemann-Pick C1-Like 1 protein (NPC1L1) in the cecum of these mice (Figure 4A). NPC1L1 is expressed on the apical surface of enterocytes, and is integral to the absorption of free cholesterol, the precursor of bile acids, from the lumen (Jia et al., 2011). Goblet cell-related proteins, specifically Mucin-19 (MUC19) and Zymogen granule 16 (ZG16), a protein localized to secretory granules (Rodríguez-Piñeiro et al., 2013), also trended upwards following ChAT$^{+}$ neuronal activation (Figure 4A). Conversely, one of the most highly downregulated proteins was an aldehyde dehydrogenase (Q3U367) encoded by the *Aldh9a1* gene, which is involved in the catalytic conversion of putrescine to gamma-aminobutyric acid (GABA) (Matsushima et al.,

1986). While GABA is the primary inhibitory neurotransmitter in the CNS, little is known about its role in the ENS. The most significantly upregulated proteins in cecal contents of $ChAT^+$-activated mice were pancreatic digestive enzymes including chymopasin (CTRL), chymotrypsinogen B1 (CTRB1), and pancreatic lipase related protein 2 (PNLIPRP2) (Figure 4A). Accordingly, network analysis of upregulated proteins revealed that KEGG pathways associated with digestion represent the majority of the network (Figure 4B). This is consistent with evidence that cholinergic, viscerofugal neurons send signals from the GI tract to other organs of the digestive system, including the pancreas (Furness et al., 2014). Cholinergic innervation of the pancreas plays a significant role in regulating pancreatic functions, such as the secretion of digestive enzymes and insulin release (Li et al., 2019).

Peripheral activation of $TH^+$ gut-associated neurons also altered the luminal proteome of the cecum. Notably, 88% (52/59) of the differentially abundant proteins ($p_{adj.}<0.25$) were distinct from those identified in $ChAT^+$-activated mice. The overall direction of the effect was also reversed: ~90% of differentially-abundant cecal proteins in $TH^+$-activated mice were upregulated (53/59), compared to ~18% in $ChAT^+$-activated mice (20/112), suggesting that activation of distinct neuronal subsets is associated with opposing changes in GI function. We observed signatures of increased protein-protein interactions in cecal contents of $TH^+$-activated mice, evidenced by more network nodes and connections (Figure 4D). Filamin B (FLNB) and spectrin beta chain, non-erythrocytic 1 (SPTBN1) were two of the most significantly enriched proteins following $TH^+$ neuron activation (Figure 4C). Both are associated with the intestinal brush border and membrane vesicles (Donowitz et al., 2007; McConnell et al., 2011). Accordingly, coatomer proteins also trended upward (COPA and COPB2) (Figure 4C) and vesicle-mediated transport was one of the major protein

networks altered (Figure 4D). Other upregulated protein interaction networks were associated with metabolic pathways, ribosomal activity, and the immune system (Figure 4D). For example, the immune-related proteins immunoglobulin heavy constant alpha (IGHA) (in ChAT$^+$-activated), immunoglobulin heavy constant gamma 2C (IGHG2C), and complement component 3 (in TH$^+$-activated) trended upward (Figures 4A and 4C).

Perhaps the most intriguing observation was the strong depletion of acidic mammalian chitinase (CHIA) upon activation of TH$^+$ neurons (Figure 4C). Chitin is a natural polysaccharide that is a major component of fungal cell walls (Latgé, 2007), but intestinal chitinases are poorly studied in mice. This result prompted us to query the pan-proteomic dataset against a microbial protein database, which revealed that the decrease in CHIA abundance following TH$^+$ neuron activation was accompanied by a large bloom in fungal-associated peptides in the microbiome (~59% of peptides mapped to any microbe) (Figure 4E). In contrast, fungal peptides represented only ~0.4% of enriched peptides in the lumen of ChAT$^+$-activated mice (Figure 4F). Unfortunately, we were unable to corroborate these proteomic data with metagenomics since the DNA extraction method we used was not optimized for fungi. However, these findings suggest that the reduced chitinase production of activated TH$^+$ cells is directly associated with a dramatic increase in fungal proteins, which, if experimentally validated in future, would represent a novel circuit by which the gut-associated neurons of mice regulates fungal load in the gut.

**Activation of ChAT$^+$ and TH$^+$ neurons alters the intestinal transcriptome**

Given the changes to the gut microbiome, proteome and metabolome that we observed, we were interested in the tissue-level impact of neuronal activation on the intestinal

transcriptome. We therefore profiled gene expression with QuantSeq, a quantitative 3' mRNA-sequencing technology, in 1 cm of tissue from the distal SI and proximal colon harvested one hour after the last C21 injection. Rapid and transient expression of immediate early genes (IEGs) is widely used as a measure of increased neuronal activity (Wu et al., 2017), and the IEGs *Fos*, *Egr1*, *Jun*, and *Klf2* were among the most significantly upregulated transcripts we identified in the SI and colon of both $ChAT^+$- and $TH^+$-activated mice (Figures 5A-5D). These IEGs are also known to be upregulated during growth and differentiation of highly active cell types such as immune cells (Bahrami and Drabløs, 2016; Ramirez-Carrozzi et al., 2009), smooth muscle cells (Miano et al., 1993), and intestinal epithelial cells (Flandez et al., 2008).

In the distal SI, we found similar numbers of differentially-expressed genes (DEGs; $p_{adj.}<0.05$) in $ChAT^+$-activated mice (162 DEGs) and $TH^+$-activated mice (165 DEGs) (Figures 5A and 5C). The direction of regulation differed, however, with ~73% of DEGs upregulated upon $ChAT^+$ activation (118 up, 44 down) and ~58% of DEGs downregulated upon $TH^+$ activation (69 up, 96 down). IEGs followed this overall pattern, with 29 upregulated in the distal SI of $ChAT^+$-activated mice but only two upregulated in $TH^+$-activated mice (Figure 5E), and three (i.e., *Hbegf, Soca3, Mcl1*) downregulated (Figure 5C). Similar proportions of DEGs were upregulated in the proximal colon of both $ChAT^+$-activated (169 up, 84 down) and $TH^+$-activated mice (130 up, 62 down) (Figures 5B and 5D). Given the enrichment in fungal proteins and reduction in the level of the CHIA protein in the $TH^+$-activated mice, we explored potential immune responses to fungi but found no obvious inflammatory signals compared to control mice (Table S3).

To gain insight into the cellular functions of DEGs, we used Gene Set Enrichment Analysis (GSEA) (Figures 5F-I; Table S2). Notably, the most highly enriched gene ontology (GO) term for the distal SI of ChAT$^+$-activated mice was "regulation of smooth muscle cell proliferation" (Figure 5F), whereas in TH$^+$-activated mice it was "response to bacteria" (Figure 5H), consistent with the increase in immune-related responses suggested by our proteomic dataset. In the proximal colon, we observed similar GO pathways in ChAT$^+$-activated and TH$^+$-activated mice (Figures 5G and 5I), suggesting that transcriptomic signatures may depend on the context of the activated neurons. In the SI, ChAT$^+$ neurons predominantly border muscle cells in the myenteric plexus, while TH$^+$ neurons neighbor epithelial and immune cells which respond to bacteria in the submucosal plexus of the distal SI (see Figures 1C-1E). In the colon, both neuronal subsets are abundant in the myenteric plexus (see Figure 1D). In both myenteric and submucosal plexuses, we saw a wider breadth of pathways upregulated by activation of ChAT$^+$ neurons than TH$^+$ neurons, with ChAT$^+$ neuronal activation impacting diverse cellular functions in the GI tract, involving endothelial, epithelial, immune, and adipose cells (Figure 5G; Table S2).

**Differential functional GI outcomes of activation of ChAT$^+$ and TH$^+$ neurons**

Motivated by the complexity of responses we observed following activation of neuronal populations in the gut, we decided to assay functional GI outcomes. Both ChAT$^+$ and TH$^+$ neuronal populations are known to be important for motility and secretory function (Furness, 2012; Mittal et al., 2017), but they have never been specifically modulated to study GI physiology in a freely behaving mammal. Activation of either ChAT$^+$ or TH$^+$ gut-associated neurons resulted in faster whole gut transit time, increased fecal pellet output,

and mass of cecal contents compared to control mice (Figures 6A-C). Fecal pellets from ChAT$^+$-activated, but not TH$^+$-activated, mice had increased water content, which is consistent with reports in the literature of involvement of ChAT$^+$ enteric neurons in fluid secretion (Figures 6D-6F) (Fung et al., 2018; Monane et al., 1993; Nezami & Srinivasan, 2010). This distinction is particularly notable given the higher concentration of TH$^+$ neurons than ChAT$^+$ neurons in most regions of the submucosal plexus (see Figure 1), which is largely responsible for fluid secretion and absorption (Furness, 2006). Daily administration of C21 for 9 days to control mice (no DREADD) did not cause any obvious health impairment and the mice maintained body weight throughout the experimental period (Figures S6C and S6D). TH$^+$-activated mice also maintained body weight, but ChAT$^+$-activated animals experienced slight weight loss that likely reflects the diarrhea-like phenotype over 9 consecutive days. To further examine gut motility in the absence of extrinsic innervation, we analyzed propulsive colonic migrating motor complexes (CMMCs) in an *ex vivo* system. Activation of ChAT$^+$ neurons by C21 administration resulted in more frequent migration of motor complexes (Figures 6G, 6I, and 6J; Table S4), whereas activation of TH$^+$ neurons had no effect on CMMCs (Figure 6H; Table S4). The discrepancy between the *in vivo* and *ex vivo* results we observed may be due to activation of TH$^+$ neurons in the sympathetic prevertebral ganglia that project to the gut (Furness, 2006). Overall, these data reveal that ChAT$^+$, but not TH$^+$, neurons in the gut mediate intestinal fluid balance and *ex vivo* colonic motility.

## DISCUSSION

While early pioneers of neuroscience in the 20th century focused on the ENS as a model, more recent research has centered on the brain, and our understanding of the CNS has outpaced that of other neuronal systems in the body. As a result, basic knowledge of many aspects of neuronal architecture and function within the gut remain rudimentary (Fung et al., 2018; Monane et al., 1993; Nezami & Srinivasan, 2010). Here, using a viral delivery system with enhanced tropism for the ENS, we mapped the distribution of $ChAT^+$ and $TH^+$ neurons across the mouse GI tract and assayed the complex effects of their peripheral activation on physiology and function. Although the DREADD-based activation paradigm we use in this study is inherently artificial, the results reveal strikingly different roles for neuronal populations, with nearly every feature characterized (spatial distribution, metagenomic, metabolic, transcriptional, and proteomic profiles, and even physiological output) unique to cell type.

The viral vector we used, AAV-PHP.S, can transduce other neuronal subtypes in the PNS such as those in the DRGs and, with a strong ubiquitous promoter, induce transgene expression (Chan et al., 2017). To limit this off-target effect, we utilized a weaker promoter with increased ENS specificity and focused our analyses on GI tissue and lumen. By thus excluding most known extrinsic innervation pathways, we uncover cell-type-specific effects of gut-associated neuronal activation that are independent of signaling from the brain. It was recently shown that a similar strategy using AAV-PHP.S-hSYN1 in ChAT-Cre mice also labels $ChAT^+$ neurons in cardiac ganglia, and activation of cholinergic neurons reduces heart rate and blood pressure (Rajendran et al., 2019; Roy et al., 2015). Cardiac afferent

neurons signal through the vagus nerve and jugular-nodose ganglia to the brain, and in sensory pathways through the DRGs and spinal cord (Mohanta et al., 2023). Though there is no known direct route for signaling from cardiac ganglia to gut-associated neurons, it is possible that the gut may be impacted by an indirect route involving the CNS. In the future, further refinement of AAVs through directed evolution may generate serotypes with exclusive tropism for the ENS and allow full separation of the functions of intrinsic and extrinsic activation of gut-associated neuronal subsets. Since the hSYN1 promoter we used has been shown to drive expression only in neurons (Finneran et al., 2021; Kügler et al., 2003), we did not characterize other cell types, such as enteroendocrine cells (EECs), also called neuropod cells, which were recently shown to form synapses with enteric neurons and contribute to sensory transmission from the gut to the brain through the vagus nerve. Since these cells turn over every few days (Moran et al., 2008) and have not been reported to express TH or ChAT, we think it unlikely that they are a major contributor to the activation-induced phenotypes we observed, but we cannot completely rule out their involvement.

Exposure to the external environment charges the intestines with myriad responsibilities including absorption and digestion of dietary nutrients, exclusion of xenobiotics, protection from enteric infection, and partnership with the gut microbiome. Deletion of ChAT in enteric neurons leads to microbiome dysbiosis (Johnson et al., 2018), and we observed differences in the compositional profile (both metagenomic and proteomic) of the gut microbiome specific to activation of $ChAT^{+}$ neurons. Notably, we found an expansion of Verrucomicrobia driven by *A. muciniphila*, which has been implicated in human diseases such as obesity (Everard et al., 2013; Plovier et al., 2017), multiple sclerosis (Cekanaviciute

et al., 2017; Jangi et al., 2016), and seizures (Olson et al., 2018). *A. muciniphila* metabolizes host-derived mucus as a nutrient source (Derrien et al., 2004; Van Herreweghen et al., 2017), consistent with the increase in luminal mucin proteins and digestive enzymes we observed in $ChAT^+$-activated mice. A particularly interesting host-microbial interaction emerged from activation of $TH^+$ cells, which led to a dramatic decrease in anti-fungal chitinase (CHIA) protein expression and a concomitant bloom in fungi, suggesting that neuronal circuits can regulate fungal populations in the gut. If validated, this would be a novel demonstration of a host-microbial interaction with implications for health. Our study does not, however, reveal the mechanism(s) by which ENS activation reshapes the gut microbial community structure, which may involve altered colonic motility, changes in mucus production, modulation of mucosal immune responses, and/or shifts in metabolism and nutrient availability.

The human gut microbiome possesses as much metabolic capacity as the liver; it is therefore no surprise that changes to both mouse gut physiology and the microbiome have major influences on the gut metabolome. In a striking example of mutualism, we report widespread changes to the pool of intestinal bile acids, molecules produced via host-microbial co-metabolism. Activation of $ChAT^+$ neurons, but not $TH^+$ neurons, impacted expression of NPC1L1, which is involved in cholesterol transport. In mammals, cholesterol is the substrate for production of primary bile acids, which are then metabolized exclusively by the gut microbiome into secondary bile acids. Bile acids play critical roles in fat absorption (de Aguiar Vallim et al., 2013), gut motility (Kirwan et al., 1975), hormonal signaling (Watanabe et al., 2006) and immune functions (Fiorucci et al., 2018), and neurological conditions (McMillin and DeMorrow, 2016). Expression of bile salt

hydrolases and hydratases increases the fitness of both commensal and pathogenic bacteria (Begley et al., 2005; Delpino et al., 2007; Hofmann and Eckmann, 2006; Jones et al., 2008; Sannasiddappa et al., 2017). While additional work is required to determine how the ENS affects levels and constitution of the bile acid pool, understanding the processes that regulate synthesis of secondary bile acids may have implications for organ systems throughout the body.

Our study complements recent single-cell RNAseq studies of the ENS neuronal transcriptome (Drokhlyansky et al., 2020) by giving us the ability to selectively activate specific enteric neurons and explore the dynamic interplay between cells of various lineages in the gut. Importantly, the transcriptomic changes we observed may be a consequence of direct or indirect effects of neuronal activation. Indeed, induced activation of $ChAT^{+}$ or $TH^{+}$ neurons rapidly changed GI transit and fluid secretion patterns, which are only a fraction of the processes that may feed back on epithelial or immune cells, altering their gene expression profiles. Further single-cell analysis may help dissect the roles of the various intestinal cells that collaborate to coordinate gut functions.

The ENS adapts and responds to incredibly diverse molecular cues from the environment and must do so throughout the entire length and surface area of the intestines—the largest and most extensive internal organ, with a rich network of neurons termed the “second brain” (Gershon, 2015). Exposure to molecules from the diet or the microbiome may modulate ENS function, along with signals from outside the gut such as the circulatory system. Curiously, many disorders of the brain are also associated with GI symptoms (Bhavsar et al., 2013; Cersosimo et al., 2013; Del Giudice et al., 1999; Pfeiffer,

2003; Valicenti-McDermott et al., 2008). While mechanisms linking the gut and the brain, and their consequences for health, are an active area of study, the impact of neuronal activation within the ENS has largely been unexplored. Herein, we establish an experimental system that allows controlled activation of intrinsic and extrinsic neurons of the gut, separated from inputs from the brain, and demonstrate broad changes in the gut environment and its physiology that differ by activated neuronal population. The extensive datasets on activation of two major gut-associated neuronal populations that we generated should serve as a resource for further studies on the interconnected biological systems governing the complex relationship between gut physiology and the microbiome. Future deployment of this approach could enable mapping of neuronal connections into and out of the gut, providing insights into how the ENS networks with tissues throughout the body and advancing growing research into the many functions of the GI tract, an endeavor with important consequences for human health.

# FIGURES

## Figure 1

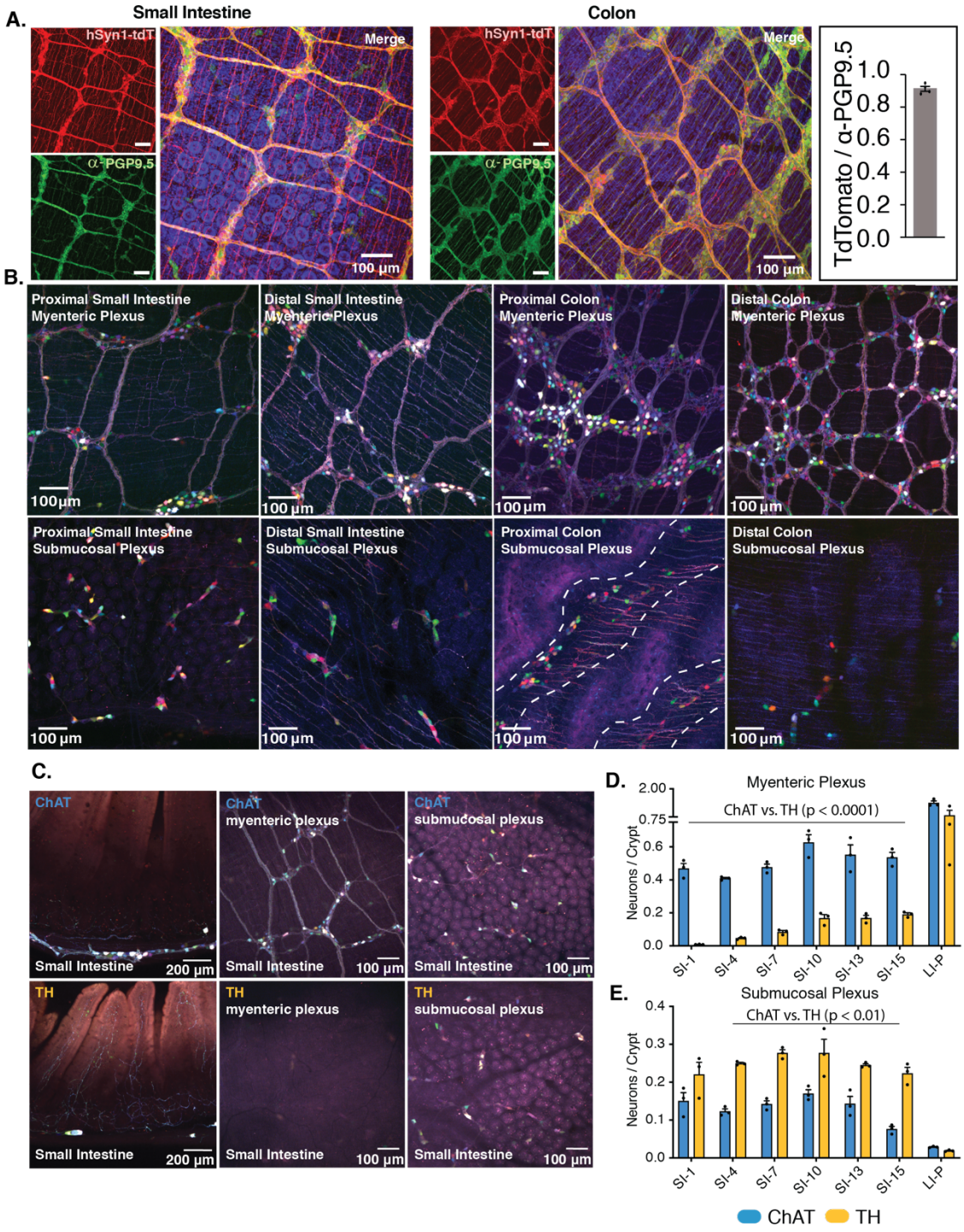

**Figure 1. ChAT$^+$ versus TH$^+$ Neuronal Distribution in the ENS**

(A) Representative images of SI and colon from mice infected with AAV-PHP.S-hSYN1-tdTomato and immunolabelled with the pan-neuronal antibody PGP9.5. Inset shows quantification of the ratio of tdTomato$^+$ cells / PGP9.5$^+$ cells (N=3 mice, each data point represents the average of 3 representative fields).

(B) Representative images of proximal and distal regions of the SI and colon from AAV-PHP.S-hSYN1-XFP infected mice. Dotted lines demarcate the rugae (folds) in the proximal colon.

(C) Representative images of cross-sections, myenteric, and submucosal plexuses in ChAT-Cre and TH-Cre mice infected with AAV-PHP.S-hSYN1-DIO-XFP.

(D-E) Density of neurons in the myenteric plexus and submucosal plexus of ChAT-Cre and TH-Cre mice normalized to the number of crypts (N=3 mice, each data point represents the average of 3 representative fields).

See also Figures S1-S5 and Video Supplement 1

**Source Data Figure 1**

https://github.com/mazmanianlab/Griffiths_Yoo_et_al/tree/main/ENS%20quantification

**Figure S1**

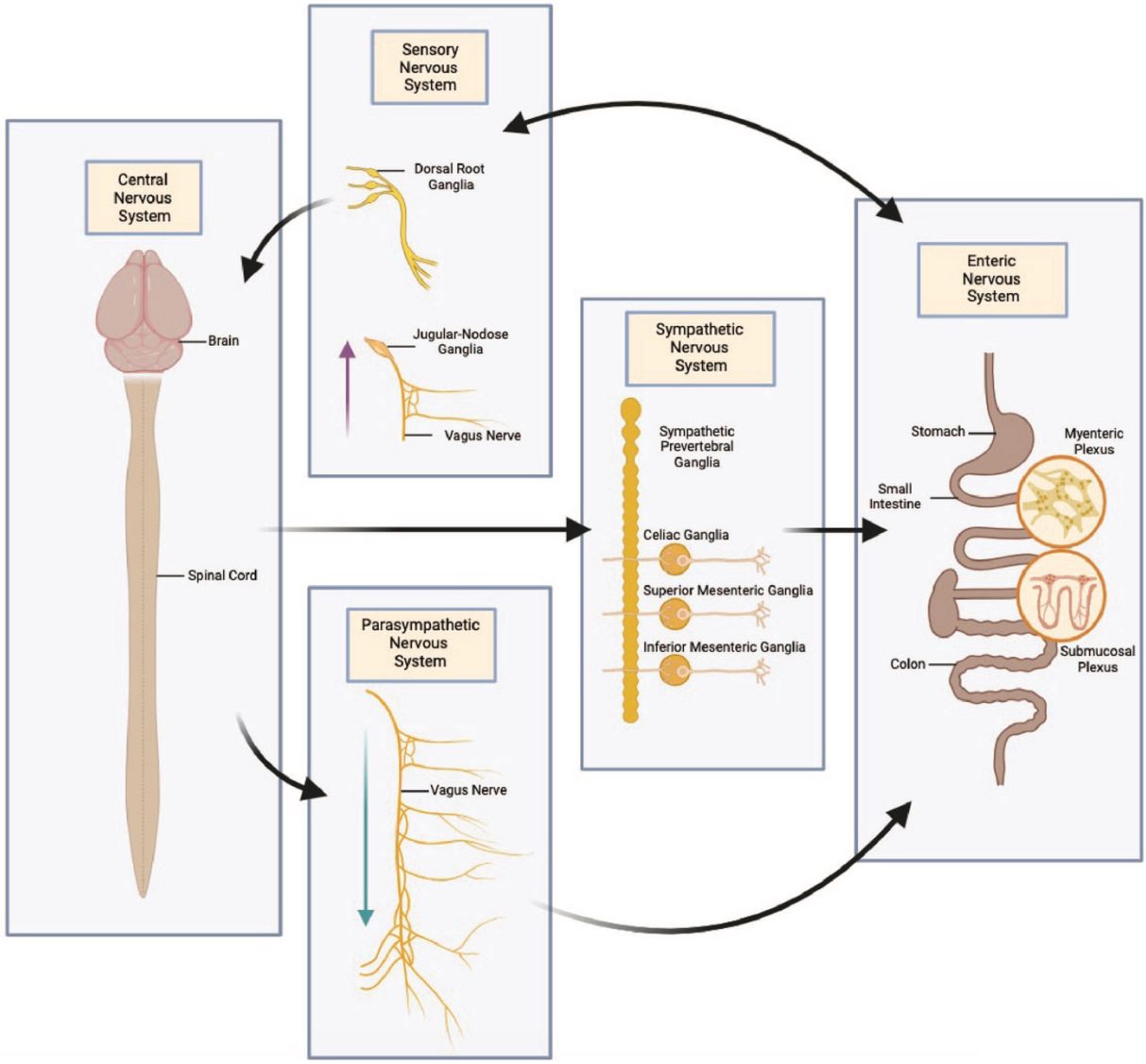
Sensory Nervous System
Dorsal Root Ganglia
Jugular-Nodose Ganglia
Vagus Nerve
Central Nervous System
Brain
Spinal Cord
Sympathetic Nervous System
Sympathetic Prevertebral Ganglia
Celiac Ganglia
Superior Mesenteric Ganglia
Inferior Mesenteric Ganglia
Enteric Nervous System
Stomach
Myenteric Plexus
Small Intestine
Colon
Submucosal Plexus
Parasympathetic Nervous System
Vagus Nerve

**Figure S1. Extrinsic and Intrinsic Innervation of the GI Tract**

Neurons of the sympathetic, parasympathetic, and sensory nervous systems extrinsically innervate the gut and have effects on GI function. In the sensory nervous system, sensory information from the gut is transmitted to the dorsal root ganglia (DRGs) and then to the spinal cord. Additionally, projections from the DRGs transmit sensory information to the gut. Other sensory signals arise from the periphery and are transmitted through the vagus nerve into the jugular-nodose ganglia and then into the brain. In the sympathetic nervous system, neurons from the spinal cord synapse onto neurons in the sympathetic prevertebral ganglia, celiac ganglia, superior mesenteric ganglia, and inferior mesenteric ganglia. These neurons then project to the gut. In the parasympathetic nervous system, the vagus nerve transmits signals from the brain to the gut. The intrinsic neurons of the gut, i.e., the enteric nervous system (ENS), reside in the myenteric and submucosal plexuses along the gut. Figure created with BioRender.com.

**Figure S2**

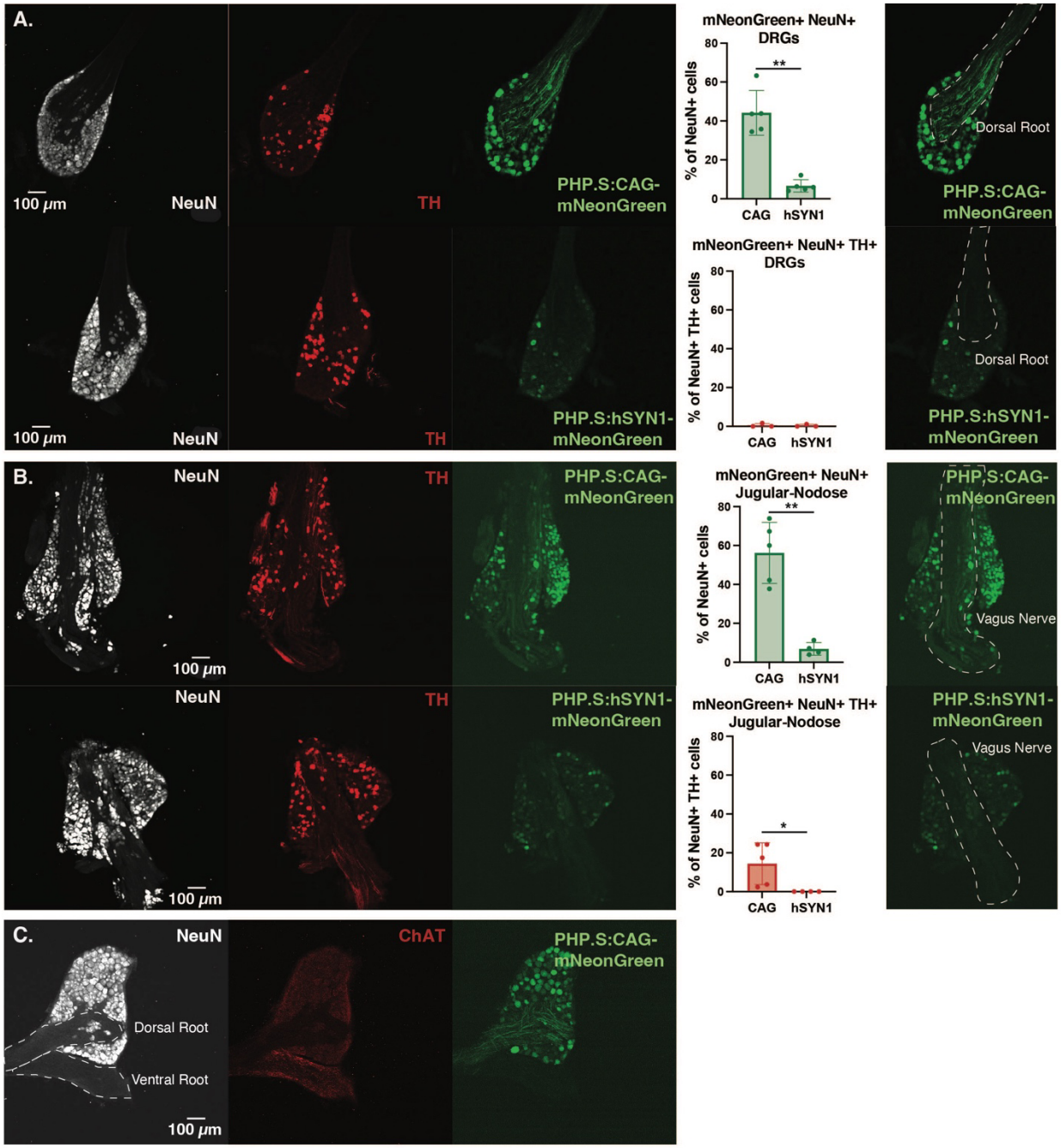
A.
NeuN
TH
PHP.S:CAG-mNeonGreen
100 μm
NeuN
TH
PHP.S:hSYN1-mNeonGreen
100 μm
mNeonGreen+ NeuN+ DRGs
% of NeuN+ cells
CAG
hSYN1
mNeonGreen+ NeuN+ TH+ DRGs
% of NeuN+ TH+ cells
Dorsal Root
PHP.S:CAG-mNeonGreen
Dorsal Root
PHP.S:hSYN1-mNeonGreen
B.
NeuN
TH
PHP.S:CAG-mNeonGreen
100 μm
NeuN
TH
PHP.S:hSYN1-mNeonGreen
100 μm
mNeonGreen+ NeuN+ Jugular-Nodose
% of NeuN+ cells
mNeonGreen+ NeuN+ TH+ Jugular-Nodose
% of NeuN+ TH+ cells
PHP.S:CAG-mNeonGreen
Vagus Nerve
PHP.S:hSYN1-mNeonGreen
Vagus Nerve
C.
NeuN
ChAT
PHP.S:CAG-mNeonGreen
Dorsal Root
Ventral Root
100 μm

**Figure S2. Viral Transduction of the Peripheral Nervous System (PNS)**

(A) Representative images showing labelling of the dorsal root ganglia (DRGs) by a single injection ($10^{12}$ vg) of either PHP.S-CAG-mNeonGreen or PHP.S-hSYN1-mNeonGreen. Cryosections were immunostained for the neuronal marker NeuN and tyrosine hydroxylase (TH). Plots show quantification of NeuN+ cells and NeuN+ TH+ cells virally labelled by AAV-PHP.S-CAG vs. AAV-PHP.S-hSyn1 in DRGs. (N=3-5 mice, each data point represents a 40 μM medial cross-section of the DRG, **p<0.01, determined by Welch's two-tailed t-test).

(B) Representative images showing labelling of the jugular-nodose ganglia by a single injection ($10^{12}$ vg) of either PHP.S-CAG-mNeonGreen or PHP.S-hSYN1-mNeonGreen. Cryosections were immunostained for the neuronal marker NeuN and TH. Plots show quantification of NeuN+ cells and NeuN+ TH+ cells virally labelled by AAV-PHP.S-CAG vs. AAV-PHP.S-hSyn1 in the jugular-nodose ganglia (N=4-5 mice, each data point represents a 40 μM medial cross-section of the jugular-nodose ganglia, **p<0.01, determined by Welch's two-tailed t-test).

(C) Representative images showing labelling of the dorsal root ganglia (DRGs), dorsal, and ventral root by a single injection ($10^{12}$ vg) of PHP.S-CAG-mNeonGreen. Cryosections were immunostained for the neuronal marker NeuN and ChAT. ChAT staining shows expected ChAT+ projections in the ventral root, but not the dorsal root or intrinsic neurons of the DRGs.

**Figure S3**

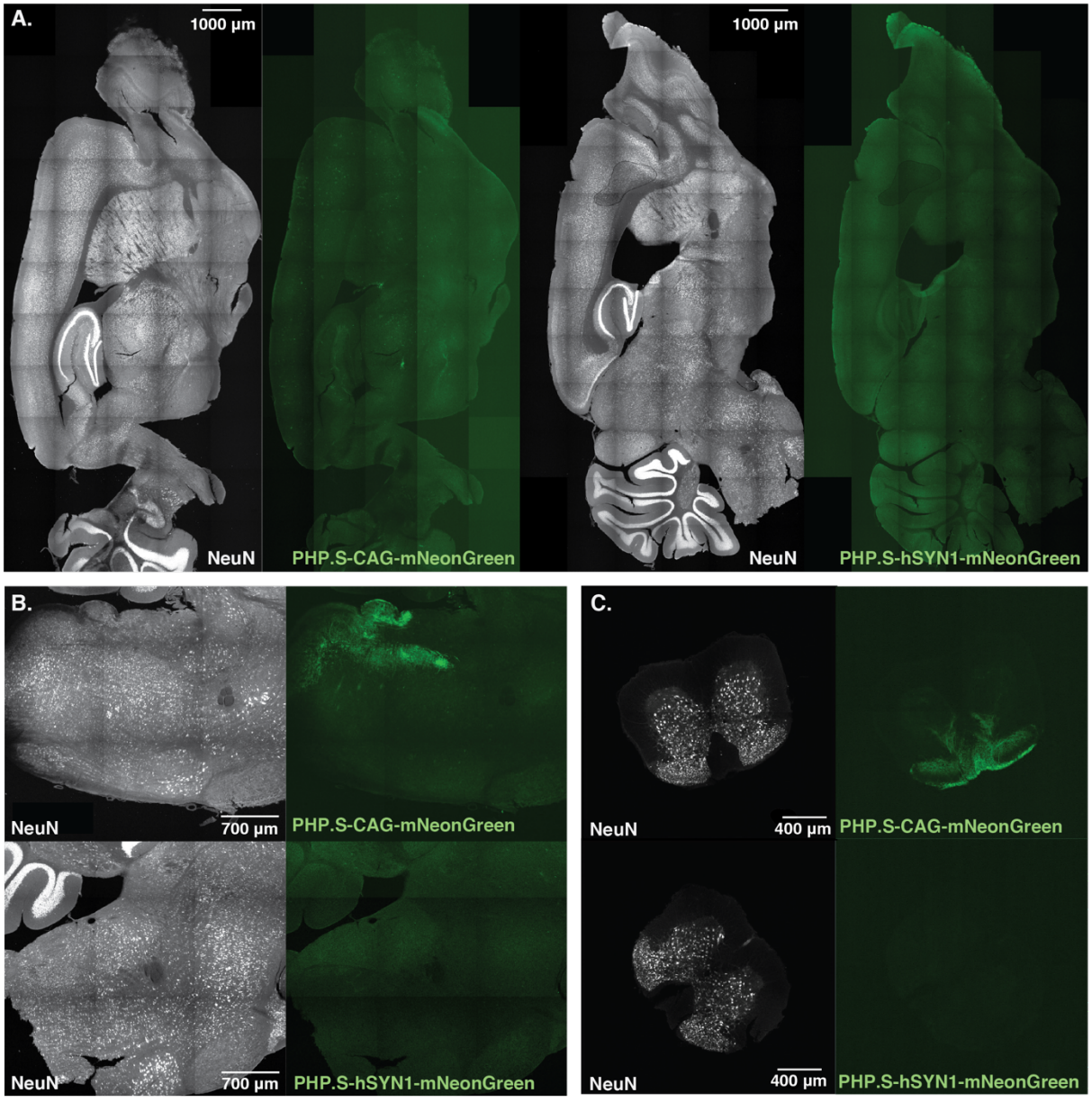
A.
1000 µm
NeuN
PHP.S-CAG-mNeonGreen
1000 µm
NeuN
PHP.S-hSYN1-mNeonGreen
B.
NeuN
700 µm
PHP.S-CAG-mNeonGreen
NeuN
700 µm
PHP.S-hSYN1-mNeonGreen
C.
NeuN
400 µm
PHP.S-CAG-mNeonGreen
NeuN
400 µm
PHP.S-hSYN1-mNeonGreen

**Figure S3. Viral Transduction of the CNS by AAV-PHP.S**

(A) Representative images showing labelling of the brain by a single injection ($10^{12}$ vg) of either AAV-PHP.S-CAG-mNeonGreen or AAV-PHP.S-hSYN1-mNeonGreen. Sections were immunostained for the neuronal marker NeuN.

(B, C) The PHP.S-hSYN1 injected mice did not show detectable mNeonGreen+ projections in the (B) brainstem or (C) spinal cord as were seen in the PHP.S-CAG injected mice.

**Figure S4**

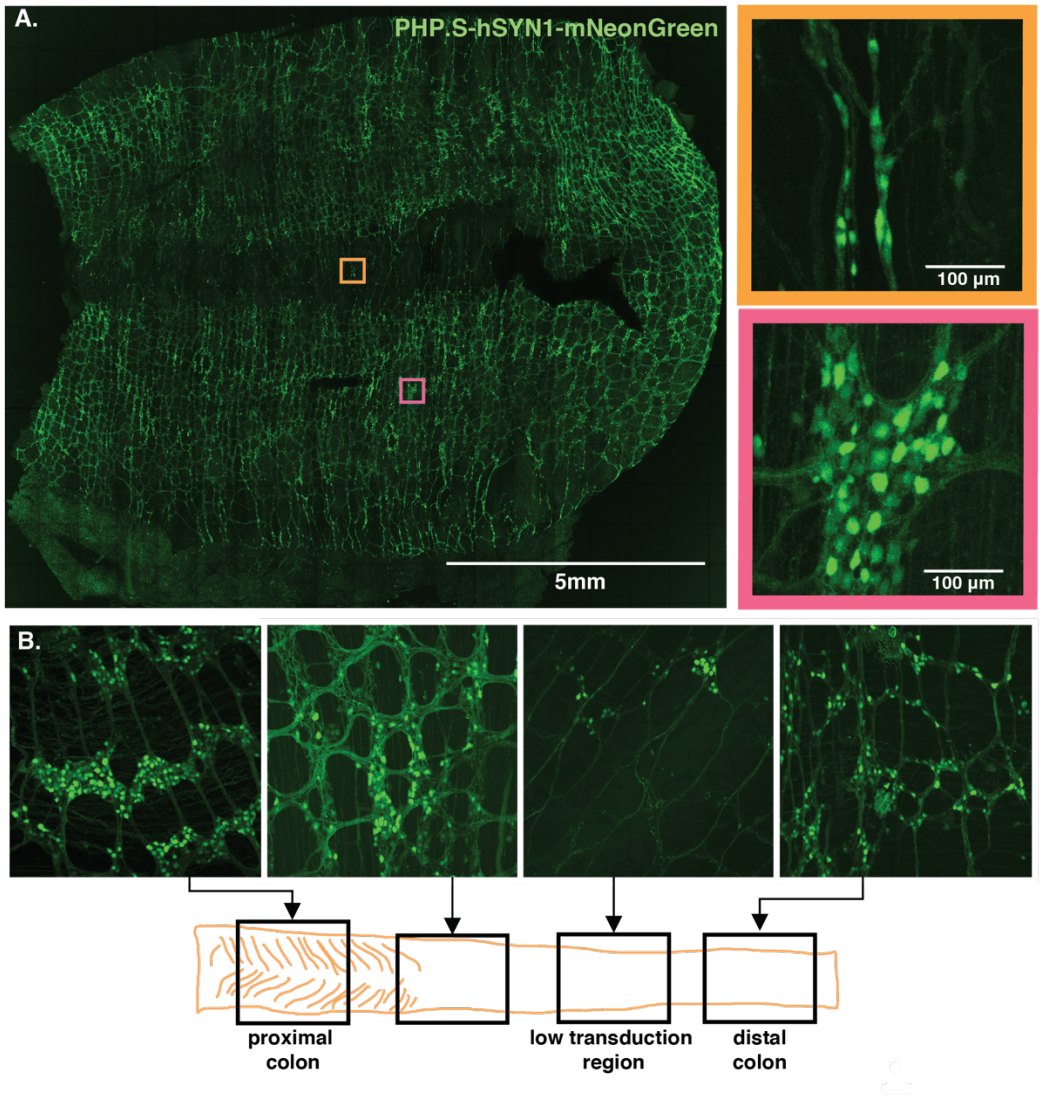
A.
PHP.S-hSYN1-mNeonGreen
5mm
100 µm
100 µm
B.
proximal colon
low transduction region
distal colon

**Figure S4. Viral Transduction by AAV-PHP.S in the Colon**

(A) Tiled, whole mount microscopy showing widespread labelling in the proximal colon (>1 cm of tissue) from a single injection of AAV-PHP.S-hSYN1-mNeonGreen ($10^{12}$ vg). Orange inset highlights a region opposite the mesenteric attachment, and pink inset highlights a central region of the tissue.

(B) Representative images showing labelling patterns along the colon, including a 1.5 cm region that AAV-PHP.S does not transduce well.

**Figure S5**

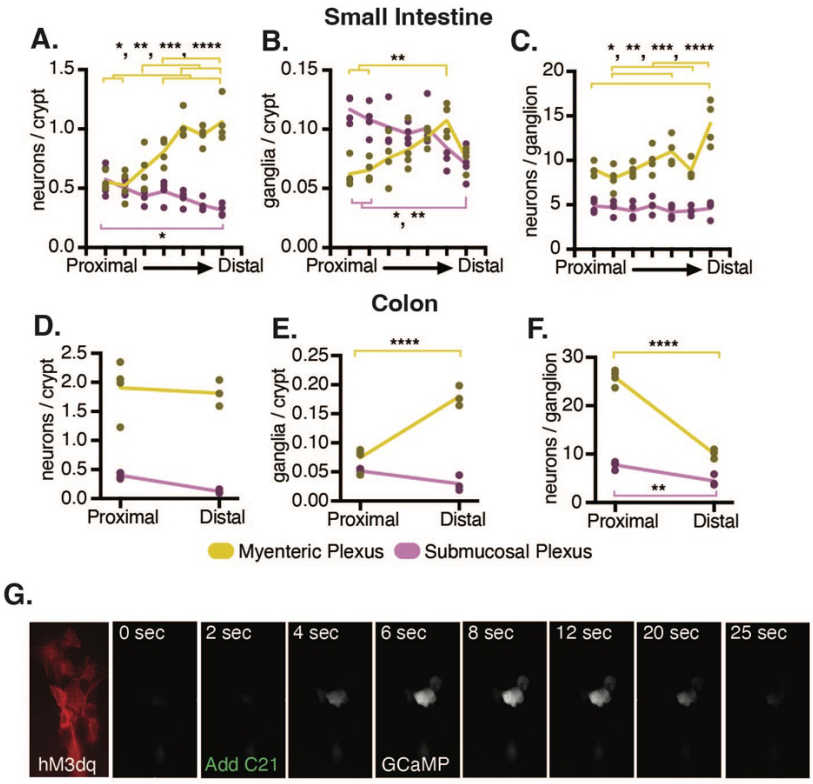
Small Intestine
A.
B.
C.
neurons / crypt
ganglia / crypt
neurons / ganglion
Proximal
Distal
Colon
D.
E.
F.
Myenteric Plexus
Submucosal Plexus
G.
0 sec
2 sec
4 sec
6 sec
8 sec
12 sec
20 sec
25 sec
hM3dq
Add C21
GCaMP

**Figure S5. ENS Architecture and ChAT$^+$ Neuronal Stimulation in the ENS**

(A-C) Quantification of neurons in 7 regions from the SI

(D-F) Quantification of neurons in 2 regions from the colon

(In A-F: N=3-4 mice per group, per intestinal region. Data points are averages from 2-3 images per mouse, per region; *: $p<0.05$, **: $p<0.01$, ***: $p<0.001$, ****: $p<0.0001$, determined by 2-way ANOVA with Sidak's multiple comparisons test).

(G) Fluorescence time course of GCaMP6f following C21 administration in an *ex vivo* preparation of ChAT$^+$ SI infected with hSYN1-DiO-hM3Dq-mRuby2 and CAG-GCaMP6f.

**Figure 2**

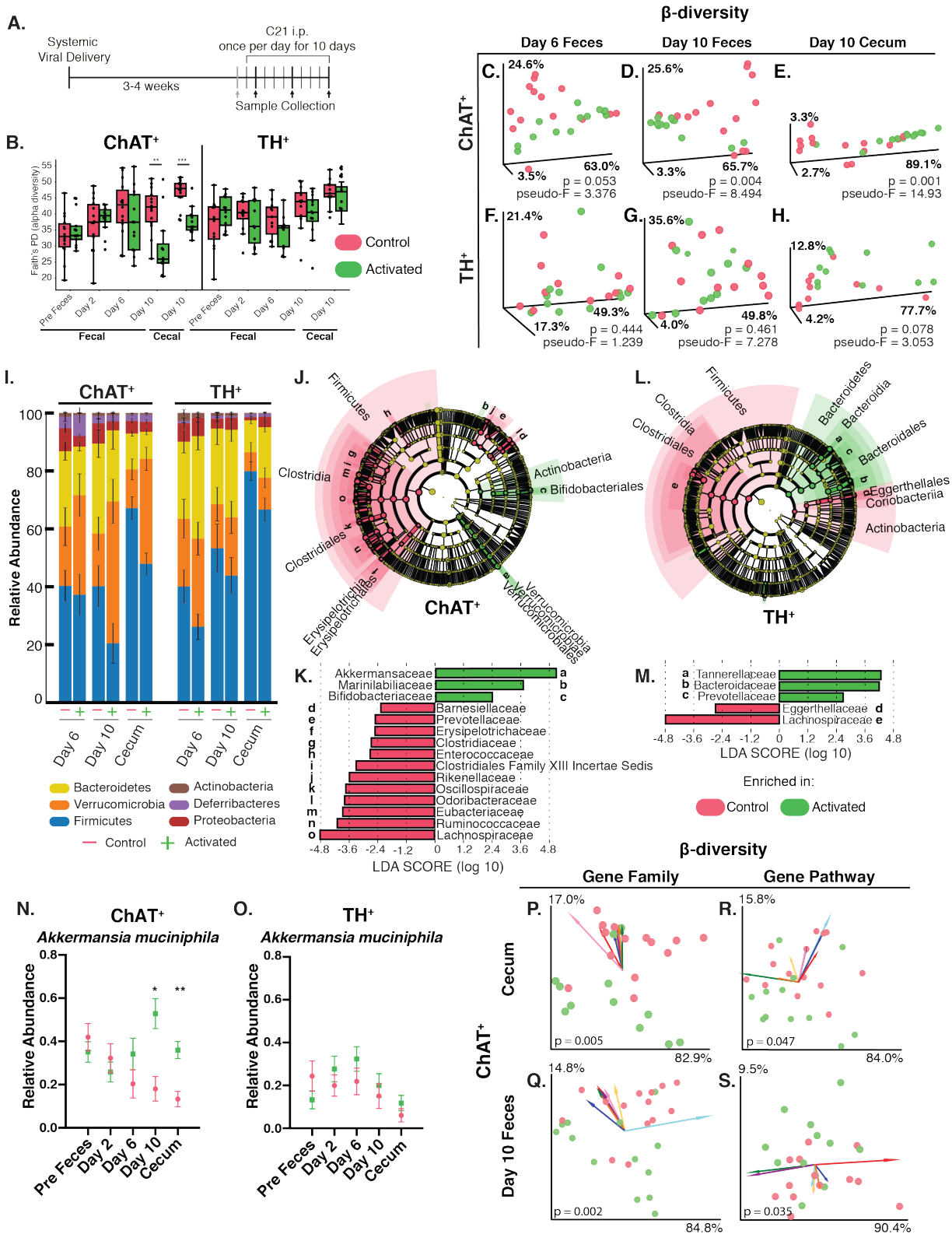
A.
Systemic Viral Delivery
C21 i.p. once per day for 10 days
3-4 weeks
Sample Collection
B.
ChAT+
TH+
Faith's PD (alpha diversity)
Pre Feces
Day 2
Day 6
Day 10
Day 10
Fecal
Cecal
Control
Activated
β-diversity
Day 6 Feces
Day 10 Feces
Day 10 Cecum
C.
D.
E.
F.
G.
H.
ChAT+
TH+
24.6%
3.5%
63.0%
p = 0.053
pseudo-F = 3.376
25.6%
3.3%
65.7%
p = 0.004
pseudo-F = 8.494
3.3%
2.7%
89.1%
p = 0.001
pseudo-F = 14.93
21.4%
17.3%
49.3%
p = 0.444
pseudo-F = 1.239
35.6%
4.0%
49.8%
p = 0.461
pseudo-F = 7.278
12.8%
4.2%
77.7%
p = 0.078
pseudo-F = 3.053
I.
ChAT+
TH+
Relative Abundance
Day 6
Day 10
Cecum
Bacteroidetes
Actinobacteria
Verrucomicrobia
Deferribacteres
Firmicutes
Proteobacteria
Control
Activated
J.
Firmicutes
Clostridia
Clostridiales
Actinobacteria
Bifidobacteriales
Erysipelotrichia
Erysipelotrichales
Verrucomicrobia
Verrucomicrobiales
ChAT+
L.
Firmicutes
Clostridia
Clostridiales
Bacteroidetes
Bacteroidia
Bacteroidales
Eggerthellales
Coriobacteriia
Actinobacteria
TH+
K.
Akkermansiaceae
Marinilabiliaceae
Bifidobacteriaceae
Barnesiellaceae
Prevotellaceae
Erysipelotrichaceae
Clostridiaceae
Enterococcaceae
Clostridiales Family XIII Incertae Sedis
Rikenellaceae
Oscillospiraceae
Odoribacteraceae
Eubacteriaceae
Ruminococcaceae
Lachnospiraceae
LDA SCORE (log 10)
M.
Tannerellaceae
Bacteroidaceae
Prevotellaceae
Eggerthellaceae
Lachnospiraceae
LDA SCORE (log 10)
Enriched in:
Control
Activated
N.
ChAT+
Akkermansia muciniphila
Relative Abundance
Pre Feces
Day 2
Day 6
Day 10
Cecum
O.
TH+
Akkermansia muciniphila
β-diversity
Gene Family
Gene Pathway
P.
R.
Q.
S.
Cecum
Day 10 Feces
ChAT+
17.0%
p = 0.005
82.9%
15.8%
p = 0.047
84.0%
14.8%
p = 0.002
84.8%
9.5%
p = 0.035
90.4%

**Figure 2. Gut-Associated ChAT$^+$ and TH$^+$ Neuronal Activation Alters the Gut Microbiome**

(A) Experimental paradigm: Cre-dependent hM3Dq was virally administered to either ChAT-Cre or TH-Cre mice. After 3-4 weeks of expression, C21 was injected daily for 10 days to induce specific neuronal activation. Feces were sampled the day prior to the first C21 injection and on days 2, 6, and 10 of C21 administration, and tissue and cecal contents were collected one hour after the last injection.

(B) Faith's phylogenetic diversity of feces and cecal contents over 10 days of neuronal activation in ChAT$^+$ and TH$^+$ mice. Feces were collected pre-experiment (1 day before first injection) and on day 2, 6, and 10. Cecal contents were collected at experimental endpoint on day 10.

(**$p<0.01$, ***$p<0.001$ determined by Kruskal-Wallis one-way ANOVA) .

(C-H) Weighted UniFrac principle coordinate analysis (PCoA) of Activated vs. Control in ChAT$^+$ and TH$^+$ mice. Statistics performed in QIIME2 as in (Bolyen et al., 2019).

(I) Stacked bar graph showing phylum-level changes in relative abundance on day 6 and day 10 of injection for feces and day 10 for cecal contents.

(J-M) Linear discriminant analysis (LDA) Effect Size (LEfSe) of the cecal microbiome. Cladograms showing differential phylogenetic clusters and family-level differences in activated and control (J,K) ChAT$^+$ and (L,M) TH$^+$ mice

(Cutoff: $\log_{10}$(LDA Score) > 2 or < -2).

(N-O) Changes in relative abundance of *Akkermansia muciniphila* in feces and cecal contents of (N) ChAT$^+$ and (O) TH$^+$ mice. (n=11-14 mice per group, per time point;

red=Control, green=hM3Dq-Activated, *p<0.05, **p<0.01, determined by multiple t-tests with Holm-Sidak correction for multiple comparisons).

(P-S) Beta-diversity of bacterial gene families and pathways in the (P,R) cecum and (Q,S) post-9 feces of control and activated mice. The direction and length of arrows indicate their influence in separating control and activated groups. Colors represent gene families and pathways (annotated in Figure S7).

See also Figures S6 and S7.

**Source Data Figure 2**

https://github.com/mazmanianlab/Griffiths_Yoo_et_al/tree/main/metagenomics

**Figure S6**

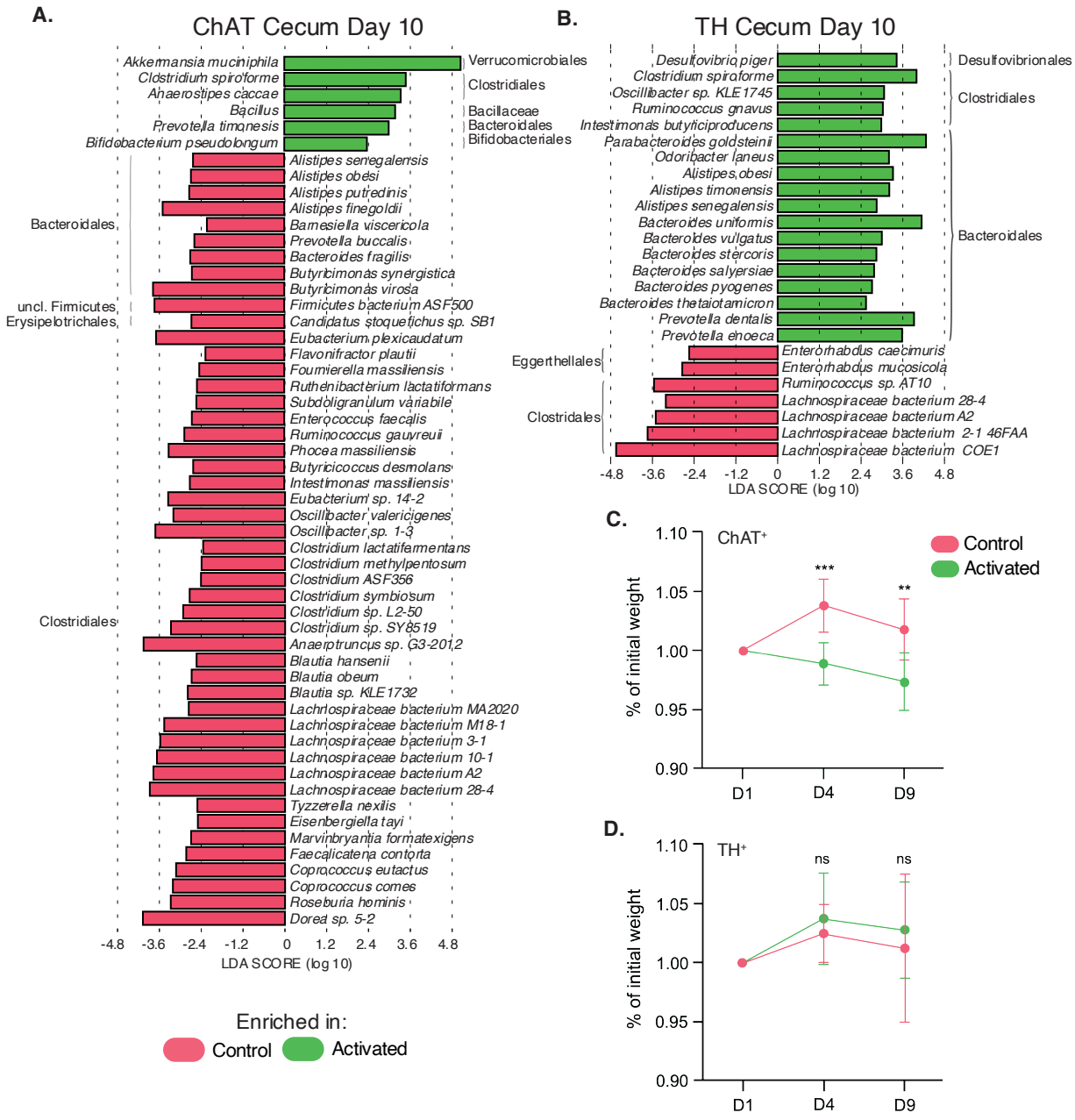
A.
ChAT Cecum Day 10
Akkermansia muciniphila
Clostridium spiroforme
Anaerostipes caccae
Bacillus
Prevotella timonesis
Bifidobacterium pseudolongum
Alistipes senegalensis
Alistipes obesi
Alistipes putredinis
Alistipes finegoldii
Barnesiella viscericola
Prevotella buccalis
Bacteroides fragilis
Butyricimonas synergistica
Butyricimonas virosa
Firmicutes bacterium ASF500
Candidatus stoquefichus sp. SB1
Eubacterium plexicaudatum
Flavonifractor plautii
Fournierella massiliensis
Ruthenibacterium lactatiformans
Subdoligranulum variabile
Enterococcus faecalis
Ruminococcus gauvreuii
Phocea massiliensis
Butyricicoccus desmolans
Intestimonas massiliensis
Eubacterium sp. 14-2
Oscillibacter valericigenes
Oscillibacter sp. 1-3
Clostridium lactatifermentans
Clostridium methylpentosum
Clostridium ASF356
Clostridium symbiosum
Clostridium sp. L2-50
Clostridium sp. SY8519
Anaeroptruncus sp. G3-201,2
Blautia hansenii
Blautia obeum
Blautia sp. KLE1732
Lachnospiraceae bacterium MA2020
Lachnospiraceae bacterium M18-1
Lachnospiraceae bacterium 3-1
Lachnospiraceae bacterium 10-1
Lachnospiraceae bacterium A2
Lachnospiraceae bacterium 28-4
Tyzzerella nexilis
Eisenbergiella tayi
Marvinbryantia formatexigens
Faecalicatena contorta
Coprococcus eutactus
Coprococcus comes
Roseburia hominis
Dorea sp. 5-2
Verrucomicrobiales
Clostridiales
Bacillaceae
Bacteroidales
Bifidobacteriales
Bacteroidales,
uncl. Firmicutes,
Erysipelotrichales,
Clostridiales
-4.8 -3.6 -2.4 -1.2 0 1.2 2.4 3.6 4.8
LDA SCORE (log 10)
Enriched in:
Control
Activated
B.
TH Cecum Day 10
Desulfovibrio piger
Clostridium spiroforme
Oscillibacter sp. KLE1745
Ruminococcus gnavus
Intestimonas butyriciproducens
Parabacteroides goldsteinii
Odoribacter laneus
Alistipes obesi
Alistipes timonensis
Alistipes senegalensis
Bacteroides uniformis
Bacteroides vulgatus
Bacteroides stercoris
Bacteroides salyersiae
Bacteroides pyogenes
Bacteroides thetaiotamicron
Prevotella dentalis
Prevotella enoeca
Enterorhabdus caecimuris
Enterorhabdus mucosicola
Ruminococcus sp. AT10
Lachnospiraceae bacterium 28-4
Lachnospiraceae bacterium A2
Lachnospiraceae bacterium 2-1 46FAA
Lachnospiraceae bacterium COE1
Desulfovibrionales
Clostridiales
Bacteroidales
Eggerthellales
Clostridiales
-4.8 -3.6 -2.4 -1.2 0 1.2 2.4 3.6 4.8
LDA SCORE (log 10)
C.
ChAT+
Control
Activated
***
**
% of initial weight
1.10
1.05
1.00
0.95
0.90
D1 D4 D9
D.
TH+
ns
ns
% of initial weight
1.10
1.05
1.00
0.95
0.90
D1 D4 D9

**Figure S6. Annotated changes in gut bacteria (Related to Figure 2 and Figure 6)**

(A,B) Species-levels differences in cecal bacteria after 10 days of C21 injection in (A) $ChAT^+$ and (B) $TH^+$ mice.

(C,D) Analysis of activation-mediated changes in body weight of (C) $ChAT^+$ and (D) $TH^+$ mice over 9 days of C21 administration.

(N = 10-11 mice per group; **: $p<0.01$, ***: $p<0.001$, determined by 2-way ANOVA with Sidak's method for multiple comparisons).

## Figure S7

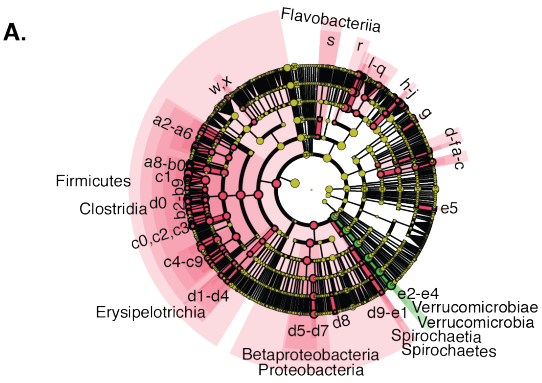


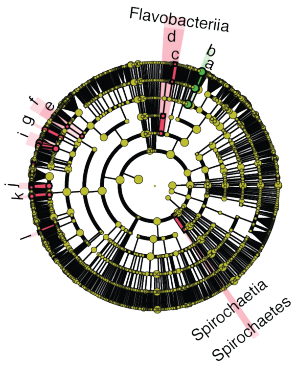


**ChAT-Cre Day 10 Feces**

| ID | Microbial Taxon | ID | Microbial Taxon | ID | Microbial Taxon | ID | Microbial Taxon |
|---|---|---|---|---|---|---|---|
| a | Bifidobacterium | p | Parabacteroides | b4 | Dorea | d0 | Clostridiales |
| b | Bifidobacteriaceae | q | Tannerellaceae | b5 | Eisenbergiella | d1 | Candidatus Stoquefichus |
| c | Bifidobacteriales | r | Marinilbiliales | b6 | Faecalicatena | d2 | Faecalitalea |
| d | Cellulomonas | s | Flavobacteriales | b7 | Lachnoclostridium | d3 | Erysipelotrichaeceae |
| e | Cellulomondaceae | w | Enterococcus | b8 | Marvinbryantia | d4 | Erysipelotrichales |
| f | Micrococcales | x | Enterococcaceae | b9 | Sellimonas | d5 | Parasutterella |
| g | Adlercreutzia | a2 | Intestinimonas | c0 | Tyzzerella | d6 | Sutterellaceae |
| h | Barnsiella | a3 | Pseudoflavonifractor | c1 | Lachnospiraceae | d7 | Burkholderiales |
| i | Coprobacter | a5 | Clostridium | c2 | Oscillibacter | d8 | Lawsonia |
| j | Barnesiellaceae | a6 | Clostridiaceae | c3 | Oscillospiraceae | d9 | Treponema |
| k | Prevotella | a8 | Anaerofustis | c5 | Anaerotruncus | e0 | Spirochaetaceae |
| l | Prevotellaceae | a9 | Eubacterium | c6 | Ruminiclostridium | e1 | Spirochaetales |
| m | Alistipes | b0 | Eubacteriaceae | c7 | Ruminococcus | e2 | Akkermansia |
| n | Rikenella | b2 | Blautia | c8 | Ruthenibacterium | e3 | Akkermansiaceae |
| o | Rikenellaceae | b3 | Coprococcus | c9 | Ruminococcaceae | e4 | Verrucomicrobiales |
| | | | | | | e5 | Varicellovirus |

**TH-Cre Day 6 Feces**

| ID | Microbial Taxon |
|---|---|
| a | Parabacteroides |
| b | Tannerellaceae |
| c | Fluviicola |
| d | Flavobacteriales |
| e | Streptococcus |
| f | Streptococcaceae |
| g | Pseudoflavonifractor |
| i | Clostridium |
| j | Blautia |
| k | Eisenbergiella |
| l | Clostridiodes |

Enriched in:
Control
Activated

**C.**

| ChAT-Cre Cecum | | |
|---|---|---|
| ID | Gene Family | Annotation |
| 1 | K02003 | putative ABC transport system ATP-binding protein |
| 2 | K02518 | translation initiation factor IF-1 |
| 3 | K02948 | small subunit ribosomal protein S11 |
| 4 | K02950 | small subunit ribosomal protein S12 |
| 5 | K02965 | small subunit ribosomal protein S19 |
| 6 | K03205 | type IV secretion system protein VirD4 |
| 7 | K03294 | basic amino acid/polyamine antiporter, APA family |
| 8 | K03496 | chromosome partitioning protein |
| **ID** | **Gene Pathway** | **Annotation** |
| 1 | HISDEG-PWY | L-histidine degradation I |
| 2 | ILEUSYN-PWY | L-isoleucine biosynthesis I (from threonine) |
| 3 | PWY-6122 | 5-aminoimidazole ribonucleotide biosynthesis II |
| 4 | PWY-6595 | superpathway of guanosine nucleotides degradation (plants) |
| 5 | PWY-6606 | guanosine nucleotides degradation II |
| 6 | PWY-7111 | pyruvate fermentation to isobutanol (engineered) |
| 7 | PWY-7219 | adenosine ribonucleotides de novo biosynthesis |
| 8 | VALSYN-PWY | L-valine biosynthesis |

**D.**

| ChAT-Cre Day 10 Feces | | |
|---|---|---|
| ID | Gene Family | Annotation |
| 1 | K02003 | putative ABC transport system ATP-binding protein |
| 2 | K02518 | translation initiation factor IF-1 |
| 3 | K02913 | large subunit ribosomal protein L33 |
| 4 | K02946 | small subunit ribosomal protein S10 |
| 5 | K02948 | small subunit ribosomal protein S11 |
| 6 | K02950 | small subunit ribosomal protein S12 |
| 7 | K02965 | small subunit ribosomal protein S19 |
| 8 | K03205 | type IV secretion system protein VirD4 |
| **ID** | **Gene Pathway** | **Annotation** |
| 1 | ILEUSYN-PWY | L-isoleucine biosynthesis I (from threonine) |
| 2 | PWY-6151 | S-adenosyl-L-methionine cycle I |
| 3 | PWY-6700 | queuosine biosynthesis I (de novo) |
| 4 | PWY-6859 | all-trans-farnesol biosynthesis |
| 5 | PWY-7111 | pyruvate fermentation to isobutanol |
| 6 | PWY-7219 | adenosine ribonucleotides de novo biosynthesis |
| 7 | PWY0-1296 | purine ribonucleosides degradation |
| 8 | VALSYN-PWY | L-valine biosynthesis |

**Figure S7. Gut-Associated Activation-Mediated Changes in the Fecal Microbiome (Related to Figure 2)**

(A) LEfSe cladograms and annotations for feces on Day 10 of C21 administration in $ChAT^+$ mice.

(B) LEfSe Cladograms and annotations for feces on Day 6 of C21 administration in $TH^+$ mice.

(C-D) Microbial gene family and pathway annotations for the feature arrows in Figures 2P-2S. Colors in the ID column refer to the colors of the arrows in the main figure.

## Figure 3

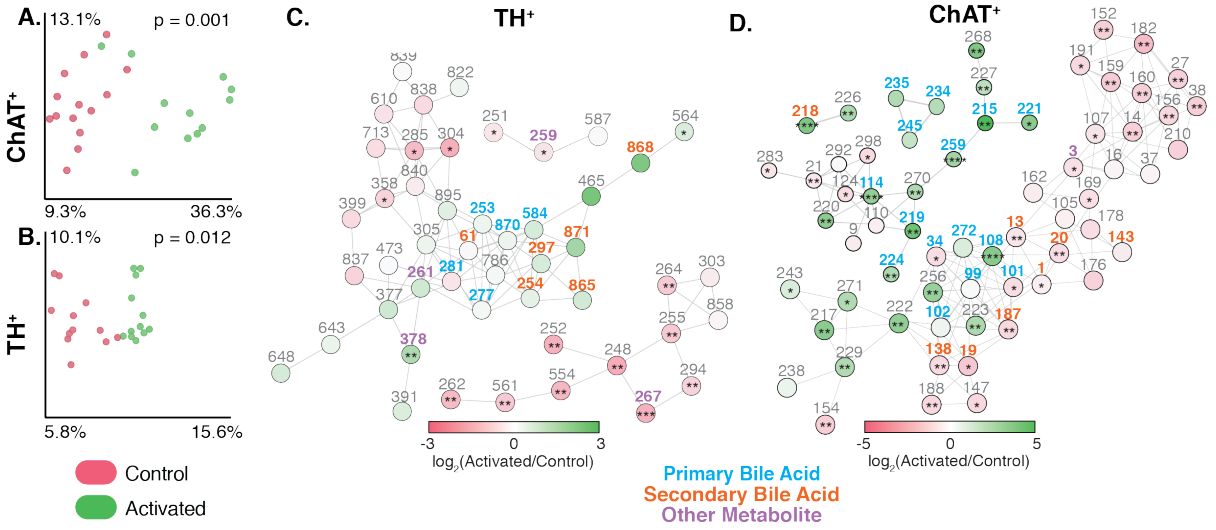


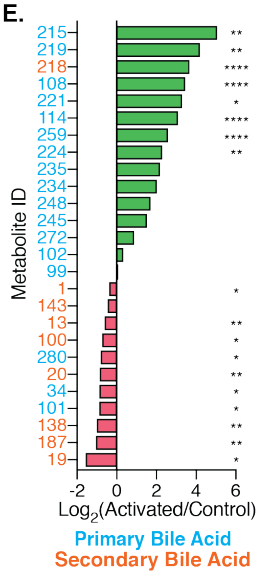


F.

**ChAT+ Cecum**

| Activated > Control | | | Activated < Control | | |
|---|---|---|---|---|---|
| ID | GNPS Annotation | Adduct | ID | GNPS Annotation | Adduct |
| 215 | Cholic acid | 2M+H | 19 | Spectral Match to 12-Ketodeoxycholic acid (NIST14) | M+H |
| 219 | Cholic acid | 2M+Na | 187 | hyocholic acid | M-2H2O+H |
| 218 | 7-Keto-3.alpha.,12-.alpha.-dihydroxycholanic acid | M+H-3H2O | 138 | Spectral Match to 12-Ketodeoxycholic acid (NIST14) | M+H |
| 108 | Cholic acid | M-3H2O+H | 101 | .beta.-Muricholic acid | M+H-3H2O |
| 221 | Cholic acid | 3M+H | 34 | 3.alpha.-Hydroxy-7-oxo-5.beta.-cholanic acid | M+H-H2O |
| 114 | Cholic acid | M+Na | 20 | .alpha.-Hyodeoxycholic acid methyl ester | M+H-CH6O2 |
| 259 | Cholic Acid | [M+NH4]+ | 280 | .gamma.-Muricholic acid/hyocholic acid | M+H-H2O |
| 224 | Cholic acid | 3M+Na | 100 | Spectral Match to Deoxycholic acid (NIST14) | 2M+H |
| 235 | taurohyocholic acid | M+H | 13 | Spectral Match to Ursodeoxycholic acid (NIST14) | M+H-H2O |
| 234 | Spectral Match to Taurocholic acid (NIST14) | M+H | 143 | .beta.-Hyodeoxycholic acid | M+H-H2O |
| 248 | Spectral Match to Taurocholic acid (NIST14) | M+Na | 1 | .beta.-Hyodeoxycholic acid | M+H-2H2O |
| 245 | taurohyocholic acid | M-2H2O+H | | | |
| 272 | Spectral Match to Cholic acid (NIST14) | M+H-2H2O | | | |
| 102 | .beta.-Muricholic acid | M+H-H2O | | | |
| 99 | hyocholic acid | M-2H2O+H | | | |

Primary Bile Acid
Secondary Bile Acid

**Figure 3. Gut-Associated ChAT$^+$ or TH$^+$ Neuronal Activation Alters Host and Microbe-Derived Luminal Metabolites**

(A-B) Canberra PCoA of the cell-free, luminal metabolome of cecal contents from control (red) and activated (green) ChAT$^+$ and TH$^+$ mice. Statistical analyses were performed in QIIME2 as in (Bolyen et al., 2019).

(C-D) Metabolic networks constructed from identified cecal metabolites in TH$^+$ and ChAT$^+$ mice. Each node is colored by its upregulation (green) or downregulation (red) in the activated group and is labelled with an ID number corresponding to annotation, mass-to-charge ratio, retention time, fold change, and significance value in Table S1.

(E) Fold changes of specific bile acids identified as upregulated (green bars) or downregulated (red bars) in activated ChAT$^+$ mice.

(F) Annotations of bile acids highlighted in (E). Metabolite IDs are colored according to annotation as primary (blue) or secondary (orange) bile acids. Metabolite IDs are specific to each sample (N=12-14 for each group analyzed, *: $p<0.05$, **: $p<0.01$, ***: $p<0.001$, ****: $p<0.0001$).

See also Table S1.

**Figure 4**

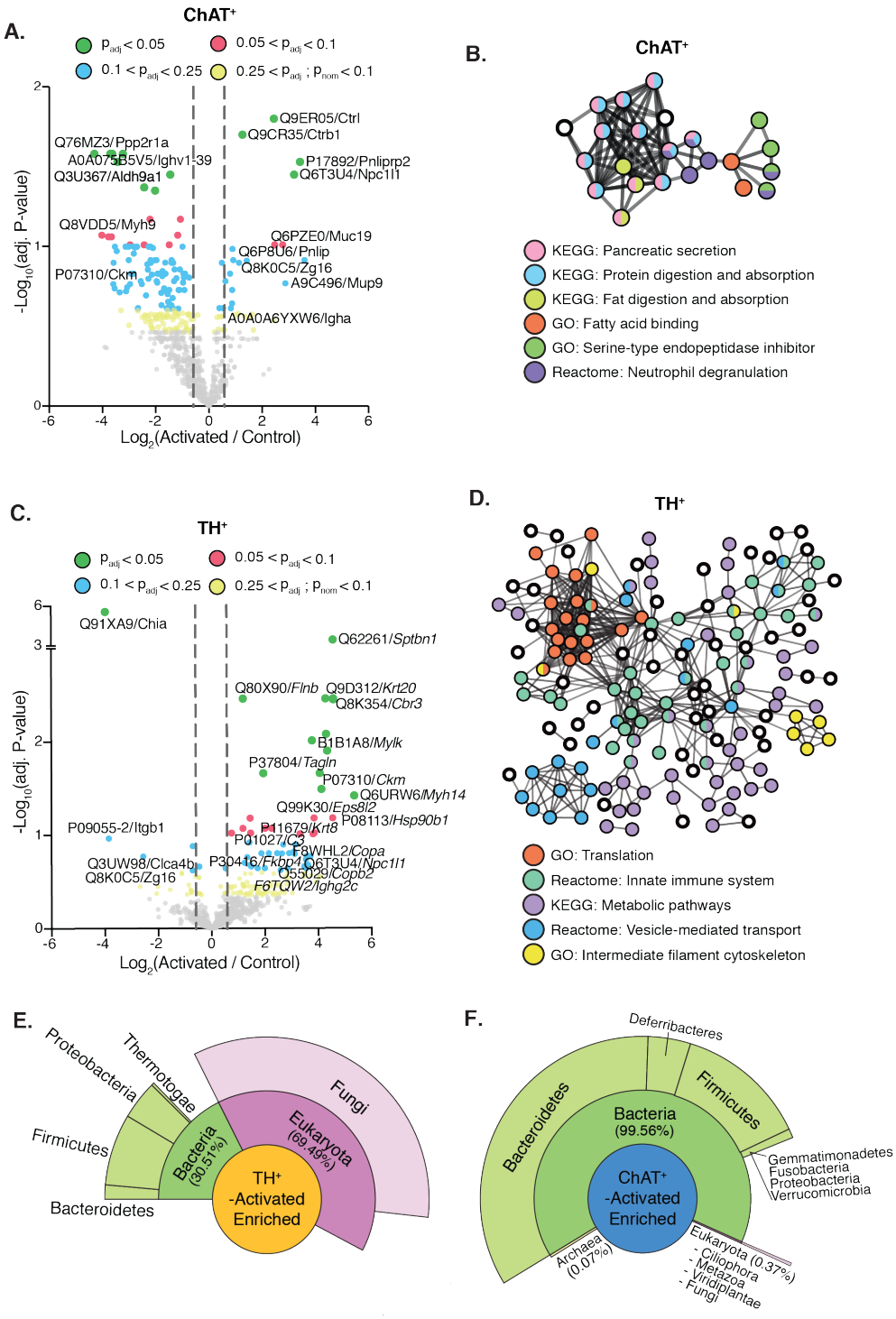
A.
ChAT+
$p_{adj} < 0.05$
$0.05 < p_{adj} < 0.1$
$0.1 < p_{adj} < 0.25$
$0.25 < p_{adj}$ ; $p_{nom} < 0.1$
Q9ER05/Ctrl
Q9CR35/Ctrb1
Q76MZ3/Ppp2r1a
A0A075B5V5/Ighv1-39
P17892/Pnliprp2
Q3U367/Aldh9a1
Q6T3U4/Npc1l1
Q8VDD5/Myh9
Q6PZE0/Muc19
Q6P8U6/Pnlip
P07310/Ckm
Q8K0C5/Zg16
A9C496/Mup9
A0A0A6YXW6/Igha
-Log10(adj. P-value)
Log2(Activated / Control)
B.
ChAT+
KEGG: Pancreatic secretion
KEGG: Protein digestion and absorption
KEGG: Fat digestion and absorption
GO: Fatty acid binding
GO: Serine-type endopeptidase inhibitor
Reactome: Neutrophil degranulation
C.
TH+
$p_{adj} < 0.05$
$0.05 < p_{adj} < 0.1$
$0.1 < p_{adj} < 0.25$
$0.25 < p_{adj}$ ; $p_{nom} < 0.1$
Q91XA9/Chia
Q62261/Sptbn1
Q80X90/Flnb
Q9D312/Krt20
Q8K354/Cbr3
B1B1A8/Mylk
P37804/Tagln
P07310/Ckm
Q6URW6/Myh14
Q99K30/Eps8l2
P08113/Hsp90b1
P09055-2/Itgb1
P11679/Krt8
P01027/C3
F8WHL2/Copa
Q3UW98/Clca4b
P30416/Fkbp4
Q6T3U4/Npc1l1
Q8K0C5/Zg16
Q55029/Copb2
F6TQW2/Ighg2c
-Log10(adj. P-value)
Log2(Activated / Control)
D.
TH+
GO: Translation
Reactome: Innate immune system
KEGG: Metabolic pathways
Reactome: Vesicle-mediated transport
GO: Intermediate filament cytoskeleton
E.
Proteobacteria
Thermotogae
Fungi
Firmicutes
Bacteria (30.51%)
Eukaryota (69.49%)
TH+ -Activated Enriched
Bacteroidetes
F.
Deferribacteres
Bacteroidetes
Firmicutes
Bacteria (99.56%)
ChAT+ -Activated Enriched
Gemmatimonadetes
Fusobacteria
Proteobacteria
Verrucomicrobia
Archaea (0.07%)
Eukaryota (0.37%)
- Ciliophora
- Metazoa
- Viridiplantae
- Fungi

**Figure 4. Gut-Associated ChAT$^+$ or TH$^+$ Neuronal Activation Alters Host and Microbe-Derived Luminal Proteins**

(A) Volcano plot of differentially-expressed host proteins identified in the cecal contents of ChAT$^+$-activated (N=8) vs. ChAT$^+$-control mice (N=9) mice, 1 hour after final C21 administration.

(B) STRING network analysis of host proteins that were more abundant in ChAT+-activated mice ($p_{nom.} < 0.2$).

(C) Proteomic volcano plot of TH$^+$-activated vs. TH$^+$-control mice (N=7 mice per group).

(D) STRING network analysis of upregulated host proteins in TH$^+$-activated mice ($p_{nom.} < 0.2$).

(E-F) Unipept metaproteomic analysis of upregulated microbial proteins (fold change > 2, $p_{nom.} < 0.2$) in TH$^+$-activated and ChAT$^+$-activated mice (N=7-9 mice per group).

Source Data Figure 4A

https://github.com/mazmanianlab/Griffiths_Yoo_et_al/blob/main/proteomics/CHAT_proteomics_volcano.txt

Source Data Figure 4C

https://github.com/mazmanianlab/Griffiths_Yoo_et_al/blob/main/proteomics/TH_proteomics_volcano.txt

Source Data Figures 4E and 4F

https://github.com/mazmanianlab/Griffiths_Yoo_et_al/blob/main/proteomics/metaproteomics/Microbiome_associated_proteins.xlsx

# Figure 5

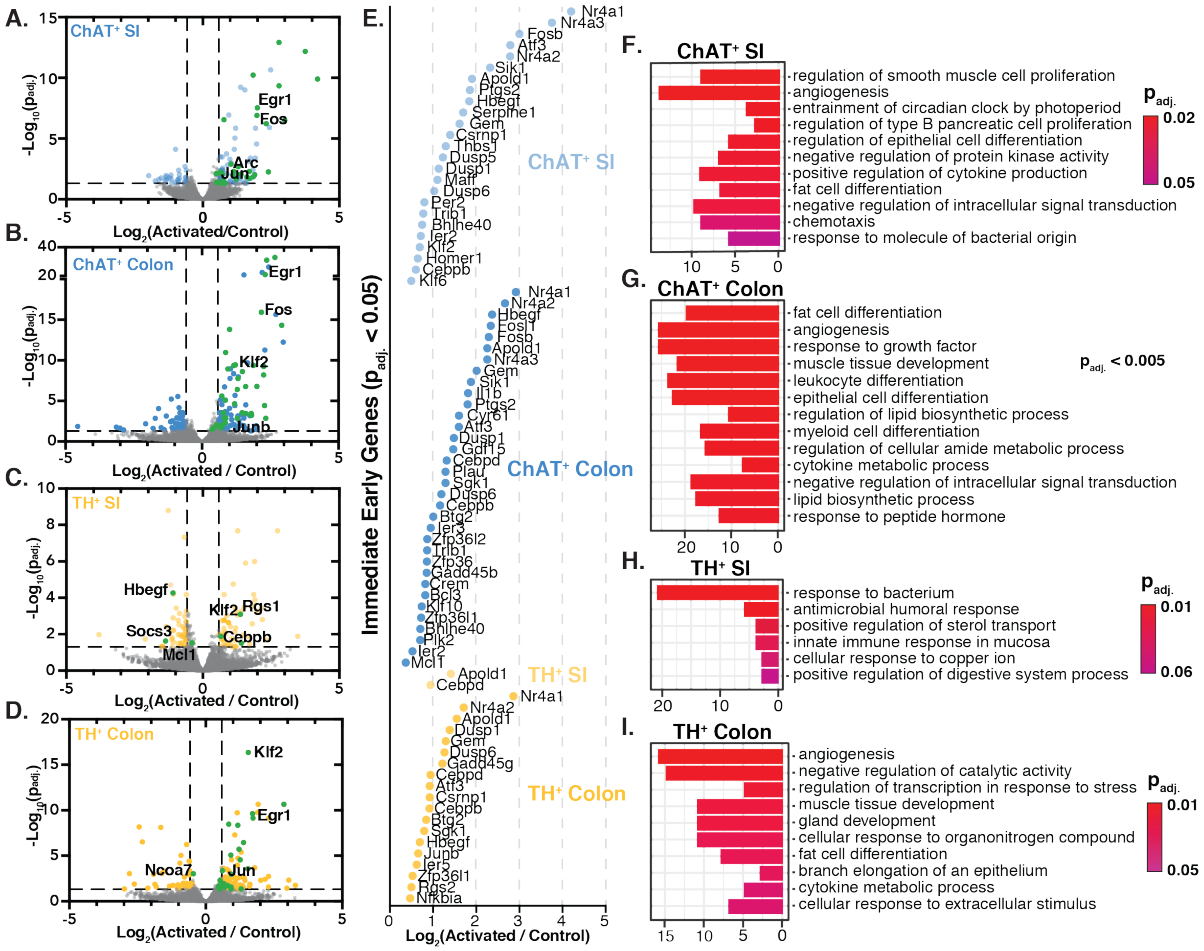
A.
ChAT⁺ SI
Egr1
Fos
Arc
Jun
-Log10(padj.)
Log2(Activated/Control)
B.
ChAT⁺ Colon
Egr1
Fos
Klf2
Junb
-Log10(padj.)
Log2(Activated / Control)
C.
TH⁺ SI
Hbegf
Klf2
Rgs1
Socs3
Cebpb
Mcl1
-Log10(padj.)
Log2(Activated / Control)
D.
TH⁺ Colon
Klf2
Egr1
Ncoa7
Jun
-Log10(padj.)
Log2(Activated / Control)
E.
Immediate Early Genes (padj. < 0.05)
ChAT⁺ SI
ChAT⁺ Colon
TH⁺ SI
TH⁺ Colon
Log2(Activated / Control)
F.
ChAT⁺ SI
regulation of smooth muscle cell proliferation
angiogenesis
entrainment of circadian clock by photoperiod
regulation of type B pancreatic cell proliferation
regulation of epithelial cell differentiation
negative regulation of protein kinase activity
positive regulation of cytokine production
fat cell differentiation
negative regulation of intracellular signal transduction
chemotaxis
response to molecule of bacterial origin
padj.
0.02
0.05
G.
ChAT⁺ Colon
fat cell differentiation
angiogenesis
response to growth factor
muscle tissue development
leukocyte differentiation
epithelial cell differentiation
regulation of lipid biosynthetic process
myeloid cell differentiation
regulation of cellular amide metabolic process
cytokine metabolic process
negative regulation of intracellular signal transduction
lipid biosynthetic process
response to peptide hormone
padj. < 0.005
H.
TH⁺ SI
response to bacterium
antimicrobial humoral response
positive regulation of sterol transport
innate immune response in mucosa
cellular response to copper ion
positive regulation of digestive system process
padj.
0.01
0.06
I.
TH⁺ Colon
angiogenesis
negative regulation of catalytic activity
regulation of transcription in response to stress
muscle tissue development
gland development
cellular response to organonitrogen compound
fat cell differentiation
branch elongation of an epithelium
cytokine metabolic process
cellular response to extracellular stimulus
padj.
0.01
0.05

**Figure 5. ChAT $^{+}$ and TH$^{+}$ Activation-Mediated Transcriptomic Changes**

(A-D) Differentially-expressed genes in DREADD-activated vs. control (A) ChAT $^{+}$ distal SI, (B) ChAT$^{+}$ proximal colon, (C) TH$^{+}$ distal SI, (D) TH$^{+}$ proximal colon. (Dashed vertical lines: Fold Change (FC) = +/- 1.5; dashed horizontal lines: $p_{adj.} < 0.05$. Transcripts of IEGs are highlighted in green and annotated. N=10 mice per group).

(E) Fold changes of upregulated IEGs ($p_{adj.} < 0.05$) as defined by Wu et al., 2017.

(F-I) Gene set enrichment analysis of gene ontology (GO) terms for (F) ChAT$^{+}$ distal SI, (G) ChAT$^{+}$ proximal colon, (H) TH$^{+}$ distal SI, (I) TH$^{+}$ proximal colon.

See also Table S2 and Table S3.

**Source Data Figure 5**

https://github.com/mazmanianlab/Griffiths_Yoo_et_al/tree/main/RNAseq

**Figure 6**

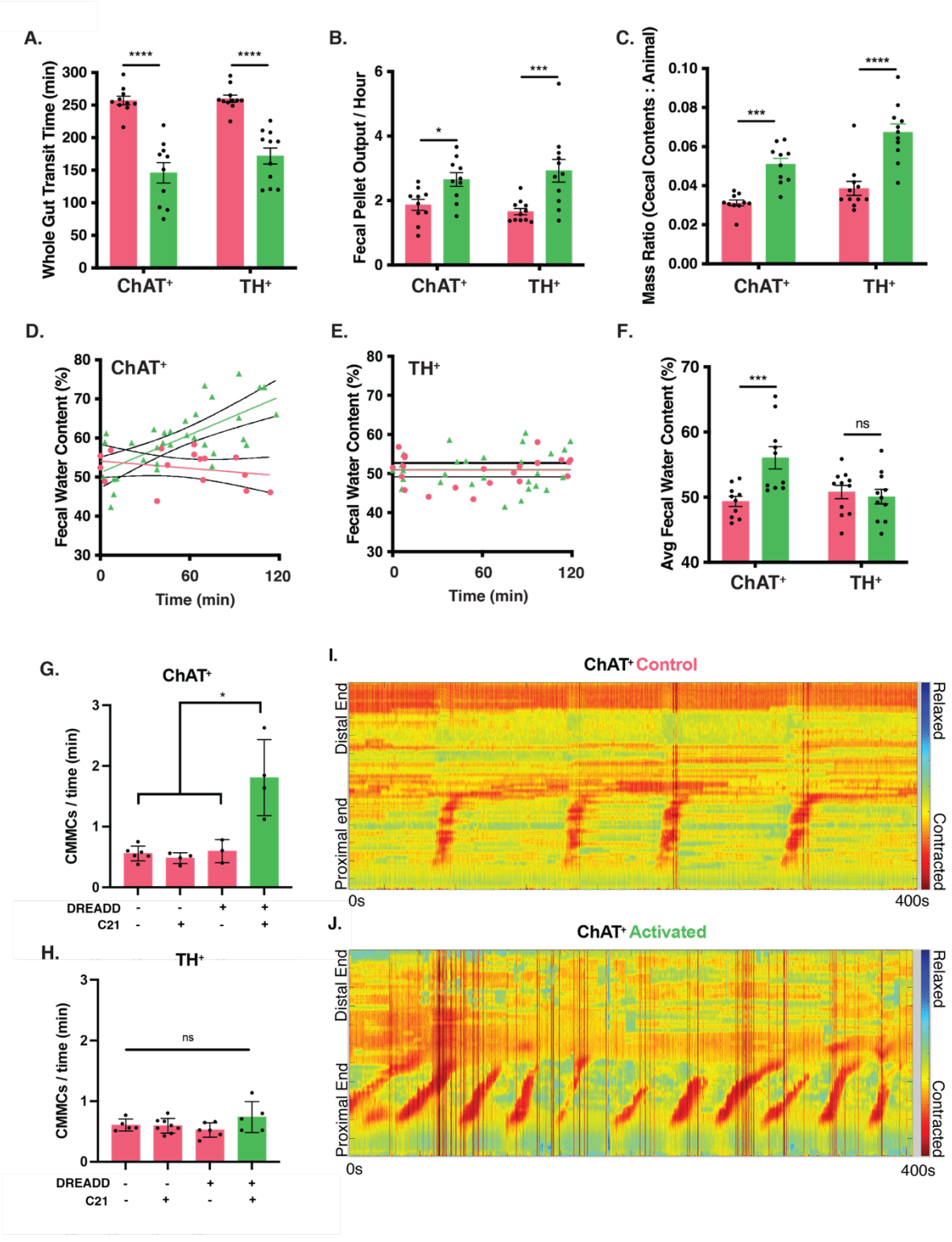
A.
Whole Gut Transit Time (min)
ChAT+
TH+
B.
Fecal Pellet Output / Hour
C.
Mass Ratio (Cecal Contents : Animal)
D.
ChAT+
Fecal Water Content (%)
Time (min)
E.
TH+
F.
Avg Fecal Water Content (%)
ns
G.
CMMCs / time (min)
DREADD
C21
H.
I.
ChAT+ Control
Distal End
Proximal end
Relaxed
Contracted
0s
400s
J.
ChAT+ Activated

**Figure 6. GI Physiology Differences in ChAT$^+$ vs. TH$^+$ mice Following Activation**

(A) Activation-mediated changes in whole gut transit time in ChAT$^+$ and TH$^+$ mice.

(B) Activation-mediated changes in fecal pellet output in ChAT$^+$ and TH$^+$ mice.

(C) Activation-mediated changes in normalized cecal content mass in ChAT$^+$ and TH$^+$ mice.

(D-E) Fecal pellet water content in (D) ChAT$^+$ and (E) TH$^+$ mice over 2 hours following C21 activation.

(F) Average fecal pellet water content in ChAT$^+$ and TH$^+$ mice following activation

(A-F: N = 10-11 mice per group; *: $p<0.05$, ***: $p<0.001$, ****: $p<0.0001$, determined by 2-way ANOVA with Sidak's method for multiple comparisons).

(G-H) Frequency of *ex vivo* CMMCs from (G) ChAT$^+$ and (H) TH$^+$ mice over 30 minutes following activation.

(N = 3-8 mice per group; *: $p<0.05$, determined by 2-way ANOVA with Sidak's method for multiple comparisons).

(I-J) Heatmaps showing frequency of CMMCs over 400 seconds following activation in *ex vivo* preps from (I) ChAT$^+$ control and (J) ChAT$^+$ DREADD-administered mice

See also Figure S6 and Table S4.

**Table S1 - Extended GNPS Annotations of Metabolite Network Nodes (Related to Figure 3).**

Extended annotations for networked (bold) MS/MS spectra from luminal cecal contents of activated $TH^+$ and $ChAT^+$ mice in Figures 3C and 3D, respectively.

**Source Data Table S1**

https://github.com/mazmanianlab/Griffiths_Yoo_et_al/blob/main/metabolomics/Table_S1-Extended_GNPS_annotations_of_Metabolite_Network_Notes_related_to_figure_3.xlsx

**Table S2 - Gene Set Enrichment Analysis of Gene Ontology (GO) Terms (Related to Figure 5).**

Gene set enrichment analysis of gene ontology (GO) terms that are upregulated in the distal SI and proximal colon of activated $ChAT^+$ and $TH^+$ mice.

**Source Data Table S2**

https://github.com/mazmanianlab/Griffiths_Yoo_et_al/blob/main/RNAseq/Table_S2-Gene_Set_Enrichment_Analysis_of_GO_related_to_figure_5.xlsx

**Table S3 – Genes Related to T helper responses (Related to Figure 5).**

List of genes in the transcriptomics dataset associated with T helper responses.

**Source Data Table S3**

https://github.com/mazmanianlab/Griffiths_Yoo_et_al/blob/main/RNAseq/Table_S3-Genes_Related_to_T_Helper_Responses.xlsx

**Table S4 – Annotations of Colonic Migrating Motor Complexes (Related to Figure 6)**

Video annotations of CMMCs in *ex vivo* colonic preparations from $ChAT^+$ and $TH^+$ mice at baseline and during activation.

**Source Data Table S4**

https://github.com/mazmanianlab/Griffiths_Yoo_et_al/blob/main/ex_vivo_motility/Table_S4%E2%80%93Annotations_of_Colonic_Migrating_Motor_Complexes_Related_to_figure_6.xlsx

**Video S1 – Calcium Imaging of $ChAT^+$ activated Gut Neurons (Related to Figure S5)**

Video of *in vivo* calcium imaging of GCaMP6f-expressing $ChAT^+$ activated neurons in the myenteric plexus at 5 Hz following C21 administration.

**Source Data Video S1**

https://github.com/mazmanianlab/Griffiths_Yoo_et_al/blob/main/ENS%20quantification/Video%20Supplement%201-%20GCaMP6F%20at%205Hz.avi

## MATERIALS & METHODS

### Mice

All mouse experiments were performed in accordance with the NIH Guide for the Care and Use of Laboratory Animals using protocols approved by the Institutional Animal Care and Use Committee at the California Institute of Technology. Mice were fed ad libitum for the entire duration of experiments. Homozygous TH-Cre (gift to V.G. from Ted Ebendal, B6.129X1-Thtm1(cre)Te/Kieg (Lindeberg et al., 2004)) and ChAT-Cre (Jackson Laboratories, Bar Harbor, ME-Stock# 028861, RRID:IMSR_JAX:028861) mice were bred to wild-type mice to yield the male and female heterozygous Cre-mice used for our studies. Wild-type specific pathogen free (SPF) C57BL/6 (Jackson Laboratories, Bar Harbor, ME-Stock #000664, RRID:IMSR_JAX:000664) males and females were used for breeding and experiments.

### Virus Production

Virus was produced using the methods described in Challis et al., 2019 and dx.doi.org/10.17504/protocols.io.bzn6p5he. Briefly, human embryonic kidney (HEK293T) cells were triple-transfected with pUCmini-iCAP-AAV-PHP.S, pHelper plasmid, and one of the following pAAV genomes: CAG-NLS-GFP, hSYN1-tdTomato, GFAP-tdTomato, hSYN1-mRuby2, hSYN1-DIO-mRuby2, hSYN1-mNeonGreen, hSYN1-DIO-mNeonGreen, hSYN1-mTurquoise2, hSYN1-DIO-mTurquoise2, hSYN1-DIO-hM3Dq-mRuby2, CAG-GCaMP6f. Cells were grown in DMEM + Glutamax + Pyruvate (Gibco, Gaithersburg, MD-Stock# 10569-010) + 5% FBS + non-essential amino acids

(Gibco, Gaithersburg, MD-Stock# 11140-050) + penicillin-streptomycin (Gibco, Gaithersburg, MD-Stock# 15070-063). Virus was precipitated from cells and supernatant with an 8% PEG solution (wt/vol), and purified by ultracentrifugation using 15%, 25%, 40%, 60% stacked iodixanol gradients.

**Systemic Delivery of AAV**

Mice were anesthetized using 2% isoflurane. Virus was titered to $1\times10^{12}$ vg, resuspended in a volume of 100 µl with sterile PBS, and injected retro-orbitally as described in dx.doi.org/10.17504/protocols.io.bzn6p5he.

**Neuronal activation of the GI tract**

See dx.doi.org/10.17504/protocols.io.bzp5p5q6. TH-Cre and ChAT-Cre mice were used for these experiments. “Activated” mice were infected with AAV-PHP.S-hSYN1-DIO-hM3Dq-mRuby2 and “Control Mice” were infected with AAV-PHP.S-hSYN1-DIO-mRuby2. This was to control for both AAV-PHP.S-mediated expression and the effects of Compound 21 dihydrochloride (C21) (HelloBio, Princeton, NJ-HB6124). C21 was injected intraperitoneally (i.p.) at a dose of 3 mg/kg for 10 consecutive days to both groups of mice. Mice for timecourse experiments were single-housed in sterile cages with autoclaved water following the first C21 administration. Injections of C21 were administered at the same time every day (10AM). Mice were sacrificed one hour after the day 10 injection.

**Tissue Preparation, Immunohistochemistry, Imaging, and Quantification**

Procedures are described in dx.doi.org/10.17504/protocols.io.bzp6p5re. 100 mg/kg of pentobarbital (Euthasol - Virbac, Carros, France) was administered i.p., and tissues were perfused with 30 mL of phosphate-buffered saline (PBS) and then cold 4% paraformaldehyde (PFA) in PBS. GI tract was post-fixed in 4% PFA overnight at 4 °C, and stored in PBS + 0.025% sodium azide. Tissues that underwent subsequent immunohistochemistry were made transparent by the passive CLARITY technique (PACT) (Treweek et al., 2015). Briefly, perfused and fixed tissues were embedded with polymerized 4% (wt/vol) acrylamide, and lipids were eliminated using 8% (wt/vol) SDS solution. Jugular-nodose ganglia and dorsal root ganglia tissues were cryoprotected in 10% then 30% sucrose in PBS for 1 day each. Tissues were embedded and flash frozen in OCT and cryostat sectioned into 40 µM sections. Spinal cord and brain tissues were vibratome sectioned into 50 µM sections. Tissues were blocked in 3% donkey serum and permeabilized with PBS + 0.3% Triton (PBST). Primary antibodies were incubated in PBST for 48 hours and washed with PBST for 24 hours (replacing the wash solution 3 times). Tissues were next incubated in secondary antibodies (and DAPI) for 24 hours and washed in PBS for 48 hours, intermittently replacing the wash solution with fresh PBS. Primary antibodies used were rabbit anti-PGP9.5 (1:300; Millipore Cat# AB1761-I, RRID:AB_2868444), chicken anti-GFAP (1:500, BioLegend Cat# 829401, RRID:AB_2564929), rabbit anti-tyrosine hydroxylase (1:500, Abcam Cat# ab112, RRID:AB_297840), rabbit anti-choline acetyltransferase, (1:250, Abcam Cat# ab178850, RRID:AB_2721842), and mouse anti-NeuN (1:300, Abcam Cat# ab104224, RRID:AB_10711040). Secondary antibodies used were goat anti-chicken Alexa 647 (Thermo Fisher Scientific Cat# A32933TR, RRID:AB_2866500), donkey anti-rabbit Alexa

568 (Thermo Fisher Scientific Cat# A10042, RRID:AB_2534017), goat anti-rabbit Alexa 647 (Thermo Fisher Scientific Cat# A-21245 (also A21245), RRID:AB_2535813), and goat anti-mouse Alexa 594 (Thermo Fisher Scientific Cat# A-11032, RRID:AB_2534091). GI tissues imaged for virally-expressed, endogenous fluorescence were made transparent using a sorbitol-based optical clearing method, Sca*l*eS (Hama et al., 2015).

Tissues were mounted in method-respective mounting media (RIMS and Scales S4) on a glass slide with a 0.5mm spacer (iSpacer, SunJin Lab Co.). Images were acquired on Zeiss LSM 780 or 880, and microscope, laser settings, contrast, and gamma remained constant across images that were directly compared. All confocal images were taken with the following objectives: Fluar 5× 0.25 M27 Plan-Apochromat, 10× 0.45 M27 (working distance 2.0 mm) and Plan-Apochromat 25× 0.8 Imm Corr DIC M27 multi-immersion. Neurons in each ganglion were counted by counting cells that were of a distinct color. Colonic ganglia were defined as distinct if separated by a width of 3 or more neurons.

**GCaMP6f Fluorescence in *Ex Vivo* Intestinal Preparations**

As described in dx.doi.org/10.17504/protocols.io.bzqap5se, small intestinal tissue was quickly harvested from ChAT-Cre mice, flushed, and placed in oxygenated (95% $O_2$, 5% $CO_2$), ice cold Krebs-Henseleit solution for 1 hour followed by 15 min at room temperature. A segment was cut along the mesenteric attachment and pinned flat (mucosa facing down) on a Sylgard-lined recording chamber (Warner Instruments, PH1) in oxygenated Krebs-Henseleit solution. C21 was added at 10nM and GCaMP6f fluorescence was detected on an upright microscope (Zeiss, Oberkochen, Germany-Examiner D1).

## Metagenomics

Procedures are described in dx.doi.org/10.17504/protocols.io.bzqep5te.

### *Fecal collection*

AAV-PHP.S-hSYN1-hM3Dq-mRuby2 ($10^{12}$ vg) was delivered systemically to TH-Cre and ChAT-Cre mice. 3-4 week after infection, C21 (3 mg/kg) was administered daily for 10 consecutive days. Fecal pellets were collected in sterile containers one day before the initial C21 dose, and on day 2, 6, and 10 of injections.

### *Fecal sample DNA extraction and library preparation*

DNA was extracted with the Qiagen MagAttract PowerSoil DNA kit as previously described (Marotz et al., 2017).This protocol is optimized for an input quantity of 1 ng DNA per reaction. Prior to library preparation, input DNA was transferred to a 384-well plate and quantified using a PicoGreen fluorescence assay (ThermoFisher, Inc). Input DNA was then normalized to 1 ng in a volume of 3.5 μL of molecular-grade water using an Echo 550 acoustic liquid-handling robot (Labcyte, Inc). Enzyme mixes for fragmentation, end repair and A-tailing, ligation, and PCR were prepared and added in approximately 1:8 scale volumes using a Mosquito HV micropipetting robot (TTP Labtech). Fragmentation was performed at 37 °C for 20 min, followed by end repair and A-tailing at 65 °C for 30 min.

Sequencing adapters and barcode indices were added in two steps, following the iTru adapter protocol (Glenn et al., 2019). Universal “stub” adapter molecules and ligase mix were first added to the end-repaired DNA using the Mosquito HV robot and ligation

performed at 20 °C for 1 h. Unligated adapters and adapter dimers were then removed using AMPure XP magnetic beads and a BlueCat purification robot (BlueCat Bio). 7.5 µL magnetic bead solution was added to the total adapter-ligated sample volume, washed twice with 70% EtOH, and then resuspended in 7 µL molecular-grade water.

Next, individual i7 and i5 were added to the adapter-ligated samples using the Echo 550 robot. Because this liquid handler individually addresses wells, and we used the full set of 384 unique error-correcting i7 and i5 indices, we were able to generate each plate of 384 libraries without repeating any barcodes, eliminating the problem of sequence misassignment due to barcode swapping (Costello et al., 2018; Sinha et al., 2017). To ensure that libraries generated on different plates could be pooled if necessary, and to safeguard against the possibility of contamination due to sample carryover between runs, we also iterated the assignment of i7 to i5 indices each run, such that each unique i7:i5 index combination was repeated only once every 147,456 libraries. 4.5 µL of eluted bead-washed ligated samples was added to 5.5 µL of PCR master mix and PCR-amplified for 15 cycles. The amplified and indexed libraries were then purified again using magnetic beads and the BlueCat robot, resuspended in 10 µL water, and 9 µL of final purified library transferred to a 384-well plate using the Mosquito HV liquid-handling robot for library quantitation, sequencing, and storage. 384 samples were then normalized based on a PicoGreen fluorescence assay.

*Shallow shotgun metagenome sequencing and diversity analysis*

The Illumina data for each HiSeq lane was uploaded to Qiita, a tool with standardized pipelines for processing and analyzing metagenomic data (Gonzalez et al., 2018). Adapter

sequences were removed from the reads using the Atropos v.1.1.15 (RRID:SCR_023962, https://github.com/jdidion/atropos) (Didion et al., 2017) command (from the qp-shogun 0.1.5 pipeline) and the trimmed sequences were downloaded from Qiita. The reads for each sample were filtered of any potential mouse contamination using Bowtie2 v.2-2.2.3 (RRID:SCR_016368, https://bowtie-bio.sourceforge.net/bowtie2/index.shtml) (Langmead and Salzberg, 2012). The filtered reads were then aligned to the Web of Life (WoL) reference phylogeny (Zhu et al., 2019) with Bowtie2 using an adapted SHOGUN pipeline (Hillmann et al., 2018). The WoL contains 10,575 bacterial and archaeal genomes, with each genome representing an operational taxonomic unit (OTU). Sequencing reads that did not map to a single reference genome as well as reads that mapped to multiple genomes were not included in the analysis. If an OTU had a relative abundance less than 0.01% in a given sample, the OTU was not included for that sample. Additionally, OTUs with fewer than 5 assigned reads were not considered. The samples were rarefied to a depth of 12,750 reads and those with fewer than the rarefaction depth were excluded. The QIIME2 v.2019.7 (RRID:SCR_021258, https://qiime2.org/) (Bolyen et al., 2019) DEICODE plugin was used to calculate the Aitchison distances, a compositional beta diversity metric, and perform Robust Aitchison PCA to create biplots that visualize relationships between features and samples (Martino et al., 2019). The QIIME2 diversity plugin was used to calculate the other alpha- and beta-diversity metrics used in this study.

*Metagenomics-based functional profiling*

The filtered reads were also analyzed using HUMAnN2 v2.8.1 (RRID:SCR_016280, https://huttenhower.sph.harvard.edu/humann2) (Franzosa et al., 2018) to establish functional profiles for the samples. HUMAnN2 is a pipeline that begins by using MetaPhlAn 2 to compile custom databases of reference genomes based on the species detected in a sample (Truong et al., 2015). HUMAnN2 then maps the filtered reads onto these custom databases and the reads that do not map to any of the references are then subjected to a translated search against UniProt Reference Clusters or UniRef (RRID:SCR_010646, https://www.uniprot.org/help/uniref) (Suzek et al., 2007). Here, the UniRef90 database was used for the translated search and installed according to the HUMAnN2 documentation. The results from both the search performed using the custom reference genome database and the search against the UniRef90 database were combined and the gene families identified in each sample were reported in units of reads per kilobase (RPKs) to account for gene length. HUMAnN2 also compared the gene families found in a sample with the MetaCyc pathways database (RRID:SCR_007778, https://metacyc.org/) (Caspi et al., 2018) and output a table reporting the pathway abundances found in each sample. After rarefying gene family tables to a depth of 166,000 RPKs and using a depth of 22,600 for pathway abundances, the QIIME2 diversity and DEICODE plugins were used to calculate alpha- and beta-diversity metrics. The metagenomics data from this study are available from (https://github.com/mazmanianlab/Griffiths_Yoo_et_al/tree/main/metagenomics).

**Metabolomics**

Procedures are described in dx.doi.org/10.17504/protocols.io.bzqfp5tn.

*Sample preparation*

Frozen cecal samples were transported on dry ice for metabolomics analysis. The samples were weighed and an extraction solvent (1:1 methanol to water with an internal standard of 1 µM sulfamethazine) was added at a 1:10 milligram to microliter ratio. The samples were then homogenized using a TissueLyser II (Qiagen) for 5 minutes at 25 Hz followed by a 15 min centrifugation at 14,000 rpm. 120 µL of supernatant was transferred to a 96-well DeepWell plate (Eppendorf) and lyophilized using a CentriVap Benchtop Vacuum Concentrator (Labconco) and stored at −80 °C. At the time of data acquisition, the lyophilized plates were resuspended in a 1:1 methanol to water solvent spiked with 1 µM of sulfadimethoxine. The plates were vortexed for 2 minutes, centrifuged at 14,000 rpm for 15 min and 120 µL of the supernatant was transferred to a 96-well autosampler plate (Eppendorf). Plates were stored at 4 °C prior to LCMS analysis.

*Data acquisition*

The untargeted metabolomics analysis was completed using an ultra-high performance liquid chromatography system (Thermo Dionex Ultimate 3000 UHPLC) coupled to an ultra-high resolution quadrupole time of flight (qTOF) mass spectrometer (Bruker Daltonics MaXis HD). A Phenomenex Kinetex column (C18 1.7 µm, 2.1 mm x 50 mm) was used for chromatographic separation. An injection volume of 5 µL was used for each sample and a flow-rate of 0.500 mL was used throughout the analysis. The mobile phase consisted of solvent A: 100% LC-MS grade water spiked with 0.1% formic acid and solvent B: 100% LC-MS grade acetonitrile spiked with 0.1% formic acid. The chromatographic gradient was as follows: 0.0–1.0 min, 5% B; 1.0–9.0 min, 5–100% B; 9.0-11.0 min, 100% B; 11.0-11.5

min, 100-5% B; 11.5-12.5 min, 5% B. Data was collected with electrospray ionization in positive mode, and was saved as .d file folders.

*Data processing*

The raw .d data files were converted to mzXML format using Bruker Compass DataAnalysis 4.1 software. The resulting .mzXML file, the original .d file folders, and basic prep information sheet are stored in the UC San Diego MassIVE data repository under the accession number MSV000084550. For MS1 level feature detection, the open-source software MZmine version 2.51 (RRID:SCR_012040, https://mzmine.github.io/) was used. The parameters used are as follows: 1) Mass Detection (Centroid, Noise Level MS1 1E3, MS2 1E2); 2) ADAP Chromatogram Builder (Min Group size in # of scans=3, Group Intensity Threshold= 3E3, Min Highest Intensity=1E3, m/z tolerance 0.01 m/z or 10.0 ppm); 3) Chromatogram Deconvolution (Local Minimum Search>Chromatographic Threshold 0.01%, Minimum in RT range 0.50 min, <Minimum Relative Height 0.01%, Minimum Absolute Height 3E3, Min Ratio of Peak Top/Edge 2, Peak Duration Range 0.05-0.50 min; m/z Calculation Auto, m/z range for MS2 pairing 0.01 Da, and RT Range for MS2 Pairing 0.1 min); Isotopic Peaks Grouper (m/z Tolerance 0.01 m/z or 10.0 ppm, Retention Time Tolerance 0.3 min, Maximum Charge 4, Representative Ion Most Intense); Join Aligner (m/z Tolerance 0.01 m/z or 10.0 ppm, Weight for m/z 75, Retention Time Tolerance 0.3 min, Weight for RT 25); Gap-Filling Peak Finder (Intensity Tolerance 20%, m/z Tolerance 0.005 m/z or 10.0 ppm, Retention Time Tolerance 0.2 min). The resulting feature table was saved as a .csv file and .mgf file for use in GNPS and MetaboAnalyst.

*Molecular networking and statistical analysis*

Molecular networking was performed using the feature networking tool available through the Global Natural Products Social Molecular Networking (GNPS, RRID:SCR_019012, https://gnps.ucsd.edu/ProteoSAFe/static/gnps-splash.jsp) portal: https://gnps.ucsd.edu/ProteoSAFe/index.jsp?params=%7B%22workflow%22:%22FEATURE-BASED-MOLECULAR-NETWORKING%22,%22library_on_server%22:%22d.speclibs;%22%7D.

The annotations obtained using this workflow fall under MSI level 2 or 3 and were used for feature analysis (Sumner et al., 2007). Briefly, level 2 compounds are putatively annotated, meaning they are not identified using chemical reference standards but rather based on physical properties and/or spectral similarities to available spectral libraries (publicly available and purchased NIST17 CID). Level 3 compounds are putatively characterized classes of compounds identified similarly to level 2 compounds. The feature-based molecular networking workflow on GNPS (Nothias et al., 2019) was utilized in order to analyze the spectra associated with the feature tables produced using the open source software Mzmine version 2.51 (RRID:SCR_012040, https://mzmine.github.io/) (Pluskal et al., 2010). The .mgf and .csv outputs from MZmine v2.51 were used to run the workflow. The GNPS workflow parameters used were as follows: Precursor Ion Mass 0.02 Da, Fragment Ion Mass Tolerance 0.02 Da, Min Pairs Cos 0.7, Minimum Matched Fragments 6, Maximum Shift Between Precursors 500 Da, Network TopK 10, Maximum Connected Component Size (Beta) 100, and the files were row sum normalized. Default parameters were used for the rest of the settings. Visualizations and statistical analyses were performed using QIIME 2 v.2019.10 (RRID:SCR_021258) (Bolyen et al., 2019), MetaboAnalyst (RRID:SCR_015539, https://www.metaboanalyst.ca/) and Cytoscape v3.7.2

(RRID:SCR_003032, https://cytoscape.org/). The metabolomics data from this study are available from (https://github.com/mazmanianlab/Griffiths_Yoo_et_al/tree/main/metabolomics).

**Proteome Preparation**

Procedures are described in dx.doi.org/10.17504/protocols.io.bzqcp5sw.

*Protein extraction*

Mice were sacrificed 1 hour after the final C21 administration and cecal contents were isolated and resuspended in 400 µl of phosphate buffered solution and centrifuged at 20,000 xg to spin down cells and lysate. Protein was isolated from the resulting supernatant using Wessel-Flügge's methanol/chloroform extraction method (Wessel and Flügge, 1984). Briefly, MeOH and chloroform were added to the samples at a 4:1 and 1:1 ratio, respectively. Next, $dH_2O$ was added at a 3:1 ratio, samples were vortexed and centrifuged at 20,000 xg. Resulting precipitated protein was collected and washed with MeOH. Precipitated protein was centrifuged and left to air dry, and stored at −20 °C until protein digestion.

*In-solution protein digestion and desalting*

Precipitated protein samples were denatured in 40 µL of 8M Urea (100 mM Tris-HCl pH 8.5). To reduce disulfide bonds, 1.25 µL of 100 mM Tris(2-carboxyethyl)Phosphine was added and incubated at room temperature (RT) for 20 minutes. Then 1.8 µL of 250 mM iodoacetamide was added and incubated at RT in the dark to alkylate cysteines. The first

step of digestion was initiated by adding 1 µL of 0.1 µg/µL of lysyl endopeptidase. After 4 hours of incubation, the urea concentration was adjusted to 2 M by adding 120 µL of 100 mM Tris-HCl pH 8.5. The second step of digestion was done by adding 2.5 µL of 2µg/µL trypsin plus 1.6 µL of 100 mM $CaCl_2$ and incubating overnight in the dark. Formic acid was added to stop trypsin digestion. Digested peptides were desalted by HPLC using a C8 peptide microtrap (Microm Bioresources), lyophilized, and diluted to 200 ng/µl in 0.2% formic acid prior to LC-MS/MS analysis.

*LC-MS/MS*

Samples were analyzed on a Q Exactive HF Orbitrap mass spectrometer coupled to an EASY nLC 1200 liquid chromatographic system (Thermo Scientific, San Jose, CA). Approximately 200 ng of peptides were loaded on a 50 µm I.D. × 25 cm column with a 10 µm electrospray tip (PicoFrit from New Objective, Woburn, MA) in-house-packed with ReproSil-Pur C18-AQ 1.9 µm (Dr. Maisch, Ammerbuch, Germany). Solvent A consisted of 2% MeCN in 0.2% FA and solvent B consisted of 80% MeCN in 0.2% FA. A non-linear 60 minute gradient from 2% B to 40% B was used to separate the peptides for analysis. The mass spectrometer was operated in a data-dependent mode, with MS1 scans collected from 400-1650 m/z at 60,000 resolution and MS/MS scans collected from 200-2000 m/z at 30,000 resolution. Dynamic exclusion of 45 s was used.

The top 12 most abundant peptides with charge states between 2 and 5 were selected for fragmentation with normalized collision energy of 28.

*Peptide and protein identification*

Thermo .raw files were converted to .ms1 and .ms2 files using RawConverter 1.1.0.18 (He et al., 2015) operating in data dependent mode and selecting for monoisotopic m/z. Tandem mass spectra (.ms2 files) were identified by a database search method using the Integrated Proteomics Pipeline 6.5.4 (IP2, Integrated Proteomics Applications, Inc., http://www.integratedproteomics.com). Briefly, databases containing forward and reverse (decoy) (Elias and Gygi, 2007; Peng et al., 2003) peptide sequences were generated from *in silico* trypsin digestion of either the mouse proteome (UniProt; Oct. 2, 2019) or protein sequences derived from large comprehensive public repositories (ComPIL 2.0) (Park et al., 2018). Tandem mass spectra were matched to peptide sequences using the ProLuCID/SEQUEST (1.4) (Xu et al., 2015; 2006) software package. The validity of spectrum-peptide matches was assessed using the SEQUEST-defined parameters XCorr (cross-correlation score) and DeltaCN (normalized difference in cross-correlation scores) in the DTASelect2 (2.1.4) (Cociorva et al., 2007; Tabb et al., 2002) software package. Search settings were configured as follows: (1) 5 ppm precursor ion mass tolerance, (2) 10 ppm fragment ion mass tolerance, (3) 1% peptide false discovery rate, (4) 2 peptide per protein minimum, (5) 600-6000 Da precursor mass window, (6) 2 differential modifications per peptide maximum (methionine oxidation: M+15.994915 Da), (7) unlimited static modifications per peptide (cysteine carbamidomethylation: C+57.02146 Da), and (8) the search space included half- and fully- tryptic (cleavage C-terminal to K and R residues) peptide candidates with unlimited (mouse database, custom metagenomic shotgun database) or 2 missed cleavage events (ComPIL 2.0).

*Differential analysis of detected proteins using peptide-spectrum matches (spectral counts)*

Detected proteins were grouped by sequence similarity into “clusters” using CD-HIT 4.8.1 (RRID:SCR_007105, http://weizhong-lab.ucsd.edu/cd-hit/) (Fu et al., 2012; Li and Godzik, 2006; Li et al., 2001) at the following similarity cut-offs: 65%, 75%, 85%, and 95%. The following is an example command line input: “cd-hit -i fastafile.fasta -o outputfile -c 0.65 -g 1 -d 0”. Tandem mass spectra identified as peptides (peptide spectrum matches, PSMs) were mapped to CD-HIT generated clusters. PSMs mapping to >1 cluster were discarded. Cluster-PSM tables were generated and differential analysis was performed in DESeq2 (1.25.13, RRID:SCR_015687, https://bioconductor.org/packages/release/bioc/html/DESeq2.html) (Love et al., 2014). Briefly, count data (PSMs) were modeled using the negative binomial distribution, and the mean-variance relationship was estimated. Variance was estimated using an information sharing approach whereby a single feature’s (or cluster’s) variance was estimated by taking into account variances of other clusters measured in the same experiment. Feature significance calling and ranking were performed using estimated effect sizes. Multiple testing correction was performed by the Benjamini-Hochberg method within the DESeq2 package. Volcano plots were generated in Prism (GraphPad).

*Differential analysis of detected proteins using ion intensity (precursor intensity)*

Detected proteins were grouped into “clusters” by sequence similarity using CD-HIT 4.8.1 (Fu et al., 2012; Li and Godzik, 2006; Li et al., 2001) at the following similarity cut-offs: 65%, 75%, 85%, and 95%. The following is an example command line input: “cd-hit -i fastafile.fasta -o outputfile -c 0.65 -g 1 -d 0”. Using the Census software package (Park et al.; 2008) (Integrated Proteomics Pipeline 6.5.4), peptide ion intensities were calculated

from .ms1 files. Peptide ion intensities were assigned to their parent peptide, then parent peptides were mapped to their appropriate CD-HIT generated clusters. Ion intensities belonging to parent peptides that mapped to >1 CD-HIT cluster were discarded. Cluster-ion intensity tables were generated.

Ion intensity data were analyzed using the Differential Enrichment analysis of Proteomics data DEP package

(RRID:SCR_023090, https://bioconductor.org/packages/release/bioc/html/DEP.html) (Zhang et al., 2018) operating in R. Intensity values were automatically Log2 transformed in DEP. The cluster list was subsequently filtered with the 'filter_proteins' function such that clusters with missing values above a 65% threshold were discarded. Remaining intensities were further transformed by the 'normalize_vsn' function (Huber et al., 2002). Missing data in remaining clusters were imputed using a mixed approach. Clusters where either the control or treatment group contained only null entries were classified as 'missing not at random' (MNAR) and imputed with 0 values. All other groups were treated as 'missing at random' (MAR) and imputed using the maximum likelihood method ('MLE') (Gatto and Lilley, 2012). Note that for a given cluster, missing values for treatment groups were imputed separately by treatment group. Differential expression analyses were performed on filled-in cluster-ion intensity tables using the 'test_diff' function (Ritchie et al., 2015) and multiple testing correction was performed using the 'add_rejections' function.

*Network analysis using the STRING database*

Upregulated proteins with a nominal p-value < 0.2 were searched against protein-protein interactions in the STRING database (RRID:SCR_005223, http://www.string-db.org) where high confidence interactions are selected for. Briefly, the STRING database sources protein-protein interactions from primary databases consisting of genomic context predictions, high-throughput lab experiments, (conserved) co-expression, automated text mining, and previous knowledge in databases (Szklarczyk et al., 2019).

*Metaproteome analysis using Unipept*

Upregulated tryptic, microbial peptide sequences, with fold change and nominal p-value cutoffs of >2 and <0.2, respectively, were input into Unipept (http://unipept.ugent.be) (Gurdeep Singh et al., 2019; Mesuere et al., 2015), equating leucine and isoleucine and filtering duplicate peptides. Briefly, Unipept indexes tryptic peptide sequences from the UniProtKB and details peptides with NCBI's taxonomic database. Lowest common ancestor was calculated for each tryptic peptide. The proteomics data from this study are available from (https://github.com/mazmanianlab/Griffiths_Yoo_et_al/tree/main/proteomics).

**3' mRNA sequencing**

Procedures are described in dx.doi.org/10.17504/protocols.io.bzqbp5sn.

*Tissue collection and RNA extraction*

Mice were cervically dislocated and the GI tract was removed. 1 cm of tissue above and below the cecum were dissected and cleaned to represent tissue from the distal SI and

proximal colon, respectively. Tissue was homogenized in TRIzol (ThermoFisher Scientific, Waltham. MA-Cat. No. 15596018) solution using a bead-based homogenizing method, and total RNA was extracted using chloroform per manufacturer's instructions.

*Library preparation, sequencing, and analysis*

The cDNA libraries were prepared using the QuantSeq 3'mRNA-Seq Library Prep Kit FWD for Illumina (Lexogen, Greenland, NH) supplemented with UMI (unique molecular index) as per the manufacturer's instructions. Briefly, total RNA was reverse transcribed using oligo (dT) primers. The second cDNA strand was synthesized by random priming, in a manner such that DNA polymerase is efficiently stopped when reaching the next hybridized random primer, so only the fragment closest to the 3' end gets captured for later indexed adapter ligation and PCR amplification. UMIs were incorporated to the first 6 bases of each read, followed by 4 bases of spacer sequences. UMIs are used to eliminate possible PCR duplicates in sequencing datasets and therefore facilitate unbiased gene expression profiling. The basic principle behind the UMI deduplication step is to collapse reads with identical mapping coordinates and UMI sequences. This step helps increase the accuracy of sequencing read counts for downstream analysis of gene expression levels. The processed libraries were assessed for size distribution and concentration using the Bioanalyzer High Sensitivity DNA Kit (Agilent Technologies, Santa Clara, CA-Cat. No. 5067-4626 and -4627). Pooled libraries were diluted to 2 nM in EB buffer (Qiagen, Hilden, Germany, Cat. No. 19086) and then denatured using the Illumina protocol. The libraries were pooled and diluted to 2 nM using 10 mM Tris-HCl, pH 8.5 and then denatured using the Illumina protocol. The denatured libraries were diluted to 10 pM with pre-chilled hybridization

buffer and loaded onto an Illumina MiSeq v3 flow cell for 150 cycles using a single-read recipe according to the manufacturer's instructions. Single-end 75 bp reads (max 4.5M reads) were obtained. De-multiplexed sequencing reads were generated using Illumina BaseSpace.

UMI specific workflows that were developed and distributed by Lexogen were used to extract reads that are free from PCR artifacts (i.e., deduplication). First, the umi2index tool was used to add the 6 nucleotide UMI sequence to the identifier of each read and trim the UMI from the start of each read. This generated a new FASTQ file, which was then processed through trimming and alignment. Second, after the quality and polyA trimming by BBDuk (Bestus Bioinformaticus Duk, RRID:SCR_016969, https://jgi.doe.gov/data-and-tools/bbtools/bb-tools-user-guide/bbduk-guide/) and alignment by HISAT2 (version 2.1.0, RRID:SCR_015530, https://daehwankimlab.github.io/hisat2/) (Kim et al., 2015), the mapped reads were collapsed according to the UMI sequence of each read. Reads were collapsed if they had the same mapping coordinates (CIGAR string) and identical UMI sequences. Collapsing reads in this manner removes PCR duplicates. Read counts were calculated using HTSeq (RRID:SCR_005514, https://htseq.readthedocs.io/en/release_0.9.1/) (Anders et al., 2015) by supplementing Ensembl gene annotation (GRCm38.78). Raw read counts were run through ShinySeq to obtain differentially expressed genes and downstream gene ontology analyses (Sundararajan et al., 2019). The RNAseq data from this study are available from (https://github.com/mazmanianlab/Griffiths_Yoo_et_al/tree/main/RNAseq).

**Whole Gut Transit Time, Fecal Water Content, and Fecal Output**

Procedures are described in dx.doi.org/10.17504/protocols.io.36wgq3p1xlk5/v1. 6% (w/v) carmine red (Sigma-Aldrich, St. Louis, MO) with 0.5% methylcellulose (Sigma-Aldrich) was dissolved and autoclaved prior to use. ChAT-Cre and TH-Cre mice were administered C21 (3 mg/kg) intraperitoneally, and subsequently orally gavaged with 150 µL of carmine red solution. Mice were single-housed with no bedding for the duration of the experiment, and animals were not fasted beforehand. Over the 5 hours following gavage, the time of expulsion was recorded for each fecal pellet, and each pellet was collected in pre-weighed, 1.5 mL microcentrifuge tube. Each pellet collected was checked for the presence of carmine red, and the time of initial carmine red pellet expulsion was recorded as GI transit time. The mass of collected fecal pellets was determined, and pellets were left to dry in an 80 °C oven for 2 days before weighing the desiccated pellets and calculating the pellets' initial water content. Fecal output rate for each mouse was calculated as the total number of pellets expelled during the 5 hour time course post-C21 administration divided by the time the last fecal pellet was expelled.

**Colonic Migrating Motor Complexes in *Ex Vivo* Intestinal Preparations**

Procedures are described in dx.doi.org/10.17504/protocols.io.n92ldm61nl5b/v1. Intact colons were dissected from cervically-dislocated ChAT-Cre and TH-Cre mice, flushed and placed in pre-oxygenated (95% $O_2$, 5% $CO_2$) Krebs-Henseleit solution at RT. Proximal and distal ends were cannulated to 2 mm diameter tubes and secured in the center of an organ bath with continuously oxygenated Krebs-Henseleit solution at 37 °C. Syringe pumps were connected to the inlet and outlet tubes to maintain a flow of solution at a rate of 500 µL/min through the colon. The system was allowed to equilibrate for 30 minutes before recording.

Baseline recordings were taken for 30 minutes, then the Krebs solution in the organ bath was briefly removed, mixed with C21 to a final concentration of 2 μM, and replaced in the organ bath. Recordings were taken for another 30 minutes.

**REFERENCES**

Alavi, S., Mitchell, J.D., Cho, J.Y., Liu, R., Macbeth, J.C., and Hsiao, A. (2020). Interpersonal Gut Microbiome Variation Drives Susceptibility and Resistance to Cholera Infection. Cell *181*, 1533–1546.e13.

Albenberg, L.G., and Wu, G.D. (2014). Diet and the intestinal microbiome: associations, functions, and implications for health and disease. Gastroenterology *146*, 1564–1572.

Anders, S., Pyl, P.T., and Huber, W. (2015). HTSeq--a Python framework to work with high-throughput sequencing data. Bioinformatics *31*, 166–169.

Anlauf, M., Schäfer, M.K.H., Eiden, L., and Weihe, E. (2003). Chemical coding of the human gastrointestinal nervous system: cholinergic, VIPergic, and catecholaminergic phenotypes. The Journal of Comparative Neurology *459*, 90–111.

Aries, V., Crowther, J.S., Drasar, B.S., and Hill, M.J. (1969). Degradation of bile salts by human intestinal bacteria. Gut *10*, 575–576.

Bahrami, S., and Drabløs, F. (2016). Gene regulation in the immediate-early response process. Advances in Biological Regulation *62*, 37–49.

Baumuratov, A. S., Antony, P. M. A., Ostaszewski, M., He, F., Salamanca, L., Antunes, L., Weber, J., Longhino, L., Derkinderen, P., Koopman, W. J. H., Diederich, N. J. (2016). Enteric neurons from Parkinson's disease patients display ex vivo aberrations in mitochondrial structure. Scientific Reports *6*.

Begley, M., Sleator, R.D., Gahan, C.G.M., and Hill, C. (2005). Contribution of three bile-associated loci, bsh, pva, and btlB, to gastrointestinal persistence and bile tolerance of Listeria monocytogenes. Infect. Immun. *73*, 894–904.

Benskey, M.J., Kuhn, N.C., Galligan, J.J., Garcia, J., Boye, S.E., Hauswirth, W.W., Mueller, C., Boye, S.L., and Manfredsson, F.P. (2015). Targeted gene delivery to the enteric nervous system using AAV: a comparison across serotypes and capsid mutants. Mol. Ther. *23*, 488–500.

Bhavsar, A.S., Verma, S., Lamba, R., Lall, C.G., Koenigsknecht, V., and Rajesh, A. (2013). Abdominal manifestations of neurologic disorders. Radiographics *33*, 135–153.

Bolyen, E., Rideout, J.R., Dillon, M.R., Bokulich, N.A., Abnet, C.C., Al-Ghalith, G.A., Alexander, H., Alm, E.J., Arumugam, M., Asnicar, F., et al. (2019). Reproducible, interactive, scalable and extensible microbiome data science using QIIME 2. Nat Biotechnol *37*, 852–857.

Bravo, J.A., Forsythe, P., Chew, M.V., Escaravage, E., Savignac, H.M., Dinan, T.G., Bienenstock, J., and Cryan, J.F. (2011). Ingestion of Lactobacillus strain regulates emotional behavior and central GABA receptor expression in a mouse via the vagus nerve. Proceedings of the National Academy of Sciences *108*, 16050–16055.

Browning, K.N. and Travagli R.A. (2014). Central nervous system control of gastrointestinal motility and secretion and modulation of gastrointestinal functions. Compr Physiol. *4*, 1339-68.

Bruel-Jungerman, E., Davis, S., and Laroche, S. (2016). Brain Plasticity Mechanisms and Memory: A Party of Four. Neuroscientist *13*, 492–505.

Carabotti, M., Scirocco, A., Maselli, M.A., and Severi, C. (2015). The gut-brain axis: interactions between enteric microbiota, central and enteric nervous systems. Ann Gastroenterol *28*, 203–209.

Carroll, I.M., Ringel-Kulka, T., Ferrier, L., Wu, M.C., Siddle, J.P., Bueno, L., and Ringel, Y. (2013). Fecal protease activity is associated with compositional alterations in the intestinal microbiota. PloS One *8*, e78017.

Caspi, R., Billington, R., Fulcher, C.A., Keseler, I.M., Kothari, A., Krummenacker, M., Latendresse, M., Midford, P.E., Ong, Q., Ong, W.K., et al. (2018). The MetaCyc database of metabolic pathways and enzymes. Nucleic Acids Res *46*, D633–D639.

Cekanaviciute, E., Yoo, B.B., Runia, T.F., Debelius, J.W., Singh, S., Nelson, C.A., Kanner, R., Bencosme, Y., Lee, Y.K., Hauser, S.L., et al. (2017). Gut bacteria from multiple sclerosis patients modulate human T cells and exacerbate symptoms in mouse models. Proc. Natl. Acad. Sci. U.S.a. *114*, 10713–10718.

Cersosimo, M.G., Raina, G.B., Pecci, C., Pellene, A., Calandra, C.R., Gutiérrez, C., Micheli, F.E., and Benarroch, E.E. (2013). Gastrointestinal manifestations in Parkinson's disease: prevalence and occurrence before motor symptoms. J. Neurol. *260*, 1332–1338.

Challis, R.C., Ravindra Kumar, S., Chan, K.Y., Challis, C., Beadle, K., Jang, M.J., Kim, H.M., Rajendran, P.S., Tompkins, J.D., Shivkumar, K., et al. (2019). Systemic AAV vectors for widespread and targeted gene delivery in rodents. Nature Protocols *14*, 379–414.

Chan, K.Y., Jang, M.J., Yoo, B.B., Greenbaum, A., Ravi, N., Wu, W.-L., Sánchez-Guardado, L., Lois, C., Mazmanian, S.K., Deverman, B.E., et al. (2017). Engineered AAVs for efficient noninvasive gene delivery to the central and peripheral nervous systems. Nat. Neurosci. *20*, 1172–1179.

Chen, T.-W., Wardill, T.J., Sun, Y., Pulver, S.R., Renninger, S.L., Baohan, A., Schreiter, E.R., Kerr, R.A., Orger, M.B., Jayaraman, V., et al. (2013). Ultrasensitive fluorescent proteins for imaging neuronal activity. Nature *499*, 295–300.

Cociorva, D., L Tabb, D., and Yates, J.R. (2007). Validation of Tandem Mass Spectrometry Database Search Results Using DTASelect. Current Protocols in Bioinformatics *16*.

Costello, M., Fleharty, M., Abreu, J., Farjoun, Y., Ferriera, S., Holmes, L., Granger, B., Green, L., Howd, T., Mason, T., et al. (2018). Characterization and remediation of sample index swaps by non-redundant dual indexing on massively parallel sequencing platforms. BMC Genomics *19*, 332–10.

de Aguiar Vallim, T.Q., Tarling, E.J., and Edwards, P.A. (2013). Pleiotropic roles of bile acids in metabolism. Cell Metabolism *17*, 657–669.

Del Giudice, E., Staiano, A., Capano, G., Romano, A., Florimonte, L., Miele, E., Ciarla, C., Campanozzi, A., and Crisanti, A.F. (1999). Gastrointestinal manifestations in children with cerebral palsy. Brain Dev. *21*, 307–311.

Delpino, M.V., Marchesini, M.I., Estein, S.M., Comerci, D.J., Cassataro, J., Fossati, C.A., and Baldi, P.C. (2007). A bile salt hydrolase of Brucella abortus contributes to the establishment of a successful infection through the oral route in mice. Infect. Immun. *75*, 299–305.

Deneux, T., Kaszas, A., Szalay, G., Katona, G., Lakner, T., Grinvald, A., Rózsa, B., and Vanzetta, I. (2016). Accurate spike estimation from noisy calcium signals for ultrafast three-dimensional imaging of large neuronal populations in vivo. Nature Communications *7*, 12190–17.

Derrien, M., Vaughan, E.E., Plugge, C.M., and de Vos, W.M. (2004). Akkermansia muciniphila gen. nov., sp. nov., a human intestinal mucin-degrading bacterium. International Journal of Systematic and Evolutionary Microbiology *54*, 1469–1476.

Deverman, B.E., Pravdo, P.L., Simpson, B.P., Kumar, S.R., Chan, K.Y., Banerjee, A., Wu, W.-L., Yang, B., Huber, N., Pasca, S.P., et al. (2016). Cre-dependent selection yields AAV variants for widespread gene transfer to the adult brain. Nat Biotechnol *34*, 204–209.

Didion, J.P., Martin, M., and Collins, F.S. (2017). Atropos: specific, sensitive, and speedy trimming of sequencing reads. PeerJ *5*, e3720.

Donaldson, G.P., Ladinsky, M.S., Yu, K.B., Sanders, J.G., Yoo, B.B., Chou, W.C., Conner, M.E., Earl, A.M., Knight, R., Bjorkman, P.J., et al. (2018). Gut microbiota utilize immunoglobulin A for mucosal colonization. Science *360*, 795–800.

Donaldson, G.P., Lee, S.M., and Mazmanian, S.K. (2015). Gut biogeography of the bacterial microbiota. Nat Rev Micro *14*, 20–32.

Donowitz, M., Singh, S., Salahuddin, F.F., Hogema, B.M., Chen, Y., Gucek, M., Cole, R.N., Ham, A., Zachos, N.C., Kovbasnjuk, O., et al. (2007). Proteome of murine jejunal brush border membrane vesicles. J. Proteome Res. *6*, 4068–4079.

Drokhlyansky, E., Smillie, C.S., Van Wittenberghe, N., Ericsson, M., Griffin, G.K., Eraslan, G., Dionne, D., Cuoco, M.S., Goder-Reiser, M.N., Sharova, T., et al. (2020). The Human and Mouse Enteric Nervous System at Single-Cell Resolution. Cell *182*, 1606–1622.e1623.

Elias, J.E., and Gygi, S.P. (2007). Target-decoy search strategy for increased confidence in large-scale protein identifications by mass spectrometry. Nat. Methods *4*, 207–214.

Everard, A., Belzer, C., Geurts, L., Ouwerkerk, J.P., Druart, C., Bindels, L.B., Guiot, Y., Derrien, M., Muccioli, G.G., Delzenne, N.M., et al. (2013). Cross-talk between Akkermansia muciniphila and intestinal epithelium controls diet-induced obesity. Proc. Natl. Acad. Sci. U.S.a. *110*, 9066–9071.

Finneran, D.J., Njoku, I.P., Flores-Pazarin, D., Ranabothu, M. R., Nash, K.R., Morgan, D., and Gordon, M.N. (2021). Towards Development of Neuron Specific Transduction After Systemic Delivery of Viral Vectors. Frontiers in Neurology *12*, 685802.

Fiorucci, S., Biagioli, M., Zampella, A., and Distrutti, E. (2018). Bile Acids Activated Receptors Regulate Innate Immunity. Frontiers in Immunology *9*, eaao1605–eaao1617.

Flandez, M., Guilmeau, S., Blache, P., and Augenlicht, L.H. (2008). KLF4 regulation in intestinal epithelial cell maturation. Experimental Cell Research *314*, 3712–3723.

Foong, J.P.P., Tough, I.R., Cox, H.M., and Bornstein, J.C. (2014). Properties of cholinergic and non-cholinergic submucosal neurons along the mouse colon. The Journal of Physiology *592*, 777–793.

Franzosa, E.A., McIver, L.J., Rahnavard, G., Thompson, L.R., Schirmer, M., Weingart, G., Lipson, K.S., Knight, R., Caporaso, J.G., Segata, N., et al. (2018). Species-level functional profiling of metagenomes and metatranscriptomes. Nat. Methods *15*, 962–968.

Fried, D.E., and Gulbransen, B.D. (2015). In situ Ca2+ imaging of the enteric nervous system. JoVE.

Fu, L., Niu, B., Zhu, Z., Wu, S., and Li, W. (2012). CD-HIT: accelerated for clustering the next-generation sequencing data. Bioinformatics *28*, 3150–3152.

Fung, C., Koussoulas, K., Unterweger, P., Allen, A. M., Bornstein, J. C., Foong, J. P. P. (2018). Cholinergic Submucosal Neurons Display Increased Excitability Following in Vivo Cholera Toxin Exposure in Mouse Ileum. Sec. Gastrointestinal Sciences 9.

Furness, J.B. (2012). The enteric nervous system and neurogastroenterology. Nature Reviews Gastroenterology and Hepatology *9*, 286–294.

Furness, J.B., Callaghan, B.P., Rivera, L.R., and Cho, H.-J. (2014). The Enteric Nervous System and Gastrointestinal Innervation: Integrated Local and Central Control. In The Enteric Nervous System, (New York, NY: Springer New York), pp. 39–71.

Furness, J.B. (2006). The Enteric Nervous System (Wiley-Blackwell).

Gabanyi, I., Muller, P.A., Feighery, L., Oliveira, T.Y., Costa-Pinto, F.A., and Mucida, D. (2016). Neuro-immune Interactions Drive Tissue Programming in Intestinal Macrophages. Cell *164*, 378–391.

Gatto, L., and Lilley, K.S. (2012). MSnbase-an R/Bioconductor package for isobaric tagged mass spectrometry data visualization, processing and quantitation. Bioinformatics *28*, 288–289.

Gershon, M.D. (2015). The Enteric Nervous System: A Second Brain. Hospital Practice *34*, 31–52.

Glenn, T.C., Nilsen, R.A., Kieran, T.J., Sanders, J.G., Bayona-Vásquez, N.J., Finger, J.W., Pierson, T.W., Bentley, K.E., Hoffberg, S.L., Louha, S., et al. (2019). Adapterama I: universal stubs and primers for 384 unique dual-indexed or 147,456 combinatorially-indexed Illumina libraries (iTru & iNext). PeerJ *7*, e7755.

Gonzalez, A., Navas-Molina, J.A., Kosciolek, T., McDonald, D., Vázquez-Baeza, Y., Ackermann, G., DeReus, J., Janssen, S., Swafford, A.D., Orchanian, S.B., et al. (2018). Qiita: rapid, web-enabled microbiome meta-analysis. Nat. Methods *15*, 796–798.

Gottlieb, A., and Canbay, A. (2019). Why Bile Acids Are So Important in Non-Alcoholic Fatty Liver Disease (NAFLD) Progression. Cells *8*.

Grundy, D., and Brookes, S. (2011). Neural Control of Gastrointestinal Function. Colloquium Series on Integrated Systems Physiology: From Molecule to Function *3*, 1–134.

Gurdeep Singh, R., Tanca, A., Palomba, A., Van der Jeugt, F., Verschaffelt, P., Uzzau, S., Martens, L., Dawyndt, P., and Mesuere, B. (2019). Unipept 4.0: Functional Analysis of Metaproteome Data. J. Proteome Res. *18*, 606–615.

Haenraets, K., Foster, E., Johannssen, H., Kandra, V., Frezel, N., Steffen, T., Jaramillo, V., Paterna, J.-C., Zeilhofer, H.U., and Wildner, H. (2017). Spinal nociceptive circuit analysis with recombinant adeno-associated viruses: the impact of serotypes and promoters. Journal of Neurochemistry *142*, 721–733.

Hama, H., Hioki, H., Namiki, K., Hoshida, T., Kurokawa, H., Ishidate, F., Kaneko, T., Akagi, T., Saito, T., Saido, T., et al. (2015). ScaleS: an optical clearing palette for biological imaging. Nat. Neurosci. *18*, 1518–1529.

Hamnett, R., Dershowitz, L.B., Sampathkumar, V., Wang, Z., Gomez-Frittelli, J., De Andrade, V., Kasthuri, N., Druckmann, S., Kaltschmidt, J.A. (2022). Regional

cytoarchitecture of the adult and developing mouse enteric nervous system. Curr. Biol. *32*, 1–10.

Hansen, M.B. (2003). The enteric nervous system II: Gastrointestinal functions. Pharmacol. Toxicol. *92*, 249–257.

He, L., Diedrich, J., Chu, Y.-Y., and Yates, J.R. (2015). Extracting Accurate Precursor Information for Tandem Mass Spectra by RawConverter. Anal. Chem. *87*, 11361–11367.

Hennig, G.W., Gould, T.W., Koh, S.D., Corrigan, R.D., Heredia, D.J., Shonnard, M.C., and Smith, T.K. (2015). Use of Genetically Encoded Calcium Indicators (GECIs) Combined with Advanced Motion Tracking Techniques to Examine the Behavior of Neurons and Glia in the Enteric Nervous System of the Intact Murine Colon. Front. Cell. Neurosci. *9*, 13819.

Hillmann, B., Al-Ghalith, G.A., Shields-Cutler, R.R., Zhu, Q., Gohl, D.M., Beckman, K.B., Knight, R., and Knights, D. (2018). Evaluating the Information Content of Shallow Shotgun Metagenomics. mSystems *3*, 457.

Hofmann, A.F., and Eckmann, L. (2006). How bile acids confer gut mucosal protection against bacteria. Proceedings of the National Academy of Sciences *103*, 4333–4334.

Huber, W., Heydebreck, von, A., Sültmann, H., Poustka, A., and Vingron, M. (2002). Variance stabilization applied to microarray data calibration and to the quantification of differential expression. Bioinformatics *18 Suppl 1*, S96–S104.

Hyland, N.P., and Cryan, J.F. (2010). A Gut Feeling about GABA: Focus on GABA(B) Receptors. Front Pharmacol *1*, 124.

Ichikawa, R., Takayama, T., Yoneno, K., Kamada, N., Kitazume, M.T., Higuchi, H., Matsuoka, K., Watanabe, M., Itoh, H., Kanai, T., et al. (2012). Bile acids induce monocyte differentiation toward interleukin-12 hypo-producing dendritic cells via a TGR5-dependent pathway. Immunology *136*, 153–162.

Jackson, K.L., Dayton, R.D., Deverman, B.E., and Klein, R.L. (2016). Better Targeting, Better Efficiency for Wide-Scale Neuronal Transduction with the Synapsin Promoter and AAV-PHP.B. Front. Mol. Neurosci. *9*, 116.

Jakob, MO., Kofoed-Branzk, M., Deshpande, D., Murugan, S., and Klose, C.S.N. An integrated view on neuronal subsets in the peripheral nervous system and their role in immunoregulation. Front. Immunol. *12*, 679055.

Jangi, S., Gandhi, R., Cox, L.M., Li, N., Glehn, von, F., Yan, R., Patel, B., Mazzola, M.A., Liu, S., Glanz, B.L., et al. (2016). Alterations of the human gut microbiome in multiple sclerosis. Nature Communications *7*, 12015–11.

Jarret, A., Jackson, R., Duizer, C., Healy, M.E., Zhao, J., Rone, J.M., Bielecki, P., Sefik, E., Roulis, M., Rice, T., et al. (2020). Enteric Nervous System-Derived IL-18 Orchestrates Mucosal Barrier Immunity. Cell *180*, 50–63.e12.

Jia, L., Betters, J.L., and Yu, L. (2011). Niemann-pick C1-like 1 (NPC1L1) protein in intestinal and hepatic cholesterol transport. Annu. Rev. Physiol. *73*, 239–259.

Johnson, C.D., Barlow-Anacker, A.J., Pierre, J.F., Touw, K., Erickson, C.S., Furness, J.B., Epstein, M.L., and Gosain, A. (2018). Deletion of choline acetyltransferase in enteric

neurons results in postnatal intestinal dysmotility and dysbiosis. The FASEB Journal *32*, 4744–4752.

Jones, B.V., Begley, M., Hill, C., Gahan, C.G.M., and Marchesi, J.R. (2008). Functional and comparative metagenomic analysis of bile salt hydrolase activity in the human gut microbiome. Proc. Natl. Acad. Sci. U.S.a. *105*, 13580–13585.

Kaelberer, M.M., Buchanan, K.L., Klein, M.E., Barth, B.B., Montoya, M.M., Shen, X., and Bohórquez, D.V. (2018). A gut-brain neural circuit for nutrient sensory transduction. Science *361*, eaat5236.

Kaestner, C.L., Smith, E.H., Peirce, S.G., and Hoover, D.B. (2019). Immunohistochemical analysis of the mouse celiac ganglion: An integrative relay station of the peripheral nervous system. J. Comp. Neurol. *16*, 2742-2760.

Kim, D., Langmead, B., and Salzberg, S.L. (2015). HISAT: a fast spliced aligner with low memory requirements. Nat. Methods *12*, 357–360.

Kirwan, W.O., Smith, A.N., Mitchell, W.D., Falconer, J.D., and Eastwood, M.A. (1975). Bile acids and colonic motility in the rabbit and the human. Gut *16*, 894–902.

Kotterman, M.A., and Schaffer, D.V. (2014). Engineering adeno-associated viruses for clinical gene therapy. Nat Rev Genet *15*, 445–451.

Kügler, S., Kilic, E., and Bähr, M. (2003). Human synapsin 1 gene promoter confers highly neuron-specific long-term transgene expression from an adenoviral vector in the adult rat brain depending on the transduced area. Gene Ther *10*, 337–347.

Lai, N.Y., Musser, M.A., Pinho-Ribeiro, F.A., Baral, P., Jacobson, A., Ma, P., Potts, D.E., Chen, Z., Paik, D., Soualhi, S., et al. (2019). Gut-Innervating Nociceptor Neurons Regulate Peyer's Patch Microfold Cells and SFB Levels to Mediate Salmonella Host Defense. Cell *180*, 33–49.e22.

Langmead, B., and Salzberg, S.L. (2012). Fast gapped-read alignment with Bowtie 2. Nat. Methods *9*, 357–359.

Latgé, J.P. (2007). The cell wall: a carbohydrate armour for the fungal cell. Molecular Microbiology *66*, 279–290.

Li, W., and Godzik, A. (2006). Cd-hit: a fast program for clustering and comparing large sets of protein or nucleotide sequences. Bioinformatics *22*, 1658–1659.

Li, W., Jaroszewski, L., and Godzik, A. (2001). Clustering of highly homologous sequences to reduce the size of large protein databases. Bioinformatics *17*, 282–283.

Li, W., Yu, G., Liu, Y., and Sha, L. (2019). Intrapancreatic Ganglia and Neural Regulation of Pancreatic Endocrine Secretion. Front. Neurosci *13,* 21.

Li, Z., Chalazonitis, A., Huang, Y.Y., Mann, J.J., Margolis, K.G., Yang, Q.M., Kim, D.O., Cote, F., Mallet, J., and Gershon, M.D. (2011). Essential Roles of Enteric Neuronal Serotonin in Gastrointestinal Motility and the Development/Survival of Enteric Dopaminergic Neurons. Journal of Neuroscience *31*, 8998–9009.

Lindeberg, J., Usoskin, D., Bengtsson, H., Gustafsson, A., Kylberg, A., Söderström, S., and Ebendal, T. (2004). Transgenic expression of Cre recombinase from the tyrosine hydroxylase locus. Genesis *40*, 67–73.

Long, S.L., Gahan, C.G.M., and Joyce, S.A. (2017). Interactions between gut bacteria and bile in health and disease. Mol. Aspects Med. *56*, 54–65.

Lott, E. L. & Jones, E. B. (2022). Cholinergic Toxicity. StatPearls.

Love, M.I., Huber, W., and Anders, S. (2014). Moderated estimation of fold change and dispersion for RNA-seq data with DESeq2. Genome Biol *15*, 1–21.

Marotz, C., Amir, A., Humphrey, G., Gaffney, J., Gogul, G., and Knight, R. (2017). DNA extraction for streamlined metagenomics of diverse environmental samples. Biotechniques. *62*, 290-293.

Martino, C., Morton, J.T., Marotz, C.A., Thompson, L.R., Tripathi, A., Knight, R., and Zengler, K. (2019). A Novel Sparse Compositional Technique Reveals Microbial Perturbations. mSystems *4*, 813.

Matheis, F., Muller, P.A., Graves, C.L., Gabanyi, I., Kerner, Z.J., Costa-Borges, D., Ahrends, T., Rosenstiel, P., and Mucida, D. (2020). Adrenergic Signaling in Muscularis Macrophages Limits Infection-Induced Neuronal Loss. Cell *180*, 64–78.e16.

Matsushima, S., Hori, S., and Matsuda, M. (1986). Conversion of 4-aminobutyraldehyde to gamma-aminobutyric acid in striatum treated with semicarbazide and kainic acid. Neurochem. Res. *11*, 1313–1319.

McConnell, R.E., Benesh, A.E., Mao, S., Tabb, D.L., and Tyska, M.J. (2011). Proteomic analysis of the enterocyte brush border. American Journal of Physiology - Gastrointestinal and Liver Physiology *300*, G914–G926.

McMillin, M., and DeMorrow, S. (2016). Effects of bile acids on neurological function and disease. Faseb J. *30*, 3658–3668.

McQuade, R. M., Singleton, L. M., Wu, H., Lee, S., Constable, R., Di Natale, M., Ringuet, M. T., Berger, J. P., Kauhausen, J., Parish, C. L., Finkelstein, D. I., Furness, J. B., Diwakarla, S. (2021). The association of enteric neuropathy with gut phenotypes in acute and progressive models of Parkinson's disease. Scientific Reports *11*.

Mesuere, B., Debyser, G., Aerts, M., Devreese, B., Vandamme, P., and Dawyndt, P. (2015). The Unipept metaproteomics analysis pipeline. Proteomics *15*, 1437–1442.

Miano, J.M., Miano, J.M., Vlasic, N., Vlasic, N., TOTA, R.R., Tota, R.R., STEMERMAN, M.B., and Stemerman, M.B. (1993). Smooth muscle cell immediate-early gene and growth factor activation follows vascular injury. A putative in vivo mechanism for autocrine growth. Arterioscler. Thromb. *13*, 211–219.

Mittal, R., Debs, L.H., Patel, A.P., Nguyen, D., Patel, K., O'Connor, G., Grati, M., Mittal, J., Yan, D., Eshraghi, A.A., et al. (2017). Neurotransmitters: The Critical Modulators Regulating Gut-Brain Axis. J. Cell. Physiol. *232*, 2359–2372.

Mohanta, S.K., Yin, C., Weber, C., Godinho-Silva, C., Veiga-Fernandes, H., Xu, Q.J., Chang, R.B., Habenicht, A.J.R. (2023). Cardiovascular Brain Circuits. Circulation Research *11*, 1546-1565.

Monane, M., Avorn, J., Beers, M.H., Everitt, D.E. (1993). Anticholinergic drug use and bowel function in nursing home patients. Arch. Intern. Med. *153*, 633-638.

Moran, G.W., Leslie F.C., Levison, S.E., Worthington, J., and McLaughlin, J.T. (2008). Enteroendocrine cells: neglected players in gastrointestinal disorders? Therap. Adv. Gastroenterol. *1*, 51-60.

Muller, P.A., Koscsó, B., Rajani, G.M., Stevanovic, K., Berres, M.-L., Hashimoto, D., Mortha, A., Leboeuf, M., Li, X.-M., Mucida, D., et al. (2014). Crosstalk between Muscularis Macrophages and Enteric Neurons Regulates Gastrointestinal Motility. Cell *158*, 1210.

Niesler, B., Kuerten, S., Demir, I.E., and Schäfer, K.H. (2021). Disorders of the enteric nervous system - a holistic view. Nat Rev Gastroenterol Hepatol. *18*, 393-410.

Nezami, B.G. & Srinivasan, S. (2013). Enteric Nervous System in the Small Intestine: Pathophysiology and Clinical Implications. Current Gastroenterology Reports *12,* 258-365.

Nishiyama, H., Nagai, T., Kudo, M., Okazaki, Y., Azuma, Y., Watanabe, T., Goto, S., Ogata, H., and Sakurai, T. (2018). Supplementation of pancreatic digestive enzymes alters the composition of intestinal microbiota in mice. Biochem. Biophys. Res. Commun. *495*, 273–279.

Nothias, L.F., Petras, D., Schmid, R., Dührkop, K., Rainer, J., Sarvepalli, A., Protsyuk, I., Ernst, M., Tsugawa, H., Fleischauer, M., et al. (2019). Feature-based Molecular Networking in the GNPS Analysis Environment. bioRxiv *38*, 812404.

Olson, C.A., Vuong, H.E., Yano, J.M., Liang, Q.Y., Nusbaum, D.J., and Hsiao, E.Y. (2018). The Gut Microbiota Mediates the Anti-Seizure Effects of the Ketogenic Diet. Cell *173*, 1728–1741.e13.

Park, S.K.R., Jung, T., Thuy-Boun, P.S., Wang, A.Y., John R Yates, I., and Wolan, D.W. (2018). ComPIL 2.0: An Updated Comprehensive Metaproteomics Database. J. Proteome Res. *18*, 616–622.

Park, S.K., Venable, J.D., Xu, T., and Yates, J.R. (2008). A quantitative analysis software tool for mass spectrometry–based proteomics. Nat. Methods *5*, 319–322.

Peng, J., Elias, J.E., Thoreen, C.C., Licklider, L.J., and Gygi, S.P. (2003). Evaluation of multidimensional chromatography coupled with tandem mass spectrometry (LC/LC-MS/MS) for large-scale protein analysis: the yeast proteome. J. Proteome Res. *2*, 43–50.

Pfeiffer, R.F. (2003). Gastrointestinal dysfunction in Parkinson's disease. Lancet Neurol *2*, 107–116.

Plovier, H., Everard, A., Druart, C., Depommier, C., Van Hul, M., Geurts, L., Chilloux, J., Ottman, N., Duparc, T., Lichtenstein, L., et al. (2017). A purified membrane protein from Akkermansia muciniphila or the pasteurized bacterium improves metabolism in obese and diabetic mice. Nature Medicine *23*, 107–113.

Pluskal, T., Castillo, S., Villar-Briones, A., and Oresic, M. (2010). MZmine 2: Modular framework for processing, visualizing, and analyzing mass spectrometry-based molecular profile data. BMC Bioinformatics *11*.

Qu, Z.D., Thacker, M., Castelucci, P., Bagyánszki, M., Epstein, M.L., Furness, J.B. (2008). Immunohistochemical analysis of neuron types in the mouse small intestine. Cell and tissue research *334*, 147–161.

Rajendran, P.S., Challis, R.C., Fowlkes, C.C., Hanna, P., Tompkins, J.D., Jordan, M.C., Hiyari, S., Gabris-Weber, B.A., Greenbaum, A., Chan, K.Y., et al. (2019). Identification of peripheral neural circuits that regulate heart rate using optogenetic and viral vector strategies. Nature Communications 10, 1944.

Rakhilin, N., Barth, B., Choi, J., Muñoz, N.L., Kulkarni, S., Jones, J.S., Small, D.M., Cheng, Y.-T., Cao, Y., LaVinka, C., et al. (2016). Simultaneous optical and electrical in vivo analysis of the enteric nervous system. Nature Communications *7*, 31.

Rakhilin, N., Garrett, A., Eom, C.-Y., Chavez, K.R., Small, D.M., Daniel, A.R., Kaelberer, M.M., Mejooli, M.A., Huang, Q., Ding, S., et al. (2019). An intravital window to image the colon in real time. Nature Communications *10*, 5647–10.

Ramirez-Carrozzi, V.R., Braas, D., Bhatt, D.M., Cheng, C.S., Hong, C., Doty, K.R., Black, J.C., Hoffmann, A., Carey, M., and Smale, S.T. (2009). A Unifying Model for the Selective Regulation of Inducible Transcription by CpG Islands and Nucleosome Remodeling. Cell *138*, 114–128.

Rao, M., and Gershon, M.D. (2016). The bowel and beyond: the enteric nervous system in neurological disorders. Nature Reviews Gastroenterology and Hepatology *13*, 517–528.

Ritchie, M.E., Phipson, B., Wu, D., Hu, Y., Law, C.W., Shi, W., and Smyth, G.K. (2015). limma powers differential expression analyses for RNA-sequencing and microarray studies. Nucleic Acids Res *43*, e47–e47.

Rodríguez-Piñeiro, A.M., Bergström, J.H., Ermund, A., Gustafsson, J.K., Schütte, A., Johansson, M.E.V., and Hansson, G.C. (2013). Studies of mucus in mouse stomach, small intestine, and colon. II. Gastrointestinal mucus proteome reveals Muc2 and Muc5ac accompanied by a set of core proteins. American Journal of Physiology - Gastrointestinal and Liver Physiology *305*, G348–G356.

Roy, A., Guatimosim, S., Prado, V.F., Gros, R., Prado, M.A. (2015). Cholinergic activity as a new target in diseases of the heart. Molecular Medicine *20*, 527–537.

Sakai, K., Makino, T., Kawai, Y., and Mutai, M. (1980). Intestinal microflora and bile acids. Effect of bile acids on the distribution of microflora and bile acid in the digestive tract of the rat. Microbiol. Immunol. *24*, 187–196.

Samulski, R.J., and Muzyczka, N. (2014). AAV-Mediated Gene Therapy for Research and Therapeutic Purposes. Annu Rev Virol *1*, 427–451.

Sang, Q., and Young, H.M. (1998). The identification and chemical coding of cholinergic neurons in the small and large intestine of the mouse. Anat. Rec. *251*, 185–199.

Sannasiddappa, T.H., Lund, P.A., and Clarke, S.R. (2017). In Vitro Antibacterial Activity of Unconjugated and Conjugated Bile Salts on Staphylococcus aureus. Front. Microbio. *8*, 1581.

Schneider, S., Wright, C.M., and Heuckeroth, R.O. (2019). Unexpected Roles for the Second Brain: Enteric Nervous System as Master Regulator of Bowel Function. Annu. Rev. Physiol. *81*, 235–259.

Segata, N., Izard, J., Waldron, L., Gevers, D., Miropolsky, L., Garrett, W.S., and Huttenhower, C. (2011). Metagenomic biomarker discovery and explanation. Genome Biol *12*, R60.

Seillet, C., Luong, K., Tellier, J., Jacquelot, N., Shen, R.D., Hickey, P., Wimmer, V.C., Whitehead, L., Rogers, K., Smyth, G.K., et al. (2020). The neuropeptide VIP confers anticipatory mucosal immunity by regulating ILC3 activity. Nat Immunol *21*, 168–177.

Shan Li, Z., Schmauss, C., Cuenca, A., Ratcliffe, E., Gershon, M. D. (2006). Physiological Modulation of Intestinal Motility by Enteric Dopaminergic Neurons and the D2 Receptor: Analysis of Dopamine Receptor Expression, Location, Development, and Function in Wild-Type and Knock-Out Mice. J Neurosci. *26*, 2798-2807.

Sinha, R., Stanley, G., Gulati, G.S., Ezran, C., Travaglini, K.J., Wei, E., Chan, C.K.F., Nabhan, A.N., Su, T., Morganti, R.M., et al. (2017). Index switching causes “spreading-of-signal” among multiplexed samples in Illumina HiSeq 4000 DNA sequencing. *29*, 1072–29.

Steele, P.A., Brookes, S.J., and Costa, M. (1991). Immunohistochemical identification of cholinergic neurons in the myenteric plexus of guinea-pig small intestine. Neuroscience *45*, 227–239.

Sumner, L.W., Amberg, A., Barrett, D., Beale, M.H., Beger, R., Daykin, C.A., Fan, T.W.M., Fiehn, O., Goodacre, R., Griffin, J.L., et al. (2007). Proposed minimum reporting standards for chemical analysis Chemical Analysis Working Group (CAWG) Metabolomics Standards Initiative (MSI). Metabolomics *3*, 211–221.

Sundararajan, Z., Knoll, R., Hombach, P., Becker, M., Schultze, J.L., and Ulas, T. (2019). Shiny-Seq: advanced guided transcriptome analysis. BMC Res Notes *12*, 432–435.

Suzek, B.E., Huang, H., McGarvey, P., Mazumder, R., and Wu, C.H. (2007). UniRef: comprehensive and non-redundant UniProt reference clusters. Bioinformatics *23*, 1282–1288.

Szklarczyk, D., Gable, A.L., Lyon, D., Junge, A., Wyder, S., Huerta-Cepas, J., Simonovic, M., Doncheva, N.T., Morris, J.H., Bork, P., et al. (2019). STRING v11: protein-protein association networks with increased coverage, supporting functional discovery in genome-wide experimental datasets. Nucleic Acids Res *47*, D607–D613.

Tabb, D.L., McDonald, W.H., and Yates, J.R. (2002). DTASelect and Contrast: tools for assembling and comparing protein identifications from shotgun proteomics. J. Proteome Res. *1*, 21–26.

Talbot, J., Hahn, P., Kroehling, L., Nguyen, H., Li, D., and Littman, D.R. (2020). Feeding-dependent VIP neuron-ILC3 circuit regulates the intestinal barrier. Nature *579*, 575–580.

Tavares-Ferreira, D., Shiers, S., Ray, P.R., Wangzhou, A., Jeevakumar, V., Sankaranarayanan, I., Cervantes, A.M., Reese, J.C., Chamessian, A., Copits, B.A., Dougherty, P.M., Gereau, R.W., Burton, M.D., Dussor, G., and Price, T.J. (2022). Spatial transcriptomics of the dorsal root ganglia identifies molecular signatures of human nociceptors. Sci. Transl. Med. *14*, eabj8186.

Thompson, K.J., Khajehali, E., Bradley, S.J., Navarrete, J.S., Huang, X.P., Slocum, S., Jin, J., Liu, J., Xiong, Y., Olsen, R.H.J., et al. (2018). DREADD Agonist 21 Is an Effective Agonist for Muscarinic-Based DREADDs in Vitro and in Vivo. ACS Pharmacol Transl Sci *1*, 61–72.

Treweek, J.B., Chan, K.Y., Flytzanis, N.C., Yang, B., Deverman, B.E., Greenbaum, A., Lignell, A., Xiao, C., Cai, L., Ladinsky, M.S., et al. (2015). Whole-body tissue stabilization and selective extractions via tissue-hydrogel hybrids for high-resolution intact circuit mapping and phenotyping. Nature Protocols *10*, 1860–1896.

Truong, D.T., Franzosa, E.A., Tickle, T.L., Scholz, M., Weingart, G., Pasolli, E., Tett, A., Huttenhower, C., and Segata, N. (2015). MetaPhlAn2 for enhanced metagenomic taxonomic profiling. Nat. Methods *12*, 902–903.

Valicenti-McDermott, M.D., McVicar, K., Cohen, H.J., Wershil, B.K., and Shinnar, S. (2008). Gastrointestinal symptoms in children with an autism spectrum disorder and language regression. Pediatr. Neurol. *39*, 392–398.

Van Herreweghen, F., Van den Abbeele, P., De Mulder, T., De Weirdt, R., Geirnaert, A., Hernandez-Sanabria, E., Vilchez-Vargas, R., Jauregui, R., Pieper, D.H., Belzer, C., et al. (2017). In vitro colonisation of the distal colon by Akkermansia muciniphila is largely mucin and pH dependent. Benef Microbes *8*, 81–96.

Vavassori, P., Mencarelli, A., Renga, B., Distrutti, E., and Fiorucci, S. (2009). The bile acid receptor FXR is a modulator of intestinal innate immunity. J Immunol *183*, 6251–6261.

Walsh, K.T., and Zemper, A.E. (2019). The Enteric Nervous System for Epithelial Researchers: Basic Anatomy, Techniques, and Interactions With the Epithelium. Cellular and Molecular Gastroenterology and Hepatology *8*, 369–378.

Wang, H. Foong, J. P. P., Harris, N. L., Bornstein, J. C. (2022). Enteric neuroimmune interactions coordinate intestinal responses in health and disease. Mucosal Immunology 15, 27-39.

Wang, M., Carver, J.J., Phelan, V.V., Sanchez, L.M., Garg, N., Peng, Y., Nguyen, D.D., Watrous, J., Kapono, C.A., Luzzatto-Knaan, T., et al. (2016). Sharing and community curation of mass spectrometry data with Global Natural Products Social Molecular Networking. Nat Biotechnol *34*, 828–837.

Watanabe, M., Houten, S.M., Mataki, C., Christoffolete, M.A., Kim, B.W., Sato, H., Messaddeq, N., Harney, J.W., Ezaki, O., Kodama, T., et al. (2006). Bile acids induce energy expenditure by promoting intracellular thyroid hormone activation. Nature *439*, 484–489.

Wess, J., Nakajima, K., and Jain, S. (2013). Novel designer receptors to probe GPCR signaling and physiology. Trends Pharmacol. Sci. *34*, 385–392.

Wessel, D., and Flügge, U.I. (1984). A method for the quantitative recovery of protein in dilute solution in the presence of detergents and lipids. Analytical Biochemistry *138*, 141–143.

Whitcomb, D.C., and Lowe, M.E. (2007). Human pancreatic digestive enzymes. Dig. Dis. Sci. *52*, 1–17.

Wu, Y.E., Pan, L., Zuo, Y., Li, X., and Hong, W. (2017). Detecting Activated Cell Populations Using Single-Cell RNA-Seq. Neuron *96*, 313–329.e316.

Xu, T., Park, S.K., Venable, J.D., Wohlschlegel, J.A., Diedrich, J.K., Cociorva, D., Lu, B., Liao, L., Hewel, J., Han, X., et al. (2015). ProLuCID: An improved SEQUEST-like algorithm with enhanced sensitivity and specificity. J Proteomics *129*, 16–24.

Xu, T., Venable, J.D., Park, S.K., Cociorva, D., Lu, Q.B., Liao, L., Wohlschlegel, J., Hewel, J., Yates, J.R., and Conciorva, D. (2006). ProLuCID, a fast and sensitive tandem mass spectra-based protein identification program.

Yang, B., Treweek, J.B., Kulkarni, R.P., Deverman, B.E., Chen, C.-K., Lubeck, E., Shah, S., Cai, L., and Gradinaru, V. (2014). Single-Cell Phenotyping within Transparent Intact Tissue through Whole-Body Clearing. Cell *158*, 945–958.

Yano, J.M., Yu, K., Donaldson, G.P., Shastri, G.G., Ann, P., Ma, L., Nagler, C.R., Ismagilov, R.F., Mazmanian, S.K., and Hsiao, E.Y. (2015). Indigenous Bacteria from the Gut Microbiota Regulate Host Serotonin Biosynthesis. Cell *161*, 264–276.

Zhang, H., Sparks, J.B., Karyala, S.V., Settlage, R., and Luo, X.M. (2015). Host adaptive immunity alters gut microbiota. Isme J *9*, 770–781.

Zhang, X., Smits, A.H., van Tilburg, G.B., Ovaa, H., Huber, W., and Vermeulen, M. (2018). Proteome-wide identification of ubiquitin interactions using UbIA-MS. Nature Protocols *13*, 530–550.

Zhu, Q., Mai, U., Pfeiffer, W., Janssen, S., Asnicar, F., Sanders, J.G., Belda-Ferre, P., Al-Ghalith, G.A., Kopylova, E., McDonald, D., et al. (2019). Phylogenomics of 10,575 genomes reveals evolutionary proximity between domains Bacteria and Archaea. Nature Communications *10*, 5477–14.

*Chapter 3*

# GENETIC AND ENVIRONMENTAL EFFECTS ON AUTISM-RELATED BEHAVIORS AND GASTROINTESTINAL DYSFUNCTION IN MICE

**Griffiths J. A.**, Thron T. M., Glynn A. T., Mazmanian S. K.

**PREFACE**

Autism impacts over 3 million people in the US, and is diagnosed based on altered social communication and repetitive behaviors. Interestingly for a neurodevelopmental condition, individuals on the autism spectrum are three times more likely to experience chronic gastrointestinal (GI) problems than the general population. Recently, several lines of evidence have implicated a role for the gut microbiome, the trillions of bacteria living within the human intestine, as a major factor in GI symptoms and altered behaviors in autism. Individuals on the autism spectrum who have GI issues display worse behavioral outcomes than those without, and the microbiome differs between people with autism and the general population. A first-of-its-kind human trial conducted fecal microbiota transplants (FMT) in children on the autism spectrum and reported a significant reduction in GI symptoms and some alleviation of autism-associated behaviors.

This project explores the genetic and environmental interactions in an established mouse model of autism by studying the gut and gut microbiome and identifying changes in neurotransmitter release, immune responses, and GI function.

Testing the contribution of an autism risk gene to GI function is important for advancing knowledge into potential causes for intestinal issues and, possibly, altered behavioral patterns. Understanding the biology behind how the gut impacts disease-relevant outcomes in a mouse model of autism promises to be an important step toward developing safe and effective therapies for autism.

## INTRODUCTION

It is estimated that between 1% and 2% of individuals in the United States have autism[1]. Autism is likely a collection of complex and heterogeneous disorders with numerous genetic etiologies, many relating to synaptic transmission between neurons[2]. One example is *SHANK3*, a gene that codes for a scaffolding protein in the synapse of glutaminergic (excitatory) neurons that binds many postsynaptic density proteins important for neurotransmission[3]. Variants of *SHANK3*, including de novo insertions in exon 21 and a deletion of terminal 22q13 associated with Phelan-McDermid Syndrome (PMS), are found in ~1% of autism cases[3].

Gastrointestinal (GI) symptoms impact 23% to 70% of individuals on the autism spectrum[4]. These GI issues include chronic constipation, diarrhea, gastroesophageal reflux, abdominal pain, bloating, and vomiting[4,5]. Interestingly, problems such as constipation, diarrhea, and vomiting may occur at higher rates in individuals with PMS and other *SHANK3* mutations than in the general population of individuals with autism[4,6–8]. Additionally, dozens of studies have found altered microbiomes in individuals on the autism spectrum compared to the general population[9], and a single study that replaced the microbiome communities of children on the autism spectrum with fecal transplants reported improved behavior and markedly reduced GI symptoms[10].

It was recently reported that *Shank3*$^{-/-}$ mice harbor microbiomes that are different than control mice, though it is unknown what factors cause this change[11]. Further, probiotic treatment with *Lactobacillus reuteri* improves altered behaviors in *Shank3*$^{-/-}$ mice[11,12].

This evidence is part of a growing body of literature suggesting that the gut microbiome profoundly impacts behavior in mouse models and human studies, including anxiety, depression, fear, aggression, and behaviors related to schizophrenia and autism[9,13–18].To explore the mechanistic underpinnings of the observations relating to autism, this work investigates the hypothesis that impaired synaptic transmission in the gut alters GI function and shifts the microbiome in subjects with autism to a state that disrupts the normal crosstalk between the gut and the brain. In other words, the signals sent from the gut to the brain may be different between individuals on the autism spectrum and the general population.

## RESULTS

### The microbiome partially mediates autism-like behaviors in *Shank3B*$^{-/-}$ mice

Several studies have suggested that environmental factors, including the microbiome, interact with genetics to trigger and modulate autism-related phenotypes[19]. Almost two dozen studies have indicated abnormal microbiome communities in children with autism[9,20–33]. Further, a fecal microbiota transplant (FMT) study conducted on a group of children with autism reported an 80% decrease in gastrointestinal (GI) symptoms and improvements in behavior[10,34]. A number of studies have implicated the gut microbiome as a contributor to GI and autism-like phenotypes in mice[14,35,36], including recent studies in full body *Shank3*-knockout models[11,12]. Thus, mounting evidence suggests a role for gut microbiota in both the GI and behavioral symptom severity in autism. Here, we explore if gut bacteria are required for the behavioral symptoms associated with mutations in the *Shank3* gene. Our studies were performed with the *Shank3B*$^{-/-}$ mouse line, which is deficient in the major isoforms of the SHANK3 protein.

Mouse models are inherently limited in recapitulating symptoms of autism[37,38]. With these constraints, behavioral paradigms have been developed to reflect the diagnostic criteria for Autism Spectrum Disorder in the fifth edition of the Diagnostic and Statistical Manual of Mental Disorders (DSM-5) released by the American Psychiatric Association: abnormal social interaction, repetitive behavior, and anxiety-like behavior, which is a common comorbidity[39,40]. The hallmark behavioral features of *Shank3B*$^{-/-}$ male mice include increased grooming in a 2-hour time period, reduced rearing in open field, decreased exploration of open arms in elevated zero maze, and decreased social

interaction in the three-chamber social interaction test[41]. To test if the absence of a microbiome effects anxiety and autism-like behaviors in the *Shank3B*$^{-/-}$ mouse model, we rederived *Shank3B*$^{-/-}$ mouse line into the germ-free (GF) condition in gnotobiotic isolators and performed an expanded set of behavioral tests with mice raised in the GF condition to compare to the SPF phenotype (Table 1).

| Test | Purpose |
|---|---|
| Grooming | Repetitive behavior |
| Direct Social Interaction | Social Behavior |
| Ultrasonic Vocalization | Social Behavior |
| Elevated Zero Maze | Anxiety-like behavior |
| Open Field Test | Anxiety-like behavior |

**Table 1. Purpose of mouse behavioral tests used to assay autism-related behaviors**

To test anxiety related behavior, we exposed *Shank3B*$^{-/-}$ and WT mice in both the SPF and GF condition to the open-field test and elevated zero maze (Figures 1 & 2). We found that the presence of a microbiome did not affect anxiety-related behavior. Unexpectedly, we did not observe a difference in anxiety-related behavior between SPF *Shank3B*$^{-/-}$ mice and SPF WT controls in three repetitions of behavioral experiments with different cohorts, as was reported in the original publication[41]. In support of this contradictory data, a similar mouse model with a larger deletion of the *Shank3* gene (exons 4-22) also does not show prominent anxiety phenotypes[42].

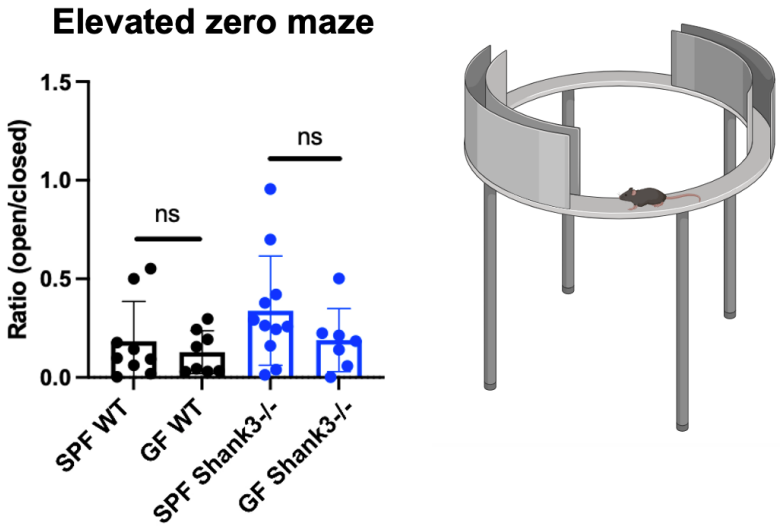


**Figure 1. Elevated zero maze.** *Shank3B*$^{-/-}$ male mice spent less time in the open arm in the elevated zero maze. The GF condition did not affect this phenotype. Figure created with BioRender.com.

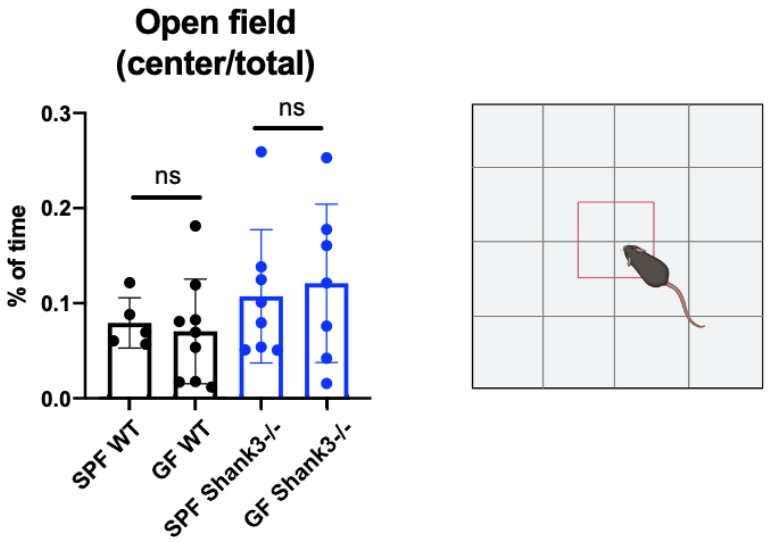


**Figure 2. Open field test.** *Shank3B*$^{-/-}$ male mice spent less time in the center region of the open field arena. The GF condition did affect this phenotype. Figure created with BioRender.com.

To examine repetitive behavior phenotypes, we quantified time spent grooming in a 10-minute period. As expected, we observed a genotype effect on grooming behavior between *Shank3B*$^{-/-}$ and WT mice (Figure 3). Notably, we identified a reduction of grooming by *Shank3B*$^{-/-}$ mice in the GF condition, which is a novel finding.

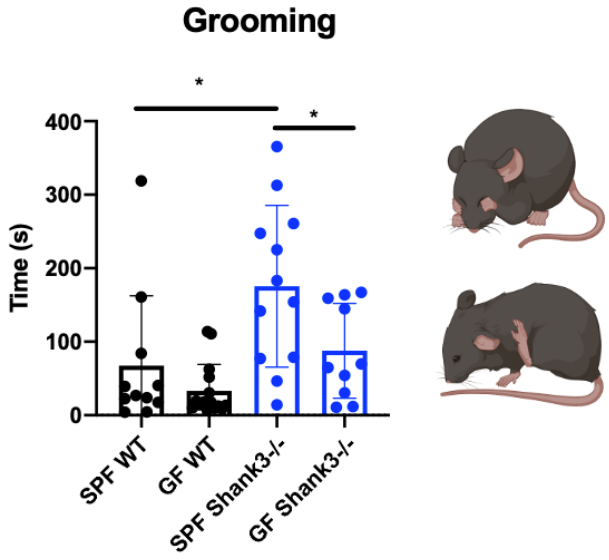


**Figure 3. Grooming.** *Shank3B*$^{-/-}$ mice spent more time self-grooming than WT controls. GF *Shank3B*$^{-/-}$ mice groomed less than the SPF condition. (*p<0.05, determined by Welch's two-tailed t-test). Figure created with BioRender.com.

As two metrics of social behavior, we tested direct social interaction (DSI) and ultrasonic vocalization (USV) in male subject mice. We observed a trending reduction in socialization in SPF *Shank3B*$^{-/-}$ mice as compared to SPF WT mice in the DSI test with an age-matched male WT mouse (Figure 4). The presence of a microbiome modulated this behavior, as GF *Shank3B*$^{-/-}$ socialized more than SPF *Shank3B*$^{-/-}$ mice. This is a surprising result, as a different study reported that the *Shank3*$^{4\text{-}22\text{-}/-}$ mice treated with antibiotics socialized less than vehicle-treated *Shank3*$^{4\text{-}22\text{-}/-}$ controls in the three-chamber

social interaction test[42]. To assess social behavior with age-matched female mice, we used the USV test to measure mating-related vocalizations. This test has shown differing results across *Shank3*$^{-/-}$ studies[43], so we did not have an anticipated outcome. We found that there was a genotype effect, as SPF *Shank3B*$^{-/-}$ male mice vocalized less to females than SPF WT male mice in both duration of call and number of calls (Figure 5). The presence of a microbiome effected the phenotype, as GF *Shank3B*$^{-/-}$ vocalized more than SPF *Shank3B*$^{-/-}$ males. An important consideration to consider regarding these social interaction findings is the lack of GF WT controls, which is addressed in a note at the end of the behavior results. Although we cannot make a direct comparison, other studies have evaluated differences in social behavior between SPF and GF WT mice. In another study performed in our lab, GF WT male mice socialized less than SPF WT male mice in a direct social interaction test, a phenotype mediated by altered stress responses and the HPA axis[44]. This finding is reinforced by another investigation, in which GF WT mice did not show the preference for the social chamber of the three-chamber social interaction test that is observed in the SPF WT case[45]. In contrast, one study reported GF WT males that socialized more than SPF WT and another reported no difference between the two groups[46,47]. The conflicting evidence makes it difficult to build a strong hypothesis about the missing GF WT control group from my findings, and also highlights the variability in behavioral results across labs. The most probable result is decreased social interaction of GF WT male mice as compared to SPF males, since the study was performed with similar methods in the same facilities and with the same equipment as my experiments. Differences in socialization of SPF or GF male mice with females have not been

characterized in the literature, so it is unclear if there would have been a phenotype between these groups in the USV test.

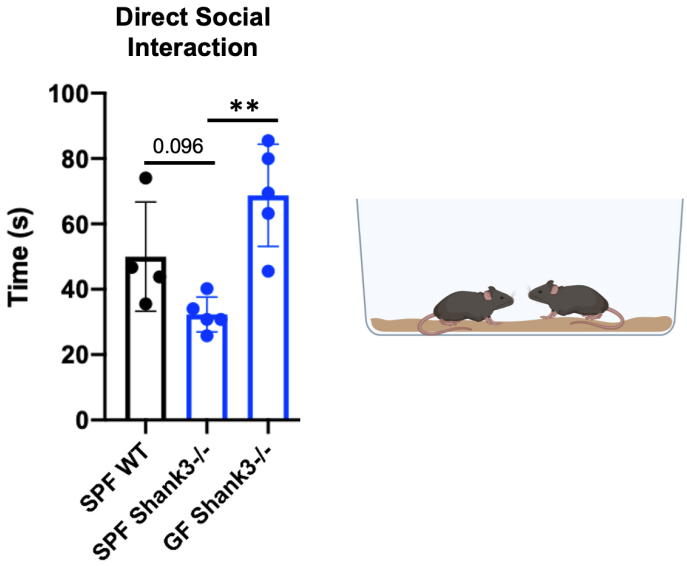


**Figure 4. Direct social interaction test.** *Shank3B*$^{-/-}$ male mice tended to spend less time socializing than WT controls in a direct social interaction test, but the result was not significant. GF Shank3B$^{-/-}$ socialized more than the SPF condition. ( **p<0.01, determined by Welch's two-tailed t-test). Figure created with BioRender.com.

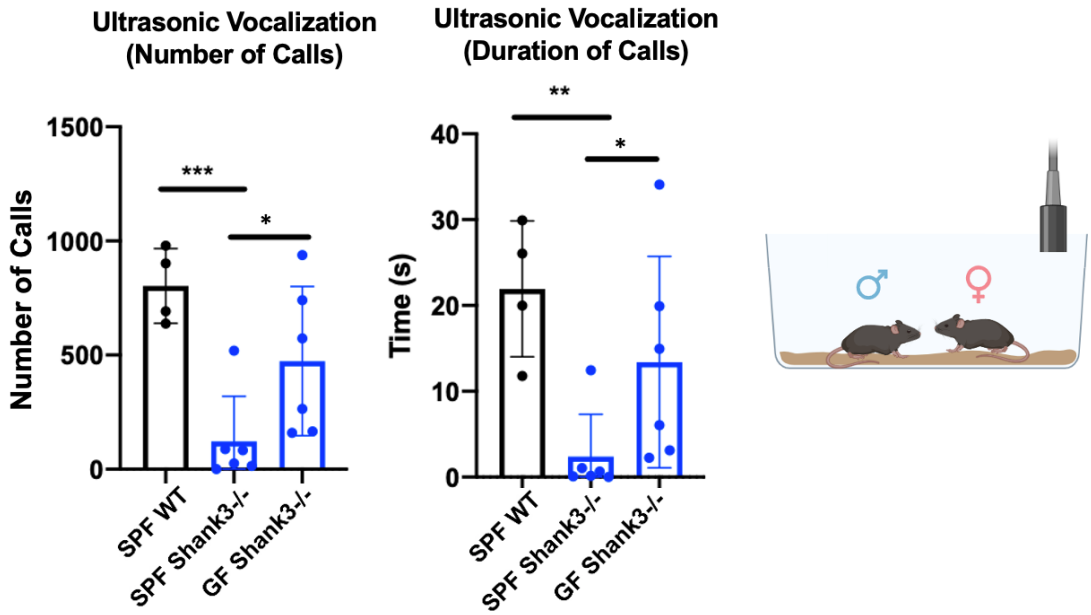

**Figure 5. Ultrasonic vocalization test.** Shank3B$^{-/-}$ male mice vocalized less with female mice than WT controls in the ultrasonic vocalization test. GF Shank3B$^{-/-}$ vocalized more than the SPF condition. (*p<0.05, **p<0.01, ***p<0.001 determined by Welch's one-tailed t-test). Figure created with BioRender.com.

Note:

Unfortunately, the lab experienced two sequential contaminations of different GF gnotobiotic isolators that contained the *Shank3B*$^{-/-}$ mice, causing us to lose the genetic line before these pilot experiments could be performed with larger cohorts. This roadblock would have taken great resources and time to overcome so we decided to focus on other experiments.

### *Shank3B*$^{-/-}$ mice have altered gastrointestinal function

Gastrointestinal (GI) symptoms are common in children with autism, and with *SHANK3* loss-of-function mutations such as those associated with PMS[4,6]. It also has been shown that knockdown of SHANK3 leads to intestinal permeability, also known as "leaky gut," after dextran sulfate sodium (DSS) induced colitis in mice[48]. Additionally, *Shank3* knockouts in zebrafish display GI abnormalities in motility and inflammation[49].

The causes of GI symptoms in people with autism and in experimental models are unknown. Studies have not yet been conducted to characterize GI dysfunction in *Shank3*$^{-/-}$ mice. GI studies have been conducted using mice with mutations in genes that interact with *Shank3*, such as the gene encoding the synaptic protein NLGN3[50,51]. *Nlgn3*$^{R451C}$ mice display abnormal GI motility, shown by video imaging of GI explants, suggesting that

mutations in synaptic proteins may contribute to GI abnormalities in autism[51]. Herein, I characterize GI dysfunction in Shank3B$^{-/-}$ mice (knockout of exons 13-16) from an immunological, microbiological, and neurological perspective.

Gastrointestinal Motility

In investigating gastrointestinal function, our initial focus was on motility due to its association with nervous system activity. As SHANK3 is a protein involved in excitatory signaling in the CNS[52], we hypothesized that it may play a similar role in the PNS. In the simplest model of GI motility, impaired excitatory signaling in the ENS would result in slower GI transit[53]. Inhibition of the excitatory cholinergic neurons in the ENS results in slower GI transit, and excitation of the same subset results in faster GI transit (Chapter 2)[54–57]. To test motility, we performed a whole gut transit time assay with carmine red dye. Surprisingly, Shank3B$^{-/-}$ had faster transit time compared to WT controls (Figure 6A). To dissect the biology behind this phenotype, we performed additional motility tests to test motility of different GI locations. We used a small intestinal transit assay with Evans blue dye and observed that Shank3B$^{-/-}$ mice did not have altered GI transit in the small intestine (Figure 6B). This was an unanticipated result, as we expected GI transit to be similarly disturbed across different regions of the GI tract. To further investigate transit in the colon, we used an *ex vivo* apparatus to quantify colonic migrating motor complexes (CMMCs) in colon explants. Migrating motor complexes (MMCs) are the propagating constriction of the muscles around the gut, which propels luminal material to the distal end of the gut[51]. Shank3B$^{-/-}$ mice initiated more CMMCs per unit time than WT controls (Figure 7). This suggests that the colon is the primary contributor to the motility phenotype.

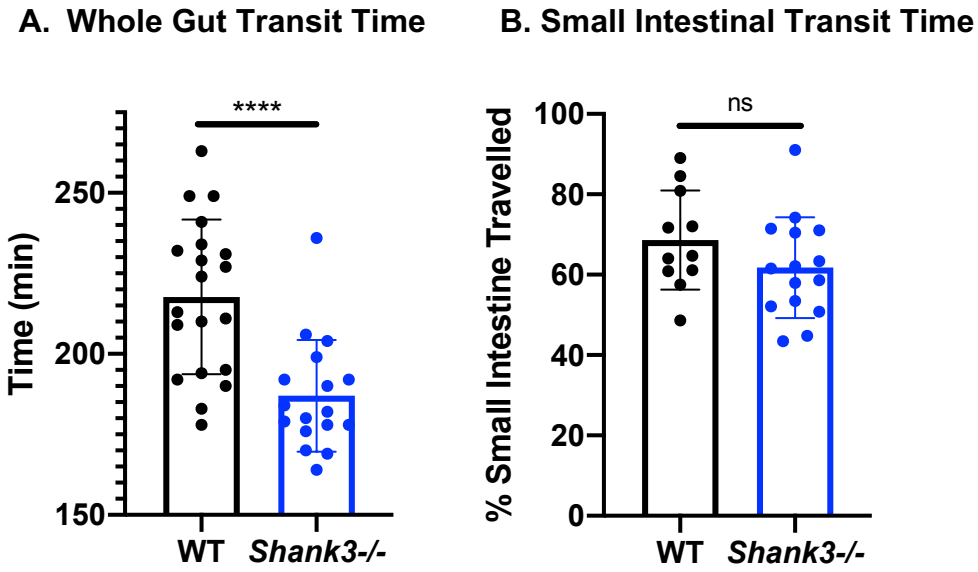


**Figure 6. In vivo gastrointestinal transit time.** Whole gut transit time and small intestinal transit time of Shank3B$^{-/-}$ and WT mice. (****p<0.0001, determined by Welch's two-tailed t-test)

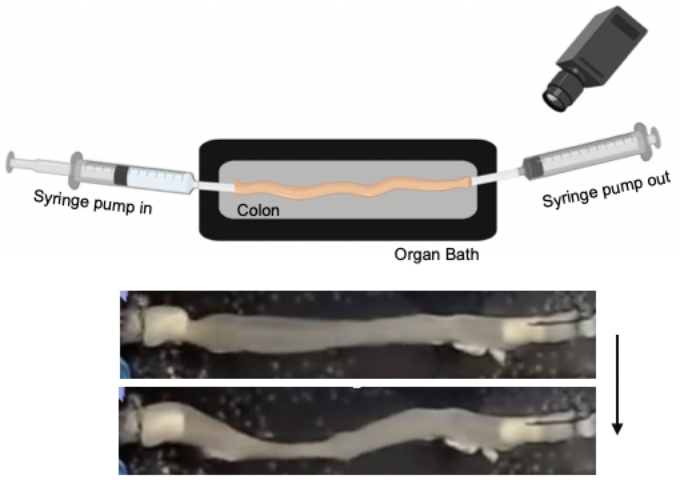


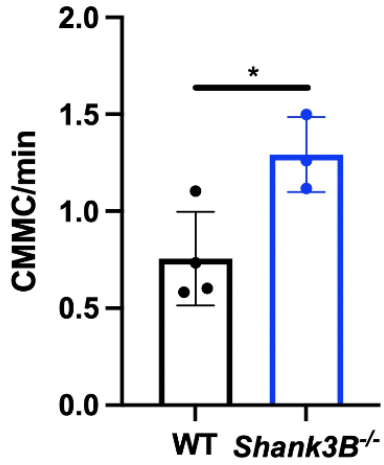


**Figure 7. Ex vivo colonic migrating motor complexes.** Number of motor complexes per minute in WT and Shank3B$^{-/-}$ mice (*$p<0.05$ determined by Welch's two-tailed t-test). Figure created with BioRender.com.

In a more complete model of GI physiology, motility is affected by many factors besides enteric neurons. Diet, microbiome, hormones, and enteric glia, as well as inputs from the CNS and prevertebral ganglia all influence this phenotype[58–66]. Since multiple publications

have reported microbiome differences in *Shank3*$^{-/-}$ mice, we hypothesized that the gut microbiome may contribute to altered motility[11,12,42,67]. To separate the role of the microbiome on motility, we treated mice with a broad-spectrum antibiotic cocktail (ampicillin, vancomycin, neomycin, and metronidazole) known to effectively deplete the microbiome to a near GF condition[44,68]. The lack of microbiome almost doubled GI transit time in both groups, and the altered motility phenotype between the Shank3B$^{-/-}$ and WT mice disappeared (Figure 8). Prolonged intestinal transit is a known phenotype in GF and antibiotic-treated animals, influenced by a loss of enteric neurons and reduced expression of microbially-modulated genes important for GI transit[69]. Taking these factors into account, the motility data with and without antibiotic treatment suggests that the interaction between the microbiome and genotype influences the difference in whole gut transit time. Other microbiome perturbation experiments should be performed before strong conclusions are made.

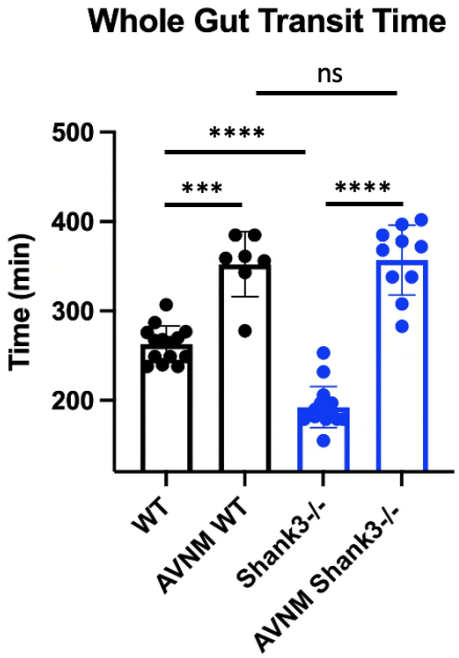

**Figure 8. Whole gut transit time after treatment with a broad-spectrum antibiotic cocktail (ampicillin, vancomycin, neomycin, and metronidazole)** (***$p<0.001$, ****$p<0.0001$, determined by Welch's two-tailed t-test)

Another modulator of GI motility is serotonin[70–73]. In fact, serotonin receptor agonists and antagonists are used to treat patients with GI motility disorders[70]. Peripheral serotonin is known to play a role in peristalsis and accelerated gut motility through the activation of the pacemaker interstitial cells of Cajal and muscle contraction[71]. Prior research shows than 90% of serotonin in the body is synthesized by the gut and microbes can secrete serotonin[74,75]. Additionally, elevated whole blood serotonin (hyperserotonemia) is correlated with ASD, although the mechanism is not understood[76]. Given this information, we hypothesized that serotonin levels would be higher in the blood and tissues of the Shank3B$^{-/-}$ mice. We isolated serum and GI tissue supernatant from Shank3B$^{-/-}$ and WT mice and quantified levels of serotonin using ELISAs. Unexpectedly, the results show that Shank3B$^{-/-}$ have trending lower levels of serotonin in the serum and ileum, proximal colon, and distal colon tissue samples (Figure 9). The functional outcome of this change is unclear, but likely does not contribute to the accelerated transit phenotype in Shank3B$^{-/-}$ mice.

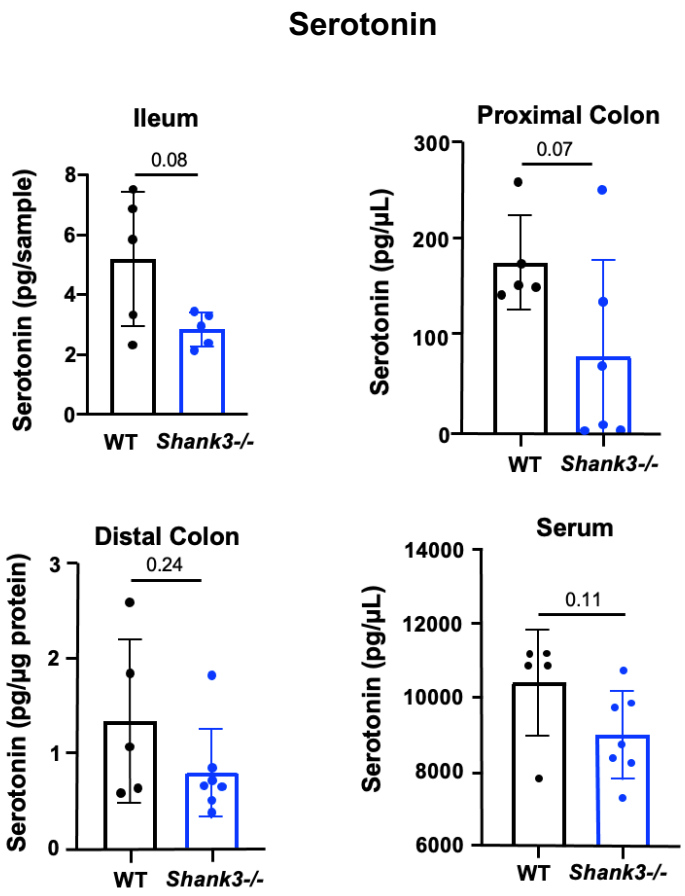


**Figure 9. Serotonin levels.** Serotonin levels detected in tissue lysate or serum by ELISA.

Gut Pathology and Inflammation

Another important role of the gut is to maintain immunological homeostasis[62,77–80]. Studies in humans and animal models have revealed bidirectional links between gut inflammation and adverse neurological phenotypes[81–84]. In autism, prenatal inflammation increases likelihood of an autism diagnosis, individuals with autism have increased inflammatory cytokines, and certain autism genetic factors regulate the immune system [24,85–87]. Considering the relevance of inflammation to autism in humans, we conducted experiments to investigate inflammatory responses in Shank3B$^{-/-}$ mice. First, we studied susceptibility to inflammation using DSS-induced colitis, which is a commonly used murine colitis model due to its noninvasive delivery method and similarity to human ulcerative colitis[88].

In a low-dose administration paradigm of DSS (2% DSS for 3 days), male Shank3B$^{-/-}$ mice lost weight, unlike the WT controls (Figure 10A). Female Shank3B$^{-/-}$ mice showed a similar trend, though it was not significant (Figure 10A). Weight loss is a measure of severity of inflammation and general health of the animal, since DSS-induced colitis causes diarrhea and reduced food intake[89]. This result was expected due to a study in a different Shank3-knockout mouse model which found that Shank3$^{-/-}$ mice are more susceptible to DSS-induced colitis[48]. Since DSS-induced colitis causes widespread epithelial damage in the gut, we decided to measure intestinal permeability through measurement of orally-gavaged FITC-dextran in serum. Though DSS-treated groups had higher levels of FITC-dextran in serum, there was no evidence of a genotype effect after treatment or at baseline (Figure 10B). To study colitis recovery, mice were treated with a more severe paradigm (2% DSS for 7 days), and allowed to recover for 2.5 weeks. At the completion of the experiment, colon lengths were measured as a marker of inflammation. Shank3B$^{-/-}$ mice did not appear to make a complete recovery since their colons were 1 cm shorter than controls, whereas DSS-treated WT mice had equivalent colon lengths to vehicle-treated WT mice (Figure 10C). Interestingly, vehicle-treated Shank3B$^{-/-}$ mice also had shorter colons than WT controls, though only slightly. Taken together, Shank3B$^{-/-}$ mice have increased susceptibility to colitis and impaired recovery responses which indicates a role for *Shank3* in the modulation of immune and inflammatory processes.

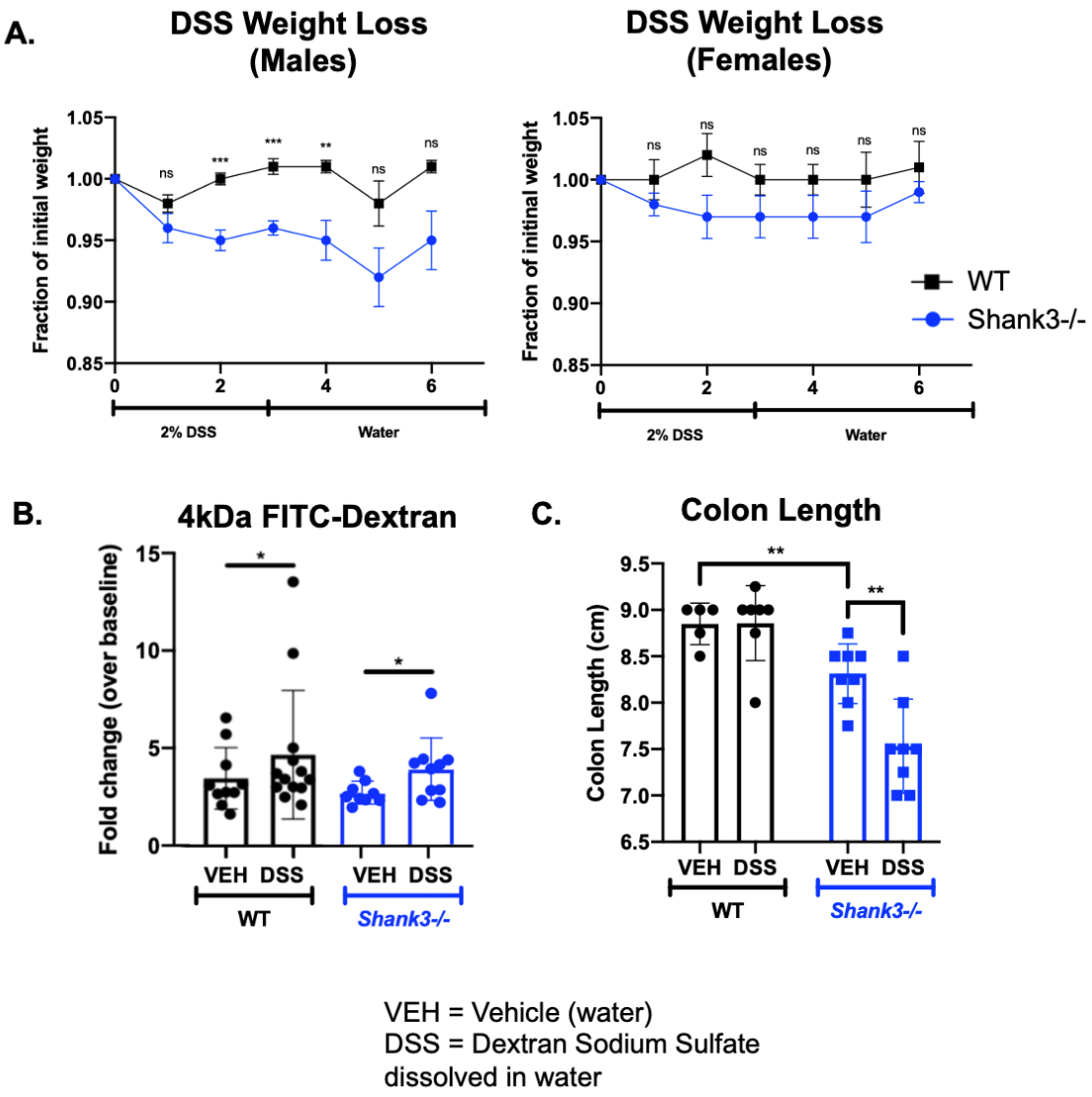


**Figure 10. DSS-induced colitis susceptibility.** (A) Weight loss of WT and Shank3B$^{-/-}$ animals during and after administration of DSS. (B) Relative levels of 4 kDa FITC-Dextran in serum of WT and Shank3B$^{-/-}$ mice at baseline or following DSS administration. (C) Colon lengths of WT and Shank3B$^{-/-}$ animals at baseline or after DSS administration. (*p<0.05, **p<0.01, ***p<0.001 determined by Welch's two-tailed t-test)

Gut Microbiome Composition

Given the impact of gut microbiota on host immunity, gut motility, and behavior, we were interested in profiling gut microbiome differences between Shank3B$^{-/-}$ and WT mice. We performed a microbiome analysis using 16S V4-V5 sequencing on fecal samples from both genotypes[90]. We surveyed microbial composition through relative abundance of individual Operational Taxonomic Units (OTUs). OTUs are sequences that are binned into clusters by sequence similarity and are used to assign taxonomy[91]. To assess the differences between Shank3B$^{-/-}$ and WT microbiomes, we plotted beta diversity, which is the difference in diversity across a set of samples[92]. Our results show that the knockout of *Shank3* affected the composition of the microbiome, since the genotypes clustered apart from each other (Figure 11A). These samples were taken from a colony that were offspring of *Shank3*$^{+/-}$ breeders, to ensure microbiomes were shaped by the genotype and not different from exposure to different bacteria. As an additional quality control metric, the samples were taken from different cages, sexes, and ages to ensure that the alterations are from genotype. This finding is consistent with the body of literature that genetic factors, including risk factors for ASD, influence microbiome composition[36,93–98]. Shank3B$^{-/-}$ mice had less phylogenetic diversity than WT mice (Figure 11B), which is similar to results from other studies using the Shank3B$^{-/-}$ mouse model, other autism mouse models, and clinical studies[11,99–101].

On a taxonomic level, Shank3B$^{-/-}$ had fewer *Rikenellaceae* and Clostridiales but more *Anaerostipes* than WT mice (Figure 11C). With this level of specificity, we performed a literature search to explore possible functional differences due to these groups of bacteria.

*Rikenellaceae* are tolerant of bile[102], can synthesize butyrate[103], and are found to be differentially abundant in high-fat diet-fed mice[104], leptin-resistant obese mice[105], and diabetic mice[106]. This family is associated with higher tryptophan and tyrosine metabolism, and lower branched-chain amino acid metabolism[107]. Clostridiales (now known as Eubacteriales) are also butyrate producers, and include both beneficial commensals and opportunistic pathogens[108]. *Anaerostipes* can produce propionate, butyrate, acetate, and lactate[109]. The role of all these groups in short-chain fatty acid (SCFA) synthesis is intriguing since SCFAs influence GI motility and inflammation, which relates to the GI function results observed in this study. Additionally, these taxonomic changes suggest differences in host and/or microbial metabolism. SCFAs can regulate energy metabolism, and differential abundance in *Rikenellaceae* is found in mouse models of metabolic disorders. This result was neither expected nor surprising, since there is not a consensus on the genetic effect of genetic Shank3 knockouts on the microbiome, as multiple studies show conflicting results[11,12,42,67]. This suggests that the different conditions in animal facilies have a large effect on the microbiome, but it would be worthwhile to perform a metagenomic analysis across different colonies to observe similarities in gene families and pathways .

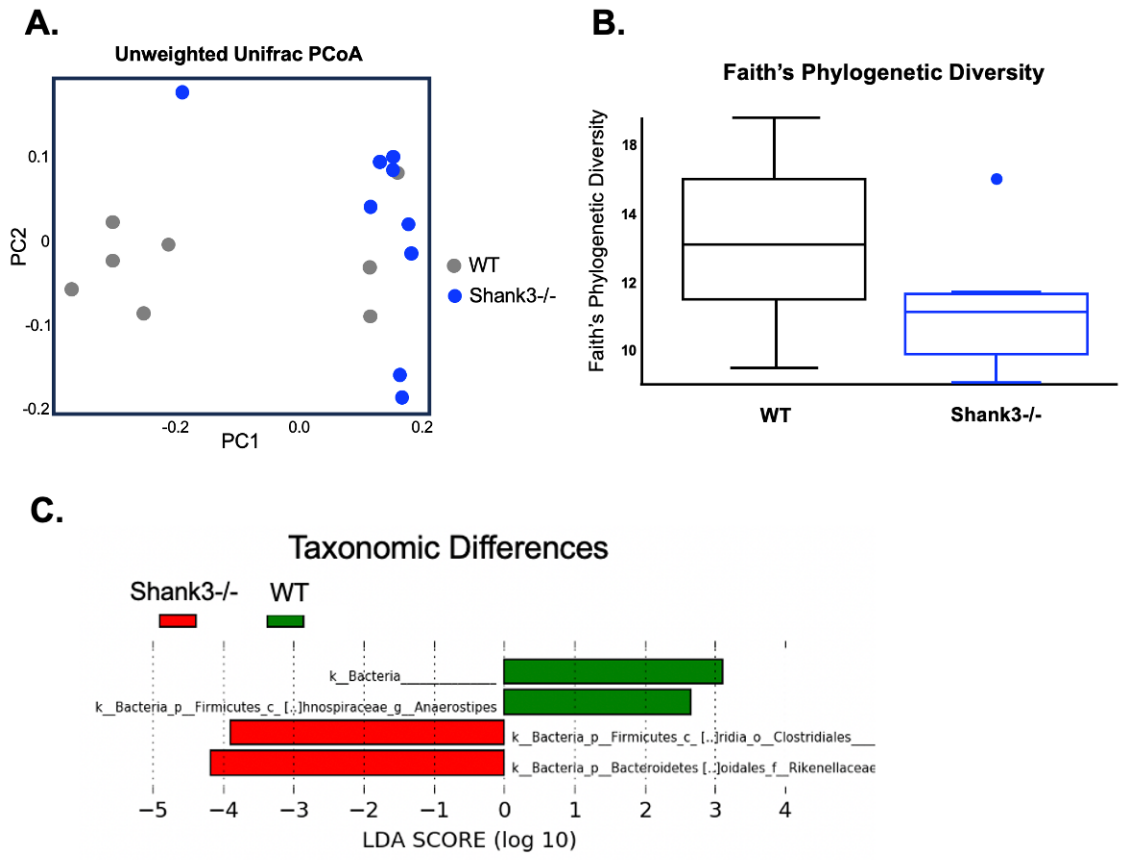


**Figure 11. Fecal microbiome differences.** (A) 16S rRNA genetic data of WT and Shank3B$^{-/-}$ fecal microbiomes shown as unweighted UniFrac PcoA, plotted by genotype. (B) Boxplots of Faith's phylogenetic diversity of WT and Shank3B$^{-/-}$ fecal microbiomes. (C) Differential abundance of specific OTUs WT and Shank3B$^{-/-}$ fecal microbiomes.

## DISCUSSION

Shank3B$^{-/-}$ mice are reported to exhibit anxiety phenotypes, social deficits, and repetitive behaviors at baseline[41]. The work performed in this study examines the combined gene and environmental effect of excluding the microbiome entirely. Though other studies have treated this autism mouse model with antibiotics to deplete the microbiome, this is the first work to analyze behavioral phenotypes in mice born and raised germ-free. Through a standard battery of behavioral tests used to assess autism-like behaviors, we did not observe the anxiety phenotypes observed in the original Shank3B$^{-/-}$ publication[41], but our finding is consistent with reports from other labs[42]. We observed a trending social deficit and significant increase in repetitive behavior, which were both ameliorated in the germ-free condition.

Shank3B$^{-/-}$ mice have a deficiency in excitatory neurotransmission in the brain[41]. Accordingly, we expected the mice to exhibit slower GI transit time. On the contrary, Shank3B$^{-/-}$ mice displayed accelerated GI transit, and an increased number of CMMCs. Shank3B$^{-/-}$ mice had equivalent small intestinal transit time, suggesting the phenotype is largely driven by changes in the large intestine. The observed difference in GI transit was absent when the microbiome of the mice was depleted by antibiotics, suggesting that microbes may play a role in this phenotype, though follow-up studies must be performed before conclusions are made. Possible experiments include cohousing mice from both genotypes to normalize microbiomes, and antibiotic-treatment followed by colonization with alternate microbiomes for by gut motility assays. The role that other biological systems, such as peripheral serotonin or SCFAs, have in the motility phenotypes remains unclear since we did not establish any mechanisms. In future studies, SCFAs and

neurotransmitter receptor agonists and antagonists could be administered either *in vivo* and/or *ex vivo* to determine if the phenotype is driven by different neuronal subsets.

Along with altered GI motility, Shank3B$^{-/-}$ mice exhibited pronounced GI inflammatory responses. When treated with DSS, which induces colitis, Shank3B$^{-/-}$ male mice begin to lose weight faster than WT controls. After a longer DSS time course followed by a 2.5 week recovery, WT male mice recovered, but Shank3B$^{-/-}$ male mice still had shorter colons. SHANK3 deficiency alters the gut microbiome and reduces phylogenetic diversity, though we have not established a link to the GI alterations. The taxonomic differences may indicate altered levels of SCFAs and host metabolism, providing a basis for future metagenomic and metabolomic experiments. For the microbiome, GI motility, and inflammation phenotypes, it is unclear if the observed phenotypes are a result of genetic alterations to the gastrointestinal environment or signals originating from the brain. RNAseq experiments on relevant tissues would be beneficial to identify candidate biological pathways that are different between the Shank3B$^{-/-}$ mice and controls.

## MATERIALS & METHODS

### Mice

All mouse experiments were performed in accordance with the NIH Guide for the Care and Use of Laboratory Animals using protocols approved by the Institutional Animal Care and Use Committee at the California Institute of Technology. Mice were fed ad libitum for the entire duration of experiments. *Shank3B*$^{+/-}$ specific pathogen free (SPF) C57BL/6 (Jackson Laboratories, Bar Harbor, ME Stock # 017688) males and females were used for breeding. *Shank3B*$^{-/-}$ and *Shank3B*$^{+/+}$ males and females were used for experiments.

### Antibiotic treatment

The gut microbiome was depleted in adult mice (6–12 weeks) with a cocktail of antibiotics for 3–4 weeks. The recipe included water with ampicillin (1 g/l), vancomycin (0.5 g/l), neomycin (1 g/l), and metronidazole (0.5 g/l), and 1% w/v of sucrose and filtered through a 0.22-μm filter. Germ-free mice were kept on this treatment when they were taken out of the gnotobiotic isolators for behavior experiments. Animals were kept in sterile cages with water changed weekly, and controls were given water with 1% w/v sucrose and filtered through a 0.22-μm filter.

### Behavior Testing

All behavior tests were performed at 6-8 weeks of age. Mice were acclimated to the testing room for at least 45 min before all behavior tests. Tests were performed 2–3 days apart for rest between tests.

*Open-field test*

The open-field test is a standard paradigm for anxiety and locomotion. The open-field apparatus is a square open arena (50 × 50 cm) bordered by opaque white plastic walls. Each mouse was placed into the arena in the center and behavior was recorded for 10 min. The center zone (17 × 17 cm) was defined as the middle of the open-field chamber. Behavior in the open field was recorded by a video camera mounted over the arena. EthoVision (Noldus Information Technology) was used to analyze the number of entries to, and the duration in, the center zone. Open-field chambers were cleaned with Rescue disinfectant (Virox Technologies) and dried between subjects.

*Elevated zero maze test*

Elevated zero maze test was performed in a circular maze with a 5 cm track width, 50 cm diameter, 20 cm wall height, with two open areas of the ring in between two walled areas. The test was recorded using an overhead camera, and tracked and analyzed using the EthoVision XT 4 software package (Noldus Information Technology). Mice were introduced to a closed arm of the arena and allowed to explore for 5 min while being tracked. The number of entries into and the time spent in open and closed arms were analyzed. Before and in between testing, the maze was disinfected using Rescue disinfectant (Virox technologies) and then allowed to dry.

*Grooming*

The open-field test is a standard paradigm for repetitive behavior. The subject was acclimated to a novel cage with no bedding or lid for 10 minutes before testing. The following 10 minutes were recorded from the side for self-grooming behavior. Grooming was manually analyzed using BORIS software.

*Direct social interaction (DSI)*

DSI is a widely-used task that tests social activity towards another novel animal. The subject was acclimated to a novel cage with clean bedding for 10 minutes before testing. A same-sex, sexually naïve, novel B6 mouse (Jackson Laboratories, Bar Harbor, ME Stock #000664) of similar age was introduced into the cage. All interactions between the two mice were video recorded for five minutes. Minimal aggressive behaviors were observed. The following social investigation behaviors constituted 'social activity' and were scored as such: anogenital sniffing, nose-nose sniffing, active approach. All behaviors were manually analyzed using BORIS software.

*Ultrasonic vocalization*

At the end of the previous behavioral tests, mice were single-housed and exposed to a new SPF C57BL/6J female for 10 min every day for 5 days before the test. On the sixth day, mice were habituated to an empty cage with a filter soaked with 10 µl of fresh pooled female urine for 10 min. Then, a novel female mouse was introduced to the cage and ultrasonic vocalizations were recorded using Avisoft UltraSoundGate 116Hme microphone (Avisoft Bioacoustics) and the Avisoft-SASLab RECORDER software (Avisoft Bioacoustics). Total vocalization and vocalization counts were recorded during 3 min sessions of male–female interaction.

**Whole Gut Transit Time**

6% (w/v) carmine red (Sigma-Aldrich, St. Louis, MO) with 0.5% methylcellulose (Sigma-Aldrich) was dissolved in water and autoclaved prior to use. Mice were orally gavaged with 150 µL of carmine red solution. Mice were single-housed with no bedding

for the duration of the experiment, and animals were not fasted beforehand. Over the 5-8 hours following gavage, the time of expulsion was recorded for each fecal pellet.

**Small Intestinal Transit Time**

5% (w/v) Evans blue dye (Sigma-Aldrich, St. Louis, MO) with 0.5% methylcellulose (Sigma-Aldrich) was dissolved in water and autoclaved prior to use. Mice were orally gavaged with 100 µL of Evans blue solution. Mice were fasted for 4 hours beforehand. 25 minutes after gavage, mice were euthanized by $CO_2$ and small intestines were immediately dissected. The distance the blue dye travelled was divided by the total length of the small intestine.

**Colonic Migrating Motor Complexes in *Ex Vivo* Intestinal Preparations**

Intact colons were dissected from cervically-dislocated mice, flushed and placed in pre-oxygenated (95% $O_2$, 5% $CO_2$) Krebs-Henseleit solution at RT. Proximal and distal ends were cannulated to 2 mm diameter tubes and secured in the center of an organ bath with continuously oxygenated Krebs-Henseleit solution at 37 ºC. Syringe pumps (Harvard Apparatus) were connected to the inlet and outlet tubes to maintain a flow of solution at a rate of 500 µL/min through the colon. The system was allowed to equilibrate for 30 minutes before recording. Recordings were taken for 30 minutes.

**Serotonin Measurements**

Mice were euthanized by $CO_2$ and blood was collected by cardiac puncture followed by separation using Sarstedt Serum-Gel microtubes (Thermo Fisher Scientific) according to

the manufacturer's specifications. Gut tissue was dissected, and luminal contents were flushed out with PBS. Tissues were separated into 1 cm sections for ileum, proximal colon, and distal colon. Serotonin levels were measured in serum and supernatant of intestinal tissue homogenates by ELISA (Eagle Biosciences). Serotonin levels from homogenates were normalized to total protein content detected by BCA assay (Thermo Pierce).

**Dextran Sodium Sulfate (DSS) Induced Colitis**

Multiple paradigms were used for DSS-induced colitis. For the mild colitis model, 2% DSS was administered orally in drinking water for 3 days, and then changed to regular water to observe recovery for 4 days. In the second paradigm, 2% DSS was administered orally in drinking water for 7 days and then changed to regular water for recovery for 2.5 weeks. Mice were weighed prior to DSS administration and weighed every day throughout the experiment to monitor weight loss to ensure mice did not lose >15% weight.

**Intestinal Permeability Test**

Mice were fasted for 4 hours prior to the experiment. Mice were gavaged with 0.6 mg/kg 4kDa FITC-dextran (total volume of 150µL) (Sigma). Four hours after gavage, mice were euthanized by $CO_2$ and blood was collected by cardiac puncture followed by separation using Sarstedt Serum-Gel microtubes (Thermo Fisher Scientific) according to the manufacturer's specifications. The concentration of FITC-dextran in serum was

measured using a spectrophotometer with an excitation of 485 nm and an emission wavelength of 528 nm.

**Fecal Microbiome Community Analysis**

Bacterial 16S rRNA genes from extracted fecal DNA were PCR-amplified with barcoded primers targeting the V4-V5 region. Sequencing was performed by Laragen, Inc. (Culver City, CA). Amplicons were sequenced according to the Earth Microbiome Protocol. Sequences were analyzed using the QIIME2 (2019.10) software package. Demultiplexed reads were filtered for quality and denoised using the DADA2 package.

**REFERENCES**


1. Data & Statistics on Autism Spectrum Disorder. *Cent. Dis. Control Prev.* (2023).
2. Giovedí, S., Corradi, A., Fassio, A. & Benfenati, F. Involvement of synaptic genes in the pathogenesis of autism spectrum disorders: the case of synapsins. *Front. Pediatr.* **2**, 94 (2014).
3. Moessner, R. *et al.* Contribution of SHANK3 mutations to autism spectrum disorder. *Am. J. Hum. Genet.* **81**, 1289–1297 (2007).
4. Chaidez, V., Hansen, R. L. & Hertz-Picciotto, I. Gastrointestinal problems in children with autism, developmental delays or typical development. *J. Autism Dev. Disord.* **44**, 1117–1127 (2014).
5. Horvath, K. & Perman, J. A. Autism and gastrointestinal symptoms. *Curr. Gastroenterol. Rep.* **4**, 251–258 (2002).
6. Soorya, L. *et al.* Prospective investigation of autism and genotype-phenotype correlations in 22q13 deletion syndrome and SHANK3 deficiency. *Mol. Autism* **4**, 18 (2013).
7. Sarasua, S. M. *et al.* Clinical and genomic evaluation of 201 patients with Phelan-McDermid syndrome. *Hum. Genet.* **133**, 847–859 (2014).
8. Phelan, K. & McDermid, H. E. The 22q13.3 Deletion Syndrome (Phelan-McDermid Syndrome). *Mol. Syndromol.* **2**, 186–201 (2012).
9. Sharon, G., Sampson, T. R., Geschwind, D. H. & Mazmanian, S. K. The Central Nervous System and the Gut Microbiome. *Cell* **167**, 915–932 (2016).
10. Kang, D.-W. *et al.* Microbiota Transfer Therapy alters gut ecosystem and improves gastrointestinal and autism symptoms: an open-label study. *Microbiome* **5**, 10 (2017).

11. Tabouy, L. *et al.* Dysbiosis of microbiome and probiotic treatment in a genetic model of autism spectrum disorders. *Brain. Behav. Immun.* **73**, 310–319 (2018).
12. Sgritta, M. *et al.* Mechanisms Underlying Microbial-Mediated Changes in Social Behavior in Mouse Models of Autism Spectrum Disorder. *Neuron* **101**, 246-259.e6 (2019).
13. Sampson, T. R. *et al.* Gut Microbiota Regulate Motor Deficits and Neuroinflammation in a Model of Parkinson's Disease. *Cell* **167**, 1469-1480.e12 (2016).
14. Hsiao, E. Y. *et al.* Microbiota modulate behavioral and physiological abnormalities associated with neurodevelopmental disorders. *Cell* **155**, 1451–1463 (2013).
15. Griffiths, J. A. & Mazmanian, S. K. Emerging evidence linking the gut microbiome to neurologic disorders. *Genome Med.* **10**, 98 (2018).
16. Golubeva, A. V. *et al.* Microbiota-related Changes in Bile Acid & Tryptophan Metabolism are Associated with Gastrointestinal Dysfunction in a Mouse Model of Autism. *EBioMedicine* **24**, 166–178 (2017).
17. Chu, C. *et al.* The microbiota regulate neuronal function and fear extinction learning. *Nature* **574**, 543–548 (2019).
18. Zheng, P. *et al.* The gut microbiome from patients with schizophrenia modulates the glutamate-glutamine-GABA cycle and schizophrenia-relevant behaviors in mice. *Sci. Adv.* **5**, eaau8317 (2019).
19. Lipkin, W. I., Bresnahan, M. & Susser, E. Cohort-guided insights into gene–environment interactions in autism spectrum disorders. *Nat. Rev. Neurol.* **19**, 118–125 (2023).

20. Coretti, L. *et al.* Gut Microbiota Features in Young Children With Autism Spectrum Disorders. *Front. Microbiol.* **9**, 3146 (2018).
21. De Angelis, M. *et al.* Fecal microbiota and metabolome of children with autism and pervasive developmental disorder not otherwise specified. *PloS One* **8**, e76993 (2013).
22. Finegold, S. M. *et al.* Pyrosequencing study of fecal microflora of autistic and control children. *Anaerobe* **16**, 444–453 (2010).
23. Gondalia, S. V. *et al.* Molecular characterisation of gastrointestinal microbiota of children with autism (with and without gastrointestinal dysfunction) and their neurotypical siblings. *Autism Res. Off. J. Int. Soc. Autism Res.* **5**, 419–427 (2012).
24. Kang, Ed. Prenatal inflammation linked to autism risk. *Natl. Inst. Health* (2013).
25. Kang, D.-W. *et al.* Differences in fecal microbial metabolites and microbiota of children with autism spectrum disorders. *Anaerobe* **49**, 121–131 (2018).
26. Kushak, R. I. *et al.* Analysis of the Duodenal Microbiome in Autistic Individuals: Association With Carbohydrate Digestion. *J. Pediatr. Gastroenterol. Nutr.* **64**, e110–e116 (2017).
27. Liu, F. *et al.* Altered composition and function of intestinal microbiota in autism spectrum disorders: a systematic review. *Transl. Psychiatry* **9**, 43 (2019).
28. Son, J. S. *et al.* Comparison of Fecal Microbiota in Children with Autism Spectrum Disorders and Neurotypical Siblings in the Simons Simplex Collection. *PloS One* **10**, e0137725 (2015).
29. Strati, F. *et al.* New evidences on the altered gut microbiota in autism spectrum disorders. *Microbiome* **5**, 24 (2017).

30. Wang, M. *et al.* Alterations in Gut Glutamate Metabolism Associated with Changes in Gut Microbiota Composition in Children with Autism Spectrum Disorder. *mSystems* **4**, (2019).
31. Williams, B. L. *et al.* Impaired carbohydrate digestion and transport and mucosal dysbiosis in the intestines of children with autism and gastrointestinal disturbances. *PloS One* **6**, e24585 (2011).
32. Gorrindo, P. *et al.* Gastrointestinal dysfunction in autism: parental report, clinical evaluation, and associated factors. *Autism Res. Off. J. Int. Soc. Autism Res.* **5**, 101–108 (2012).
33. Xu, M., Xu, X., Li, J. & Li, F. Association Between Gut Microbiota and Autism Spectrum Disorder: A Systematic Review and Meta-Analysis. *Front. Psychiatry* **10**, 473 (2019).
34. Kang, D.-W. *et al.* Long-term benefit of Microbiota Transfer Therapy on autism symptoms and gut microbiota. *Sci. Rep.* **9**, 5821 (2019).
35. Buffington, S. A. *et al.* Microbial Reconstitution Reverses Maternal Diet-Induced Social and Synaptic Deficits in Offspring. *Cell* **165**, 1762–1775 (2016).
36. Buffington, S. A. *et al.* Dissecting the contribution of host genetics and the microbiome in complex behaviors. *Cell* **184**, 1740-1756.e16 (2021).
37. Silverman, J. L. *et al.* Reconsidering animal models used to study autism spectrum disorder: Current state and optimizing future. *Genes Brain Behav.* **21**, e12803 (2022).
38. Wright, J. Why studying autism in mice may be doomed to fail. *Spectr. News* (2018).
39. Autism Diagnosis Criteria: DSM-5. *Autism Speaks*.

40. American Psychiatric Association. *Diagnostic and statistical manual of mental disorders (5th ed.).* (2013).
41. Peça, J. *et al.* Shank3 mutant mice display autistic-like behaviours and striatal dysfunction. *Nature* **472**, 437–442 (2011).
42. Osman, A. *et al.* Acetate supplementation rescues social deficits and alters transcriptional regulation in prefrontal cortex of Shank3 deficient mice. *Brain. Behav. Immun.* **114**, 311–324 (2023).
43. Premoli, M., Memo, M. & Bonini, S. A. Ultrasonic vocalizations in mice: relevance for ethologic and neurodevelopmental disorders studies. *Neural Regen. Res.* **16**, 1158–1167 (2021).
44. Wu, W.-L. *et al.* Microbiota regulate social behaviour via stress response neurons in the brain. *Nature* **595**, 409–414 (2021).
45. Desbonnet, L., Clarke, G., Shanahan, F., Dinan, T. G. & Cryan, J. F. Microbiota is essential for social development in the mouse. *Mol. Psychiatry* **19**, 146–148 (2014).
46. Arentsen, T., Raith, H., Qian, Y., Forssberg, H. & Diaz Heijtz, R. Host microbiota modulates development of social preference in mice. *Microb. Ecol. Health Dis.* **26**, 29719 (2015).
47. Gacias, M. *et al.* Microbiota-driven transcriptional changes in prefrontal cortex override genetic differences in social behavior. *eLife* **5**, e13442 (2016).
48. Wei, S.-C. *et al.* SHANK3 Regulates Intestinal Barrier Function Through Modulating ZO-1 Expression Through the PKCε-dependent Pathway. *Inflamm. Bowel Dis.* **23**, 1730–1740 (2017).

49. James, D. M. *et al.* Intestinal dysmotility in a zebrafish (Danio rerio) shank3a;shank3b mutant model of autism. *Mol. Autism* **10**, 3 (2019).

50. Hosie, S. *et al.* Gastrointestinal dysfunction in patients and mice expressing the autism-associated R451C mutation in neuroligin-3. *Autism Res. Off. J. Int. Soc. Autism Res.* **12**, 1043–1056 (2019).

51. Leembruggen, A. J. L. *et al.* Colonic dilation and altered ex vivo gastrointestinal motility in the neuroligin-3 knockout mouse. *Autism Res. Off. J. Int. Soc. Autism Res.* **13**, 691–701 (2020).

52. Grabrucker, A. M., Schmeisser, M. J., Schoen, M. & Boeckers, T. M. Postsynaptic ProSAP/Shank scaffolds in the cross-hair of synaptopathies. *Trends Cell Biol.* **21**, 594–603 (2011).

53. Holland, A. M., Bon-Frauches, A. C., Keszthelyi, D., Melotte, V. & Boesmans, W. The enteric nervous system in gastrointestinal disease etiology. *Cell. Mol. Life Sci. CMLS* **78**, 4713–4733 (2021).

54. Nezami, B. G. & Srinivasan, S. Enteric nervous system in the small intestine: pathophysiology and clinical implications. *Curr. Gastroenterol. Rep.* **12**, 358–365 (2010).

55. Qu, Z.-D. *et al.* Immunohistochemical analysis of neuron types in the mouse small intestine. *Cell Tissue Res.* **334**, 147–161 (2008).

56. Lott, E. & Jones, E. Cholinergic Toxicity. *StatPearls* (2022).

57. Monane, M., Avorn, J., Beers, M. H. & Everitt, D. E. Anticholinergic drug use and bowel function in nursing home patients. *Arch. Intern. Med.* **153**, 633–638 (1993).

58. Obata, Y. & Pachnis, V. The Effect of Microbiota and the Immune System on the Development and Organization of the Enteric Nervous System. *Gastroenterology* **151**, 836–844 (2016).

59. Camilleri, M. Gastrointestinal hormones and regulation of gastric emptying. *Curr. Opin. Endocrinol. Diabetes Obes.* **26**, 3–10 (2019).

60. Hyland, N. P. & Cryan, J. F. Microbe-host interactions: Influence of the gut microbiota on the enteric nervous system. *Enteric Nerv. Syst.* **417**, 182–187 (2016).

61. Schemann, M. Control of Gastrointestinal Motility by the "Gut Brain" - The Enteric Nervous System. *J. Pediatr. Gastroenterol. Nutr.* **41**, (2005).

62. Yoo, B. B. & Mazmanian, S. K. The Enteric Network: Interactions between the Immune and Nervous Systems of the Gut. *Immunity* **46**, 910–926 (2017).

63. Dey, N. *et al.* Regulators of gut motility revealed by a gnotobiotic model of diet-microbiome interactions related to travel. *Cell* **163**, 95–107 (2015).

64. De Palma, G. *et al.* Transplantation of fecal microbiota from patients with irritable bowel syndrome alters gut function and behavior in recipient mice. *Sci. Transl. Med.* **9**, eaaf6397 (2017).

65. Grubišić, V., Verkhratsky, A., Zorec, R. & Parpura, V. Enteric glia regulate gut motility in health and disease. *Brain Res. Bull.* **136**, 109–117 (2018).

66. Browning, K. N. & Travagli, R. A. Central nervous system control of gastrointestinal motility and secretion and modulation of gastrointestinal functions. *Compr. Physiol.* **4**, 1339–1368 (2014).

67. Sauer, A. K., Bockmann, J., Steinestel, K., Boeckers, T. M. & Grabrucker, A. M. Altered Intestinal Morphology and Microbiota Composition in the Autism Spectrum Disorders Associated SHANK3 Mouse Model. *Int. J. Mol. Sci.* **20**, (2019).

68. Ousey, J., Boktor, J. C. & Mazmanian, S. K. Gut microbiota suppress feeding induced by palatable foods. *Curr. Biol. CB* **33**, 147-157.e7 (2023).

69. Obata, Y. *et al.* Neuronal programming by microbiota regulates intestinal physiology. *Nature* **578**, 284–289 (2020).

70. Kendig, D. M. & Grider, J. R. Serotonin and colonic motility. *Neurogastroenterol. Motil.* **27**, 899–905 (2015).

71. Sikander, A., Rana, S. V. & Prasad, K. K. Role of serotonin in gastrointestinal motility and irritable bowel syndrome. *Clin. Chim. Acta Int. J. Clin. Chem.* **403**, 47–55 (2009).

72. Mawe, G. M. & Hoffman, J. M. Serotonin signalling in the gut--functions, dysfunctions and therapeutic targets. *Nat. Rev. Gastroenterol. Hepatol.* **10**, 473–486 (2013).

73. Guzel, T. & Mirowska-Guzel, D. The Role of Serotonin Neurotransmission in Gastrointestinal Tract and Pharmacotherapy. *Molecules* **27**, (2022).

74. Barandouzi, Z. A. *et al.* Associations of neurotransmitters and the gut microbiome with emotional distress in mixed type of irritable bowel syndrome. *Sci. Rep.* **12**, 1648 (2022).

75. Yano, J. M. *et al.* Indigenous bacteria from the gut microbiota regulate host serotonin biosynthesis. *Cell* **161**, 264–276 (2015).

76. Muller, C. L., Anacker, A. M. J. & Veenstra-VanderWeele, J. The serotonin system in autism spectrum disorder: From biomarker to animal models. *Neuroscience* **321**, 24–41 (2016).

77. Round, J. L. & Mazmanian, S. K. The gut microbiota shapes intestinal immune responses during health and disease. *Nat. Rev. Immunol.* **9**, 313–323 (2009).

78. Wu, H.-J. & Wu, E. The role of gut microbiota in immune homeostasis and autoimmunity. *Gut Microbes* **3**, 4–14 (2012).

79. Chung, H. & Kasper, D. L. Microbiota-stimulated immune mechanisms to maintain gut homeostasis. *Host Pathog.* ● *Immune Senescence* **22**, 455–460 (2010).

80. Mazmanian, S. K. & Lee, Y. K. Interplay between Intestinal Microbiota and Host Immune System. *jbv* **44**, 1–9 (2014).

81. Houser, M. C. & Tansey, M. G. The gut-brain axis: is intestinal inflammation a silent driver of Parkinson's disease pathogenesis? *Npj Park. Dis.* **3**, 3 (2017).

82. Park, J. & Kim, C. H. Regulation of common neurological disorders by gut microbial metabolites. *Exp. Mol. Med.* **53**, 1821–1833 (2021).

83. Bisgaard, T. H., Allin, K. H., Keefer, L., Ananthakrishnan, A. N. & Jess, T. Depression and anxiety in inflammatory bowel disease: epidemiology, mechanisms and treatment. *Nat. Rev. Gastroenterol. Hepatol.* **19**, 717–726 (2022).

84. Ma, Q. *et al.* Impact of microbiota on central nervous system and neurological diseases: the gut-brain axis. *J. Neuroinflammation* **16**, 53 (2019).

85. Hughes, H. K., R.J.Moreno & Ashwood, P. Innate immune dysfunction and neuroinflammation in autism spectrum disorder (ASD). *Brain. Behav. Immun.* **108**, 245–254 (2023).

86. Estes, M. L. & McAllister, A. K. Immune mediators in the brain and peripheral tissues in autism spectrum disorder. *Nat. Rev. Neurosci.* **16**, 469–486 (2015).

87. Choi, G. B. *et al.* The maternal interleukin-17a pathway in mice promotes autism-like phenotypes in offspring. *Science* **351**, 933–939 (2016).

88. Chassaing, B., Aitken, J. D., Malleshappa, M. & Vijay-Kumar, M. Dextran sulfate sodium (DSS)-induced colitis in mice. *Curr. Protoc. Immunol.* **104**, 15.25.1-15.25.14 (2014).

89. Britto, S. L., Krishna, M. & Kellermayer, R. Weight loss is a sufficient and economical single outcome measure of murine dextran sulfate sodium colitis. *FASEB BioAdvances* **1**, 493–497 (2019).

90. Bolyen, E. *et al.* Reproducible, interactive, scalable and extensible microbiome data science using QIIME 2. *Nat. Biotechnol.* **37**, 852–857 (2019).

91. He, Y. *et al.* Stability of operational taxonomic units: an important but neglected property for analyzing microbial diversity. *Microbiome* **3**, 20 (2015).

92. Lozupone, C., Lladser, M. E., Knights, D., Stombaugh, J. & Knight, R. UniFrac: an effective distance metric for microbial community comparison. *ISME J.* **5**, 169–172 (2011).

93. Kurilshikov, A. *et al.* Large-scale association analyses identify host factors influencing human gut microbiome composition. *Nat. Genet.* **53**, 156–165 (2021).

94. Bubier, J. A., Chesler, E. J. & Weinstock, G. M. Host genetic control of gut microbiome composition. *Mamm. Genome* **32**, 263–281 (2021).

95. Blekhman, R. *et al.* Host genetic variation impacts microbiome composition across human body sites. *Genome Biol.* **16**, 191 (2015).

96. Liu, Z. *et al.* Gene variations in autism spectrum disorder are associated with alteration of gut microbiota, metabolites and cytokines. *Gut Microbes* **13**, 1–16 (2021).

97. Kemis, J. H. *et al.* Genetic determinants of gut microbiota composition and bile acid profiles in mice. *PLoS Genet.* **15**, e1008073 (2019).

98. Korach-Rechtman Hila *et al.* Murine Genetic Background Has a Stronger Impact on the Composition of the Gut Microbiota than Maternal Inoculation or Exposure to Unlike Exogenous Microbiota. *Appl. Environ. Microbiol.* **85**, e00826-19 (2019).

99. Alamoudi, M. U. *et al.* Comparing the Gut Microbiome in Autism and Preclinical Models: A Systematic Review. *Front. Cell. Infect. Microbiol.* **12**, 905841 (2022).

100. Ding, H. *et al.* Imbalance in the Gut Microbiota of Children With Autism Spectrum Disorders. *Front. Cell. Infect. Microbiol.* **11**, 572752 (2021).

101. Sharon, G. *et al.* Human Gut Microbiota from Autism Spectrum Disorder Promote Behavioral Symptoms in Mice. *Cell* **177**, 1600-1618.e17 (2019).

102. Graf, J. The Family Rikenellaceae. *Prokaryotes Major Lineages Bact. Archaea* 857–859 (2014) doi:10.1007/978-3-642-38954-2_134.

103. Peters, B. A. *et al.* A taxonomic signature of obesity in a large study of American adults. *Sci. Rep.* **8**, 9749 (2018).

104. Wang, B. *et al.* A High-Fat Diet Increases Gut Microbiota Biodiversity and Energy Expenditure Due to Nutrient Difference. *Nutrients* **12**, (2020).

105. Geurts, L. *et al.* Altered gut microbiota and endocannabinoid system tone in obese and diabetic leptin-resistant mice: impact on apelin regulation in adipose tissue. *Front. Microbiol.* **2**, 149 (2011).

106. Cani, P. D. Gut microbiota and obesity: lessons from the microbiome. *Brief. Funct. Genomics* **12**, 381–387 (2013).

107. *Gut microbiome variation modulates the effects of dietary fiber on host metabolism.* vol. 9 (2021).

108. Djukovic, A. *et al.* Lactobacillus supports Clostridiales to restrict gut colonization by multidrug-resistant Enterobacteriaceae. *Nat. Commun.* **13**, 5617 (2022).

109. Bui, T. P. N. *et al.* Conversion of dietary inositol into propionate and acetate by commensal Anaerostipes associates with host health. *Nat. Commun.* **12**, 4798 (2021).

*Chapter 4*

# "RE-WILDING" THE MICROBIOME OF LABORATORY MICE PROMOTES SOCIABILITY

**Griffiths J. A.**, Wang, Z., Suryawinata, N., Tanaka, H., Simpson, P., Holschneider, D. P., Mazmanian S. K.

## PREFACE

Laboratory mice are essential tools in biomedical research due to their genetic, anatomical, and physiological similarity to humans. Currently, the specific pathogen-free (SPF) mice that are supplied by commercial mouse vendors have been deliberately and systematically depleted of microbiome complexity, and are maintained in rigorously cleaned animal facilities that lack gut bacterial diversity. Studies using wild or pet store mice, in comparison to SPF mice, have shown profound differences in immune system profiles and response to infection and pharmaceutical drugs. Given the established connections of both the microbiome and the immune system to brain function, this project investigated if mice with a wild-derived microbiome (WildR) not only have immunological differences, but also neurological and behavioral differences compared to mice with a SPF microbiome.

## INTRODUCTION

Both basic biological science and preclinical research rely on the use of model organisms[1]. The first model organisms, bacteria and yeast, have enabled foundational discoveries on cellular functions and biomolecular pathways[2]. As scientific inquiry grows in breadth and complexity, we require suitable organisms for the research. Mice are small, easy to maintain, reproduce quickly, have a short life cycle, and are similar in genetic and anatomical composition to humans[3,4]. For these reasons, mice have become the most widely used model organism in laboratories. This choice of model organism has been crucial to biological research progress. Mice have accelerated understanding and treatment of many genetic disorders, cancer, and infectious diseases[3,4].

Recently, scientists have become increasingly concerned about the "reproducibility crisis." In biology, over 70% of scientists cannot reproduce the results of others[5]. In mouse research, variations such as genetic drift, handling, and ambient noise can all vary between labs and influence findings[6–9]. One commonly overlooked variation between mouse colonies is the microbiome[10,11]. Mice from different research facilities and vendors have different microbiomes, which can result in different phenotypes[12–14]. Microbiomes of C57BL/6 mice from Taconic Biosciences have *Candidatus Savagella* (commonly known as segmented filamentous bacteria or SFB) which is required for the IL-17 mediated behavioral deficits seen in the maternal immune activation (MIA) mouse model[15]. Mice from Jackson Labs do not have this microbe, or the behavioral phenotype[16,17].

For more than half a century, mouse researchers have gone to great lengths to make mice "cleaner" by simplifying the microbiome and removing potential opportunistic pathogens[12,18,19]. The result is mouse microbiomes deemed "specific pathogen-free" (SPF) that are lacking a long list of microbes that have the potential to be pathogenic[20]. SPF is now the standard status of mice in biomedical experiments. Following this effort, outbreaks of specific pathogens that caused destruction of animal colonies have largely stopped[12,20]. Although the "clean" nature of laboratory mice has clear benefits, there is also cause for concern. Mouse immunity is shaped by the microbes encountered, as is ours[21–25]. The SPF microbiome is inherently artificial and highly restricts education of the immune system[11,18,19,26]. Studies comparing SPF mice to mice exposed to pet store mice or wild mice show that the increased bacterial, fungal, and viral diversity of the latter results in immune profiles that reflect humans[18,19,26–28]. These discoveries are particularly relevant given recent skepticism on the translatability of preclinical mouse research to human patients. Since the failure rate for medical treatment candidates in clinical trials is 90%, there may be a fundamental problem with using SPF mice as our model organisms[12,29,30]. Mice born with a "re-wilded" microbiome (WildR) recapitulate two disastrous clinical trial results for both innate and adaptive immunomodulatory drug candidates in people, anti-TNFα and CD28-superagonist. Anti-TNFα was developed for septic shock, and CD28SA for autoimmune/inflammatory diseases, which performed well in SPF rodents but exhibited the opposite effect in WildR mice and human patients[19]. These findings have caught the attention of many investigators, causing them to consider adding "dirty" mice to their studies[31].

The widespread shift to the SPF microbiome may have also unintentionally altered neurological phenotypes in mice, and WildR-colonized mice may reflect a more physiological state. This speculation is motivated by discoveries of the impact of the microbiome and the immune system on brain and behavior[32–34]. Individuals with depression, anxiety, and chronic stress have less diverse microbiomes[35–37]. Furthermore, humans and mice with larger social networks have increased microbiome diversity, suggesting that exposure to a large variation of conspecific-hosted microbes may contribute to behavioral phenotypes and neuropsychological wellbeing[35,38]. In support of these findings, we discovered that colonizing laboratory mice with WildR microbiomes increases sociability of male mice. To explore the neurological underpinnings of the observations relating to social behavior, this work investigates the hypothesis that the WildR microbiome alters activity patterns in brain regions implicated in known neural circuits for intraspecies interactions.

## RESULTS

### Behavioral Phenotypes of C57BL/6J Mice with SPF or WildR Microbiomes

Since this is the first known study to explore neurological differences between a clean SPF microbiome and a "dirty" mouse microbiome, we used an exploratory research approach to gather preliminary data. To survey the impact of the more diverse WildR microbiome on the brain, we performed a wide array of behavioral tests on SPF and WildR mice. These tests encompass social interaction, anxiety/fear, memory, cognition, and repetitive behaviors (Table 1).

| Test | Purpose |
|---|---|
| Grooming | Repetitive behavior |
| Direct Social Interaction | Social Behavior |
| Three-Chamber Social Interaction | Social Behavior |
| Ultrasonic Vocalization | Social Behavior |
| Elevated Plus Maze | Anxiety-like behavior |
| Open Field Test | Anxiety-like behavior |
| Light-Dark Box | Anxiety-like behavior |
| Novel Object Recognition | Memory & Cognition |
| Y maze | Memory & Cognition |

**Table 1. Tests used in this study to assay different types of behaviors in mice**

Similar studies previously performed in our lab and others show neurological differences between SPF mice and mice lacking microbiomes (germ-free or antibiotic-treated)[39–42]. A study led by a former postdoc in the lab, Dr. Wei-Li Wu, revealed that germ-free and

antibiotic-treated male mice socialize less than SPF mice in the direct social interaction (DSI) test[39]. This effect is not observed in the three-chamber social interaction test. In our study, WildR male mice socialized more than SPF mice in the DSI test, and similarly did not show a difference in the three-chamber social interaction test (Figure 1). Though the three-chamber social interaction test is the most commonly used behavioral paradigm to measure social behavior, it is only designed to assess the amount of time an animal prefers to spend in a social environment over a nonsocial one[43]. Though the simplicity of the test makes it possible to score with automatic tracking software, natural social events are much more complex. In addition, the novel mouse is restrained under a wire bar cup for the duration of the test, prohibiting free interaction, which reduces prevalence of behaviors such as aggression. In contrast, the DSI test allows for unencumbered contact and a wider spectrum of behaviors[43].

The gut microbiome has been implicated a variety of rodent behaviors beyond social interaction. Since microbially depleted mice show reduced anxiety-like behavior in open-field, light-dark box, and elevated plus maze compared to SPF mice[39–42], we hypothesized that a more diverse microbiome (WildR) would increase anxiety-like phenotypes. Results from all three anxiety behavioral tests revealed that the WildR microbiome does not modulate these behaviors in baseline conditions (Figure 2). In the tests designed to study repetitive behavior and memory and cognition, there also was no effect (Figure 3).

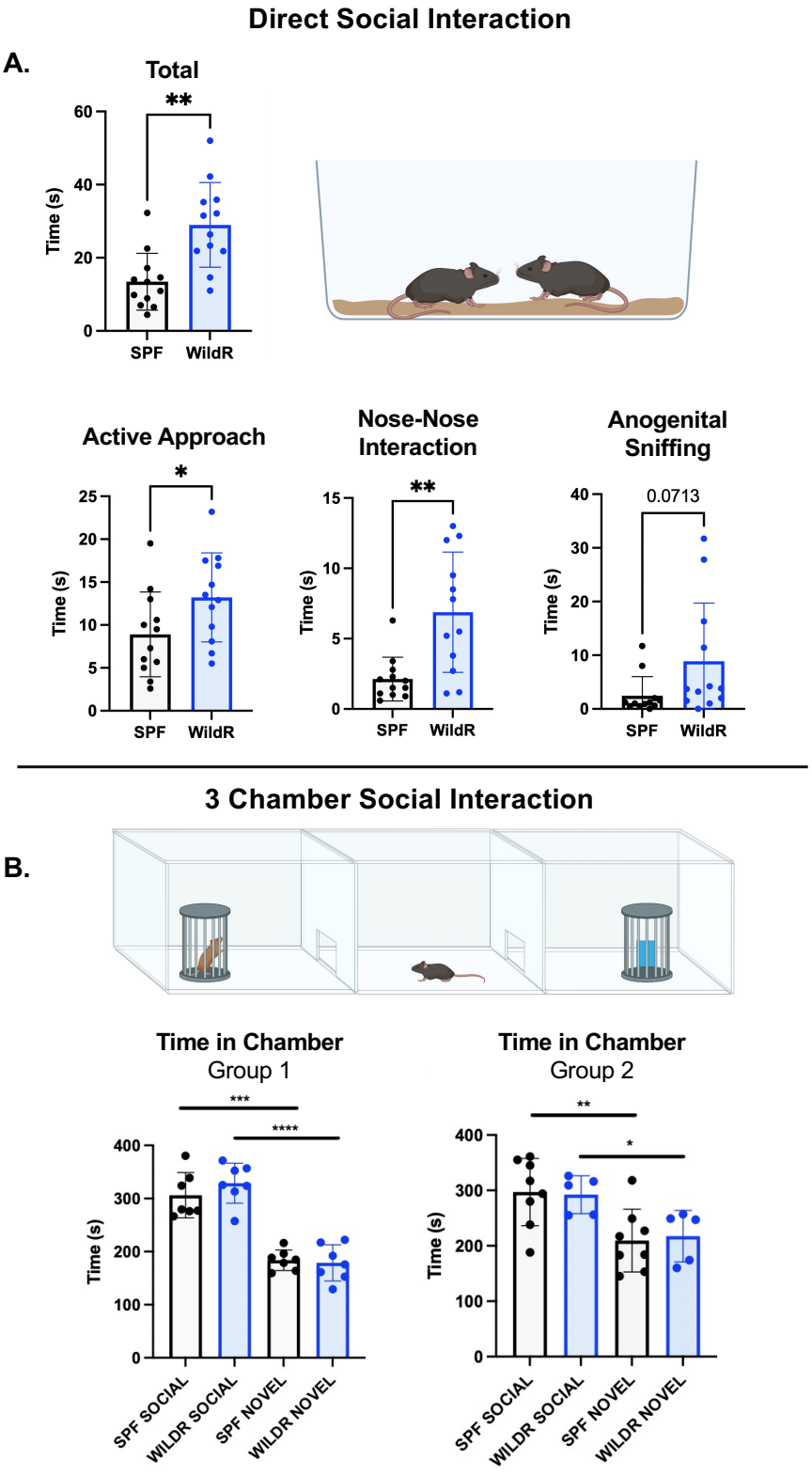


**Figure 1. WildR microbiome regulates social behavior in male mice.** (A) Direct social behavior test. WildR male mice spent more time socializing with a novel intruder mouse

(*p<0.05, **p<0.01, determined by Welch's two-tailed t-test). (B) Three-chamber social interaction test. WildR and SPF male mice spent equivalent time in chamber with a novel intruder mouse, and equivalent time in chamber with novel object. Figure created with BioRender.com.

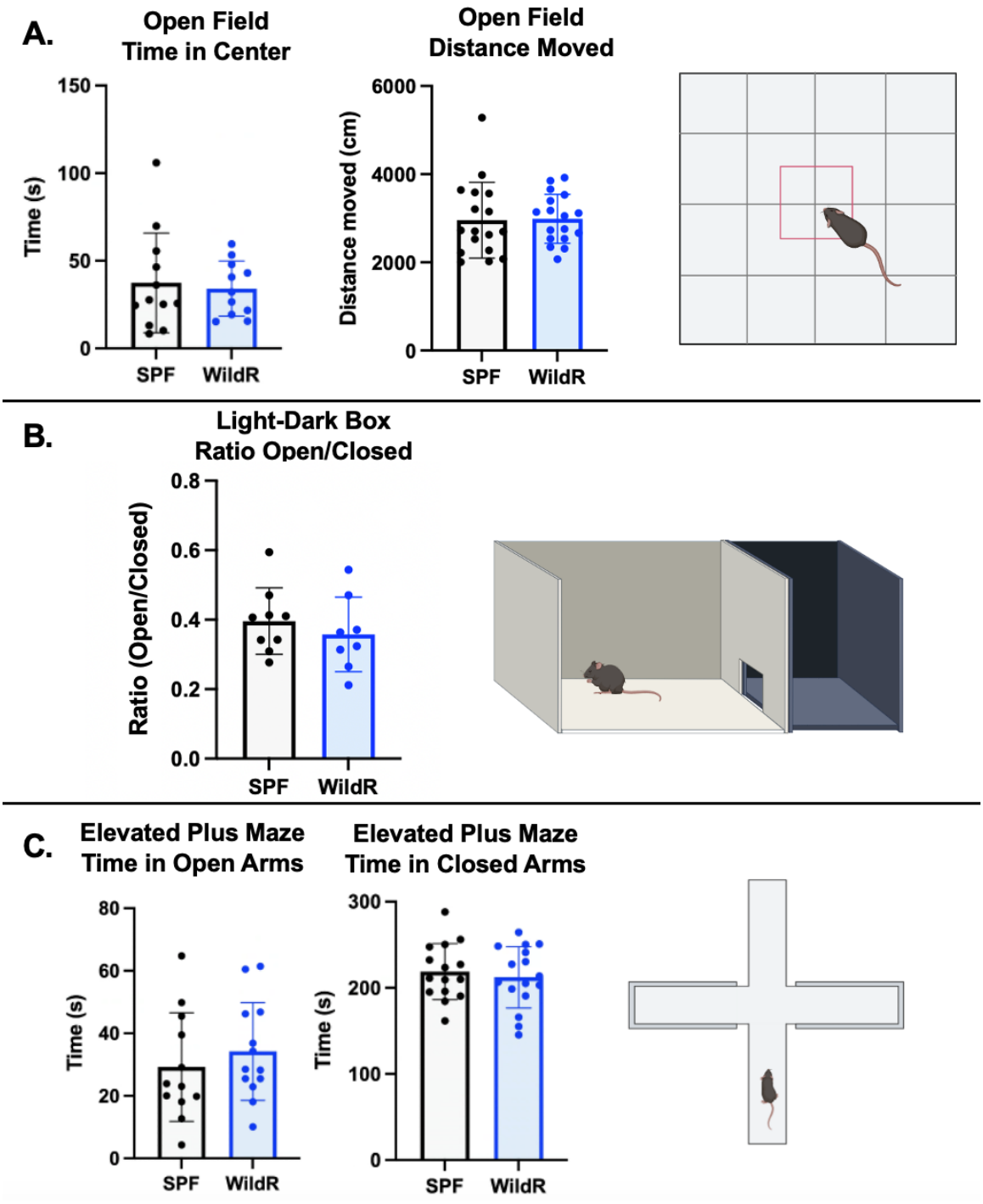


**Figure 2. WildR Microbiome does not modulate anxiety-like behaviors.** (A) Open field test. WildR mice spent the same amount of time in the exposed center region of the arena and moved the same amount as SPF mice. (B) Light-dark box test. WildR mice spent the same amount of time as SPF mice in the open chamber of the arena. (C) EPM. WildR mice

spent same amount of time as SPF mice in open arms of the arena. Figure created with BioRender.com.

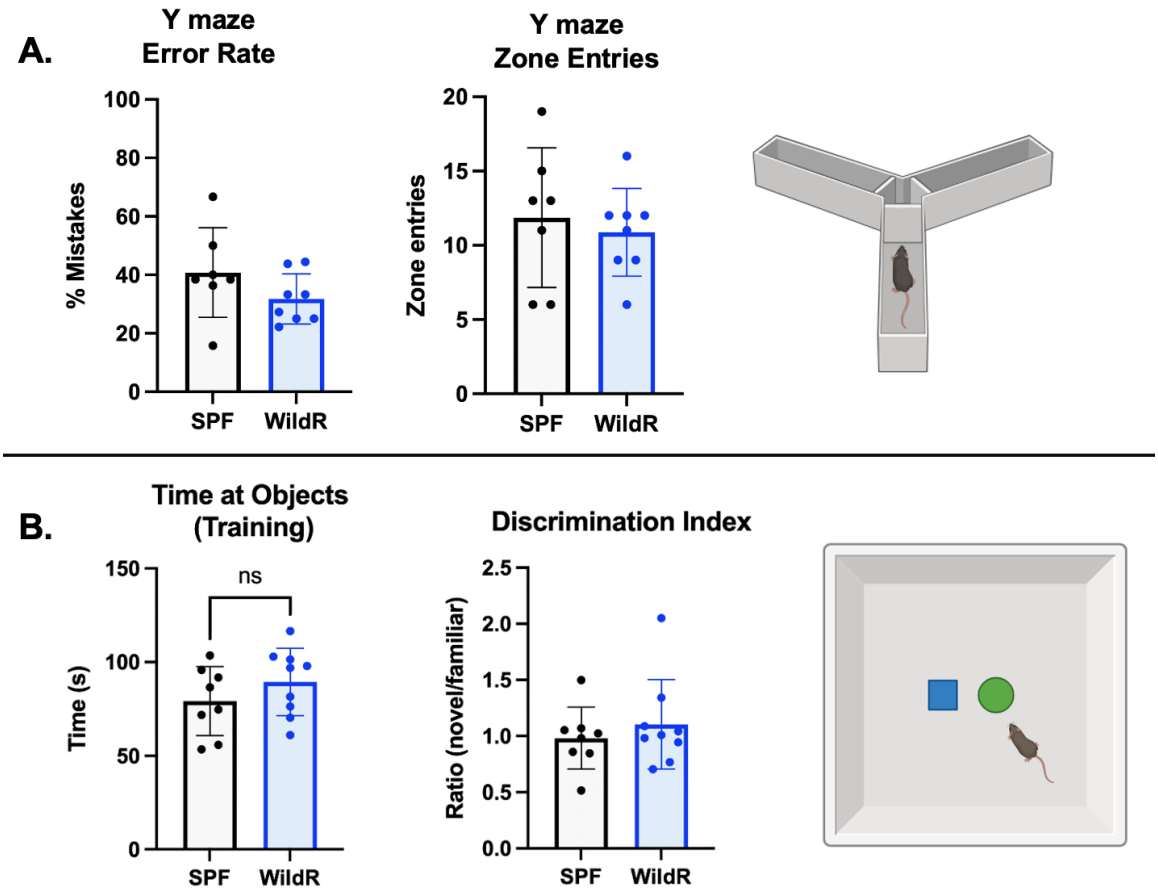


**Figure 2. WildR microbiome does not modulate cognitive behaviors.** (A) Y maze test. WildR mice made same number of mistake and arm alternations as SPF mice. (B) Novel object test. WildR mice spent the same amount of time with novel and familiar objects as the SPF mice. Figure created with BioRender.com.

Given the specificity of the microbiome behavioral effects on social interaction, we performed additional experiments to investigate this finding. Since our preliminary DSI test was conducted only with SPF intruders, we performed a similar experiment with SPF

and WildR intruders to control for the microbiome of the intruder (Figure 4). There was no effect of the intruder's microbiome on the social interaction time of the subject mice, regardless of the microbiome of the subject mouse. Additionally, identical tests performed with female mice showed no effect of the microbiome on social interaction in DSI (Figure 5). Therefore, for the purposes of investigating the social interaction phenotype, only male mice were used as the subject animals for the remainder of experiments unless otherwise stated.

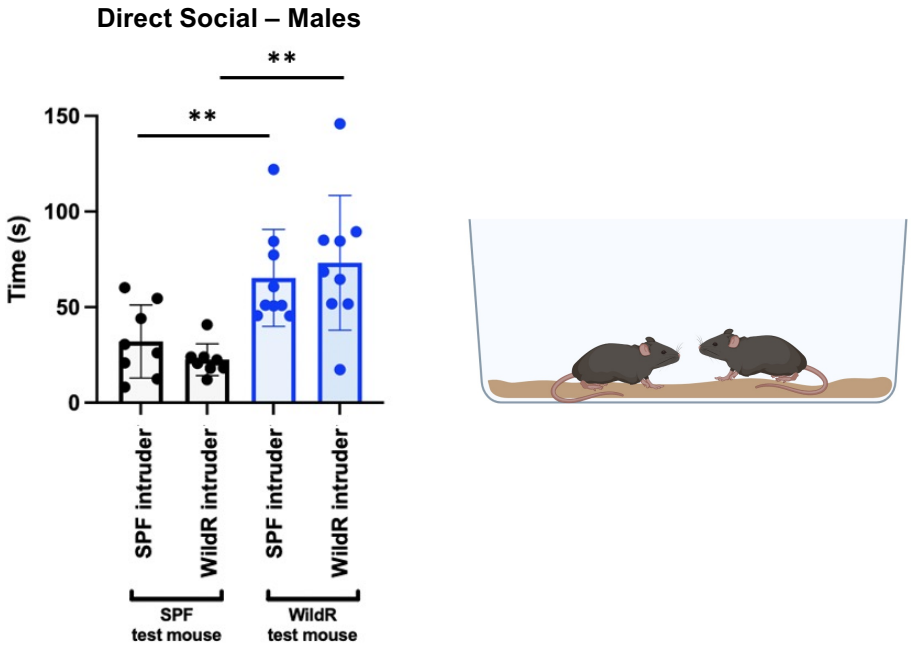


**Figure 4. Social interaction is not affected by intruder microbiome.** Direct social interaction of a male mouse with a novel SPF or WildR male intruder (**p<0.01, determined by Welch's two-tailed t-test). Figure created with BioRender.com.

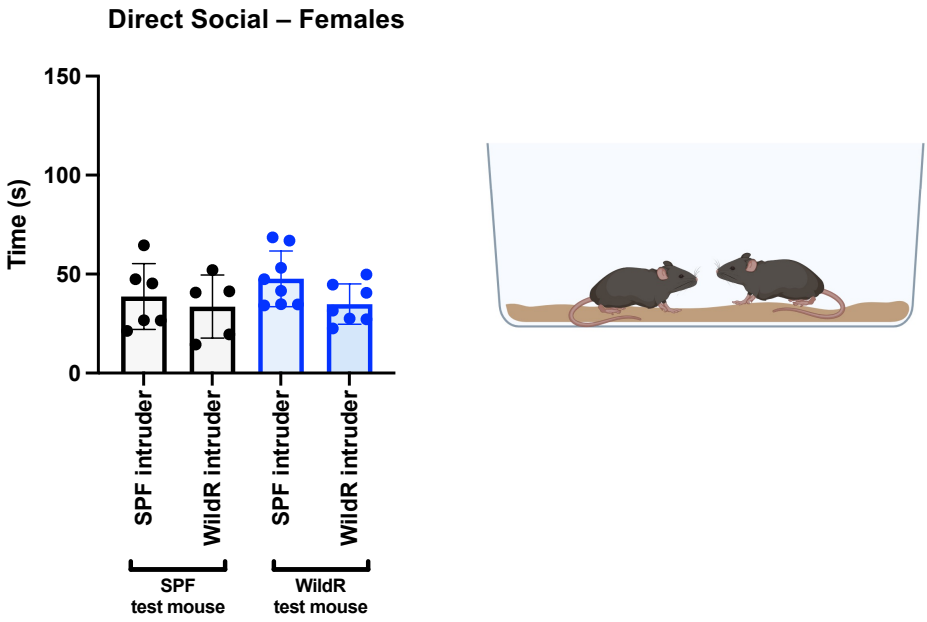


**Figure 5. WildR microbiome does not regulate social behavior in female mice.** Direct social interaction of a female mouse with a novel SPF or WildR female intruder. Figure created with BioRender.com.

Although neurobiologically distinct from male-male interactions, we assessed differences in male-female interactions using the ultrasonic vocalization (USV) test[44,45]. After exposure to a novel female mouse, WildR mice produced the same number of calls to females as SPF male mice which suggests that this phenotype is restricted to male-male encounters (Figure 6).

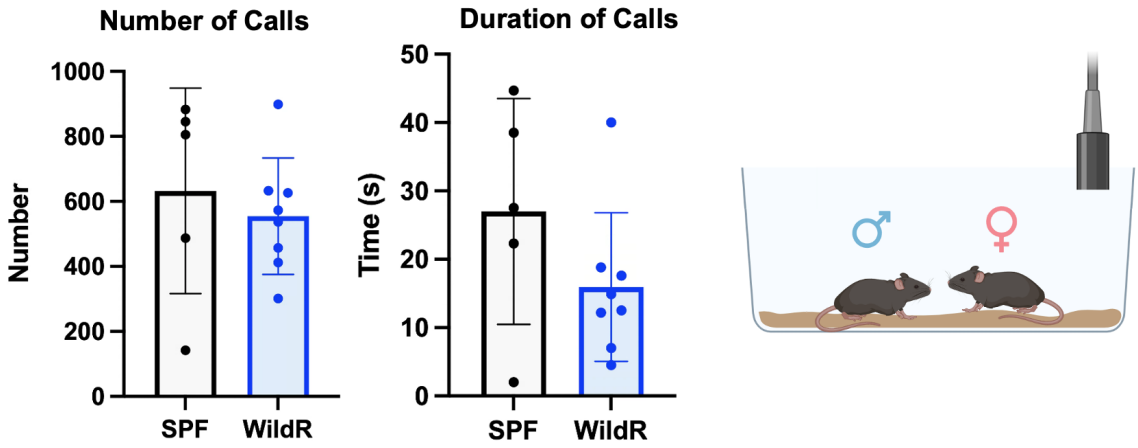


**Figure 6. WildR microbiome does not regulate male social behavior towards females.** Ultrasonic vocalizations of males exposed to a female mouse. Figure created with BioRender.com.

**Mechanism Underlying WildR Social Phenotype**

There are many different neural circuits that influence social decisions in mice[44,46–48]. Different types of sensory cues (olfactory, auditory, tactile, and visual) are detected by an individual, and activate different brain pathways that eventually lead to a behavioral response. Social reward, bonding, fear, aggression, stress, novelty, and mating are all underlying motivations or deterrents for mice to interact with one another. To determine the internal state responsible for the social behavior phenotype, we performed a battery of different experiments designed to test the many aspects of sociability.

Given the parallel results between this study and the lab's previous work performed in Wu et. al. 2021, we hypothesized that the mechanism of action of the microbiome on the brain was similar: that the social deficit was driven by alterations in stress response through the hypothalamic-pituitary-adrenal (HPA) axis[39]. Antibiotic-treated mice had higher levels of

corticosterone following a 5 minute social test, and increased number of activated neurons in the paraventricular nucleus (PVN) of the hypothalamus shown through c-Fos staining. In identical studies performed with SPF and WildR mice, there was no evidence of an altered HPA axis response since corticosterone levels between the two groups were identical at baseline and after social behavior, and equivalent numbers of c-Fos positive cells were observed in the PVN following social behavior (Figure 7).

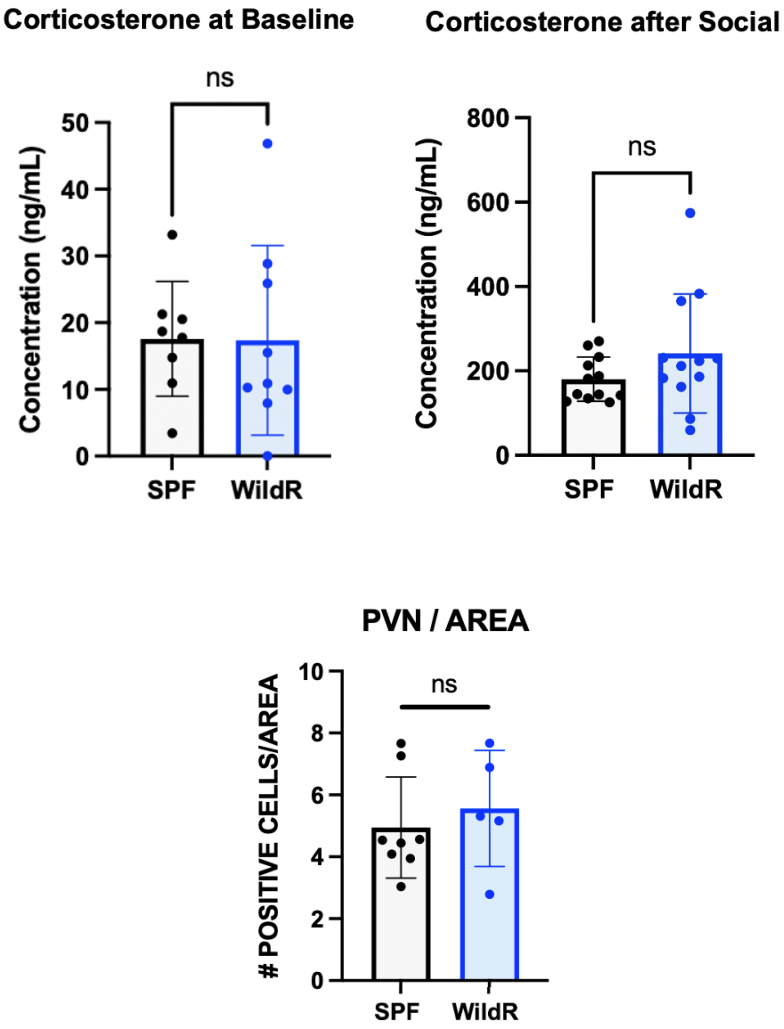


**Figure 7. Social behavior phenotype is not driven by HPA axis.** Corticosterone level in serum at (A) baseline and (B) following exposure to a novel intruder measured by ELISA.

(C) Number of c-Fos positive cells in the PVN of the hypothalamus following exposure to a novel intruder.

The hormone oxytocin is commonly known as the love or bonding hormone[49–51]. Oxytocin is released in response to touch such as hugging or cuddling[52]. In mice and humans, oxytocin is known to promote social behavior[44,51,53]. Social stimuli induce activation of oxytocin-expressing neurons in the PVN in mice, which leads to prosocial behaviors[54]. In multiple mouse models of autism, social deficits are ameliorated by oxytocin treatment[55–59]. We analyzed the number of oxytocin neurons in the PVN of SPF and WildR mice to investigate if oxytocin mediates the social behavioral phenotype (Figure 8). The lack of differences in oxytocin+ neuron density and number of c-Fos+ cells in the PVN suggest that oxytocin is not a contributor.

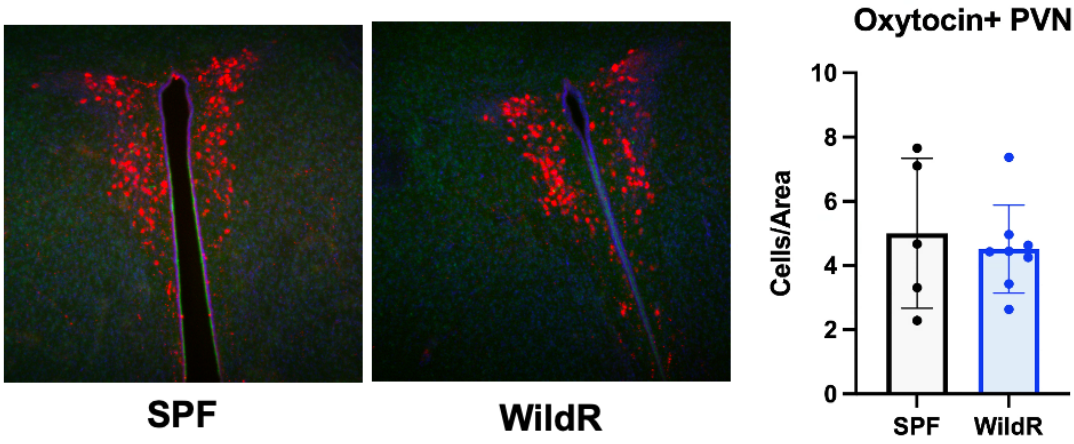


**Figure 8. Oxytocin neuron density is not different in WildR mice.** Representative images of the PVN in SPF and WildR mice, with oxytocin intensity represented in red. Density of oxytocin+ neurons in the PVN.

To investigate if WildR mice have heightened olfactory responses which may drive the social phenotype[60], we performed the olfactory habituation/dishabituation test using various non-social and social scents (Figure 9). WildR mice did not exhibit different olfactory responses to any of the scents presented.

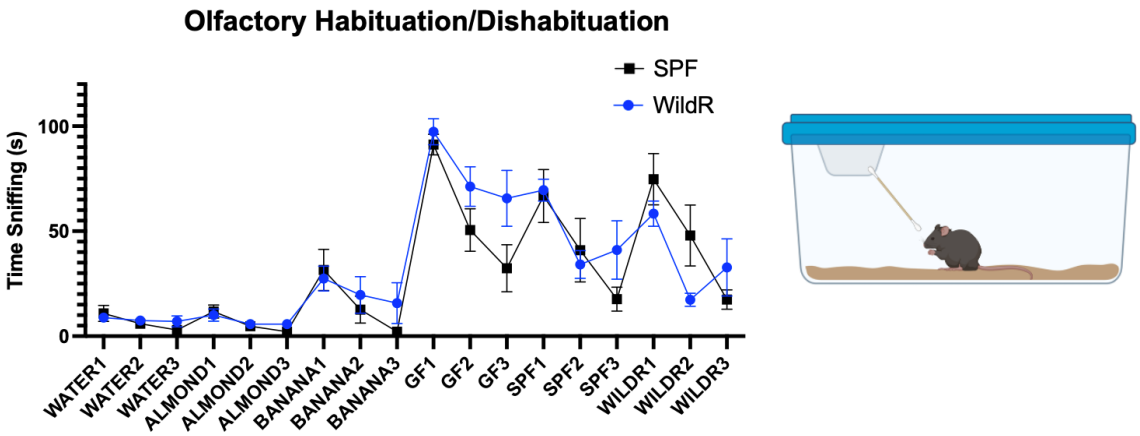


**Figure 9. Social behavior phenotype is not driven by differences in olfaction.** Time spent sniffing nonsocial and social odors in olfactory habituation/dishabituation test. Figure created with BioRender.com.

In addition to the novel object recognition test, we also used the hole-board assay to examine if the WildR mice are more exploratory than SPF mice. If true, the WildR may be more curious about intruders than the SPF mice. The results from the novel object training, novel object test, and number of nose pokes and distance moved in the hole-board assay suggest that the WildR mice are not more exploratory than SPF mice (Figures 1 & 10).

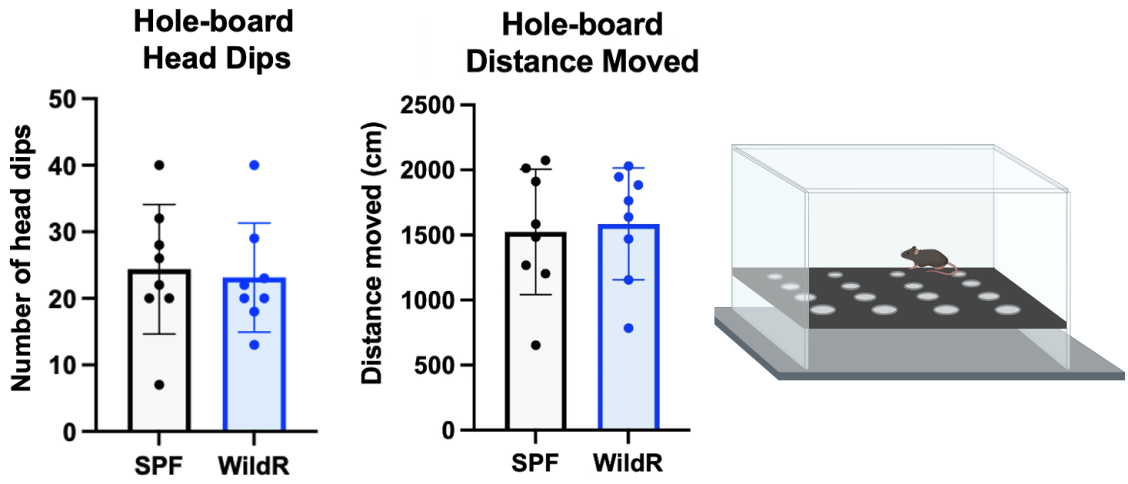


**Figure 10. Social behavior phenotype is not driven by differences in exploration.** Number of head dips and distance moved in hole-board exploration test. Figure created with BioRender.com.

The absence of a social behavior phenotype in female mice suggests that WildR male mice may be more aggressive and/or territorial than SPF male mice, since female mice do not tend to be aggressive[61,62]. Testosterone is widely implicated in male aggressive and non-aggressive behaviors[63,64], but there was no difference in measured testosterone levels in the plasma of SPF and WildR mice (Figure 11). We used the tube dominance test to explore if WildR mice are more dominant than SPF mice[65]. WildR mice "won" two-thirds of the matches with a novel SPF mouse (Figure 12). As a follow-up experiment to directly test aggression, SPF and WildR mice were single housed for two weeks to promote aggression[66,67]. When an intruder was introduced into the subject's home cage, only 1/8 mice attacked in both the SPF and WildR groups. This low attack percentage in the isolation-induced aggression test and in all DSI tests performed in this study with group-

housed animals (only observed in ~1% of all mice) suggest that WildR mice are not more social due to altered levels of aggression.

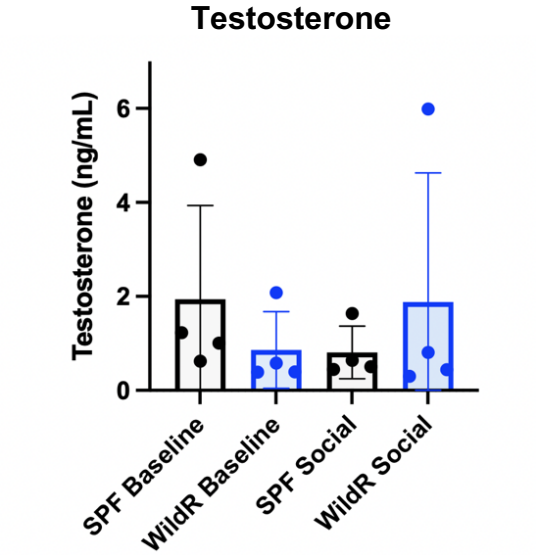


**Figure 11. Testosterone levels in SPF and WildR male mice.** Plasma levels of testosterone at baseline after exposure to a novel intruder measured by ELISA. It is common for the most dominant male in the cage to have higher testosterone levels than its cage-mates.

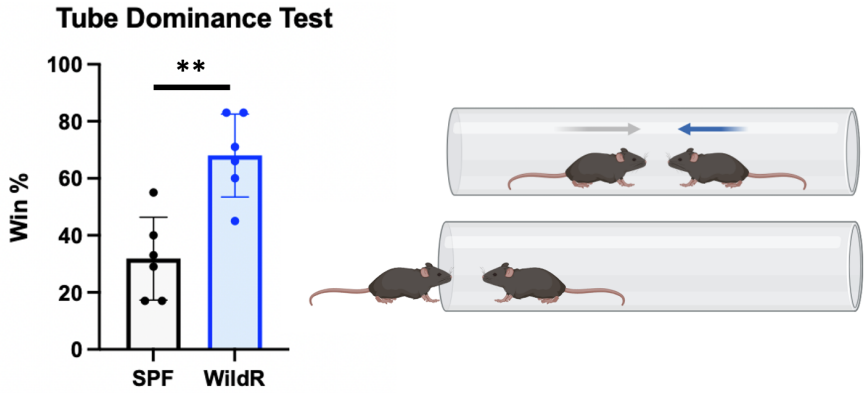


**Figure 12. WildR male mice are more dominant than SPF male mice.** WildR male mice had more "wins" in the tube dominance test than the SPF male mice. Each mouse was tested against 3 different intruders. Each data point is the result of one round. Figure created with BioRender.com.

Of all the behavioral tests performed as a follow up to the DSI test, only the tube test showed further differences between the microbiomes, indicating that WildR mice are more dominant than SPF mice. Since this test alone does not inform us about the motivation of the mice to interact with others, we utilized well characterized methods to quantify brain activity changes. The c-Fos protein, encoded by an immediate early gene, is a transcription factor that upregulates a cascade of many other genes to coordinate a response[68,69]. We repeated the DSI experiment and analyzed the brains for c-Fos expression in neurons in different regions associated with social behavior. We found increased c-Fos staining in the amygdala and decreased c-Fos staining in the hippocampal dentate gyrus (DG) in WildR mice compared to SPF mice (Figures 13 and 14) in three different coronal sections (Figure 15). No differences were observed in the bed nucleus of stria terminalis (BNST) or paraventricular nucleus of the hypothalamus (PVN), which are other brain regions implicated in pathways underlying social behavior (Figures 7 & 16)[44,46,47].

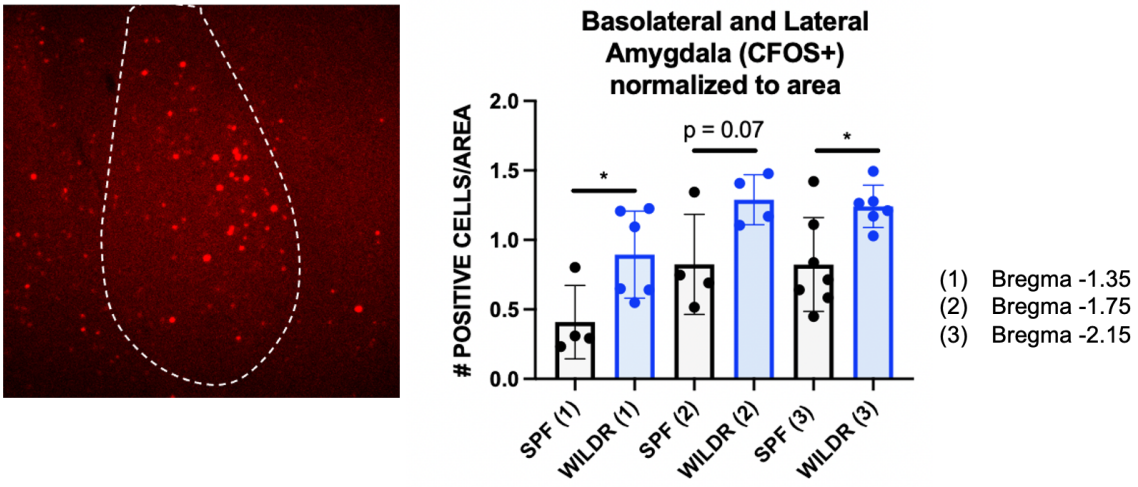


**Figure 13. Amygdala activation patterns of SPF and WildR mice following social interaction.** Representative image of the amygdala in SPF and WildR mice exposed to a

novel intruder for 5 minutes, with c-Fos intensity represented in red. Density of c-Fos+ neurons in three sections corresponding to different bregma coordinates (*p<0.05, determined by Welch's two-tailed t-test).

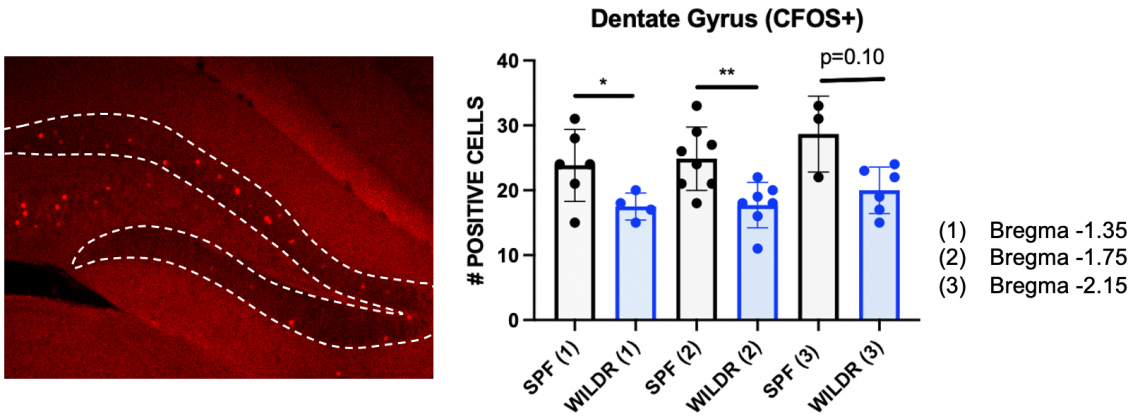


**Figure 14. Dentate gyrus activation patterns of SPF and WildR mice following social interaction.** Representative image of the dentate gyrus of the hippocampus in SPF and WildR mice exposed to a novel intruder for 5 minutes, with c-Fos intensity represented in red. Density of c-Fos+ neurons in three sections corresponding to different bregma coordinates (*p<.05, **p<0.01, determined by Welch's two-tailed t-test).

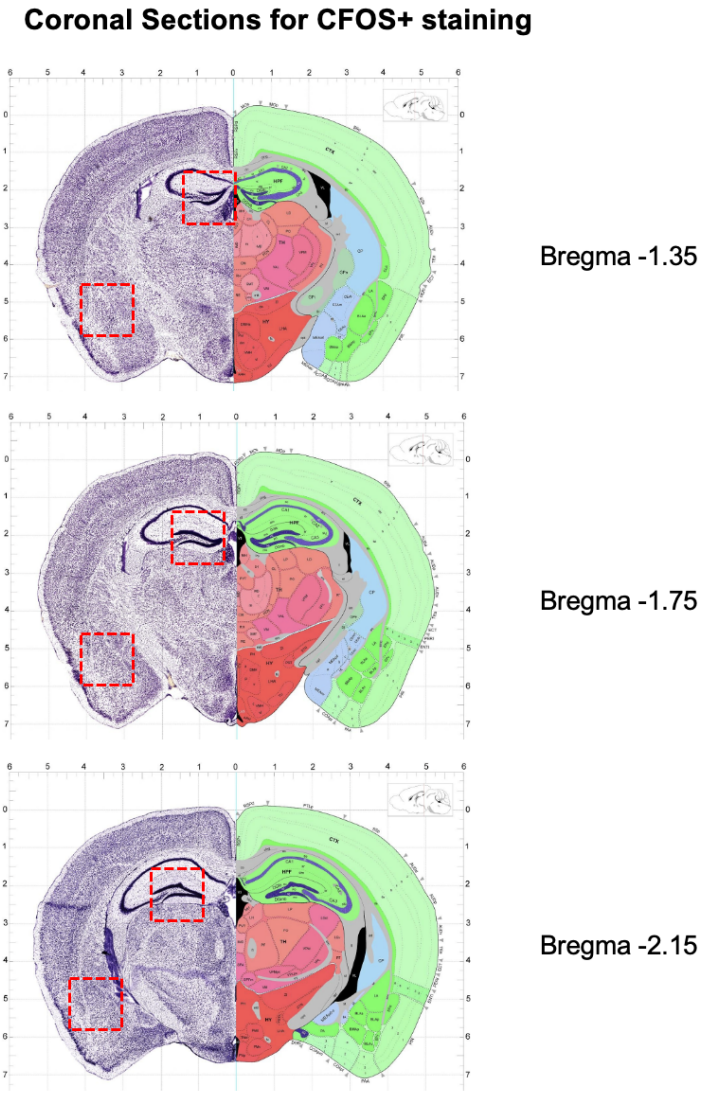


**Figure 15. Bregma coordinates for amygdala and dentate gyrus c-Fos immunohistochemistry images.** Coordinates for coronal sections in figures 13 & 14.

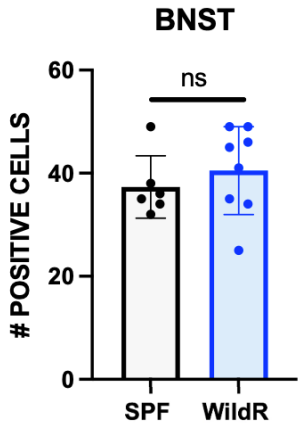


**Figure 16. BNST activation patterns of SPF and WildR mice following social interaction.** Number of c-Fos+ neurons in BNST hippocampus in SPF and WildR mice exposed to a novel intruder for 5 minutes.

In light of our c-Fos discoveries, we administered a radiolabeled tracer prior to mice exposed to a novel intruder and at baseline (alone in a cage) to explore brain activity patterns with greater precision. Results showed increased tracer uptake, and hence activity, in many regions of the brain during social behavior in the WildR mice compared to SPF mice (Figure 17). These areas include the amygdala, providing additional confirmation of the activity differences observed with c-Fos staining, as well as the nucleus accumbens, anterior cingulate cortex (ACC), bed nucleus of the stria terminalis (BNST), and hypothalamus (Table 2). The highlighted brain regions are involved in many different social behavioral circuits, including social exploration, bonding, stress, dominance, and aggression[47].

The amygdala is a brain region implicated in emotional processing, and most known for its importance in fear responses[70–72]. Many studies have shown its involvement in anxiety, autism, and addiction[73–75]. The emotions and actions initiated from signals in the amygdala can vary widely since there is an immense diversity of excitatory and inhibitory neurons that project to regions such as such as the hippocampus, hypothalamus, BNST, and prefrontal cortex (PFC)[76,77]. Overall levels of activity in this region are not sufficient to predict behavior, since it is also important for positive emotional responses provoked by rewarding experiences ranging from feeding to social interaction[44,78,79]. The amygdala is involved in the neural pathways for social investigation, dominance, aggression, and social attachment[44]. Activation of secretin (SCT) expressing excitatory neurons in the basolateral amygdala (BLA) encourages non-aggressive social interaction[80]. That finding is particularly relevant to this work since we saw increased activity in the hypothalamus of the WildR mice, which also contains $SCT^{+}$ neurons.

At baseline, the changes in brain activity were bidirectional. WildR mice had greater activity in the hippocampus, posterior thalamus, pretectal nucleus, lateral septum, and mammillary body, and less activity in the motor cortex, somatosensory cortex and amygdala. Activation of these areas are implicated in a variety of processes (Table 2), and suggest differences in learning, memory, and emotional processing between the two groups. It's worth highlighting that the amygdala activation patterns are reversed between WildR and SPF mice at baseline as compared to social exposure. Given the diversity of the behavioral and emotional states the amygdala is implicated in, it is likely that the increased activation of this particular region in SPF mice at baseline is a result of distinct neuronal

circuits with different functional outcomes. Additionally, increased activation of the VTA, caudate putamen, prefrontal cortex, and hippocampus in WildR mice suggests upregulation of dopaminergic signaling pathways. This may indicate that the WildR microbiome affects reward or motivation circuitry[81,82].

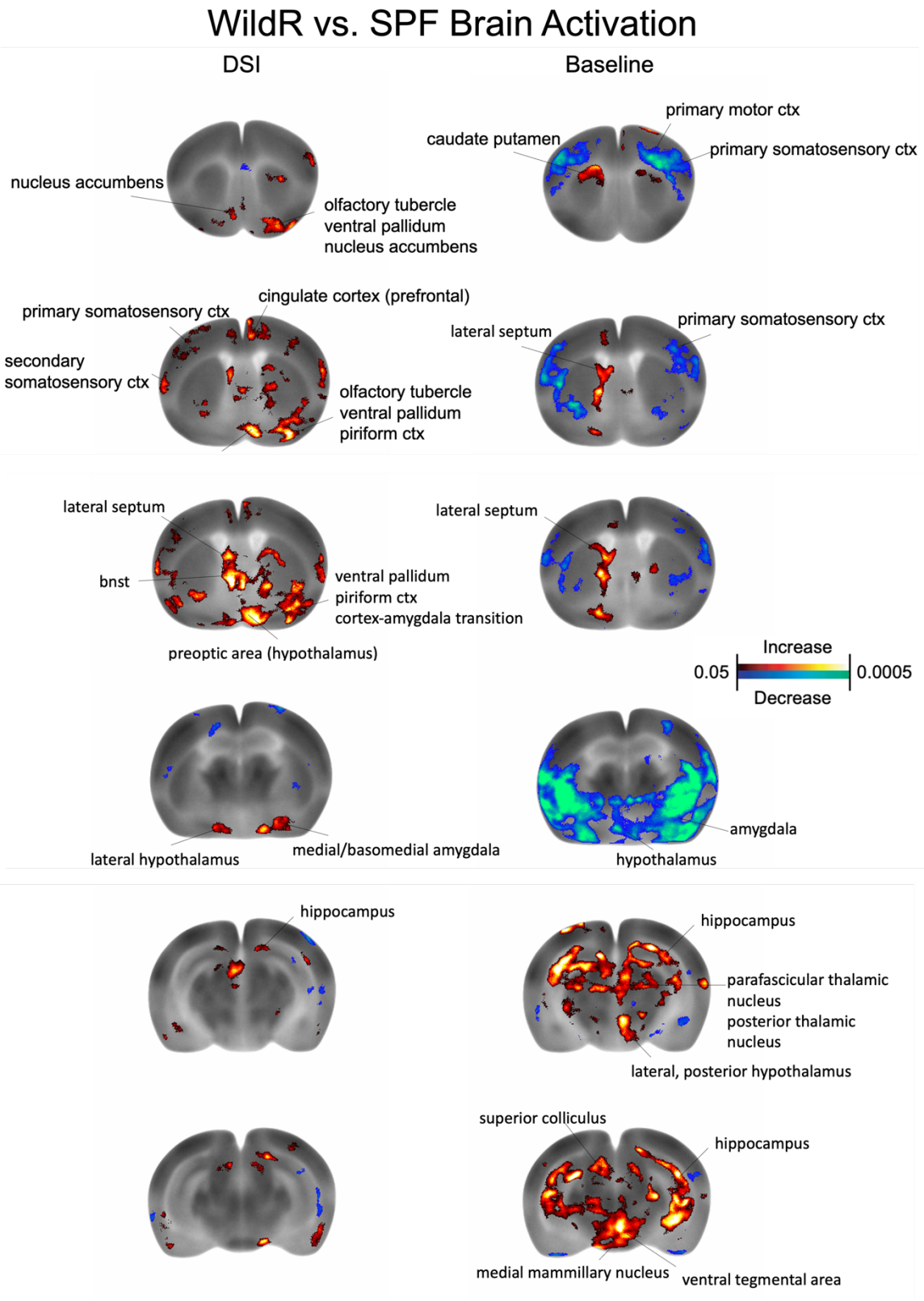
WildR vs. SPF Brain Activation
DSI
Baseline
nucleus accumbens
olfactory tubercle
ventral pallidum
nucleus accumbens
primary motor ctx
caudate putamen
primary somatosensory ctx
primary somatosensory ctx
cingulate cortex (prefrontal)
secondary
somatosensory ctx
olfactory tubercle
ventral pallidum
piriform ctx
lateral septum
primary somatosensory ctx
lateral septum
bnst
ventral pallidum
piriform ctx
cortex-amygdala transition
preoptic area (hypothalamus)
lateral septum
Increase
0.05
0.0005
Decrease
lateral hypothalamus
medial/basomedial amygdala
amygdala
hypothalamus
hippocampus
hippocampus
parafascicular thalamic
nucleus
posterior thalamic
nucleus
lateral, posterior hypothalamus
superior colliculus
hippocampus
medial mammillary nucleus
ventral tegmental area

**Figure 17. Brain activation patterns are altered in WildR mice.** Color-coded maps showing differences in brain glucose uptake between WildR and SPF male mice at baseline and following the DSI test. Displayed over representative coronal brain sections. (n=10-11 per group, p values determined by one-tailed t-tests)

| Test | Purpose |
|---|---|
| Nucleus accumbens | Behavioral response to reward and reinforcement[83] |
| Paraventricular thalamus (PVT) | Emotional processing[54] |
| Perifascicular thalamic nucleus | Attention and arousal[84] |
| Motor cortex | Coordination of movement[85] |
| Hippocampus | Learning and memory[86] |
| Posterior thalamus | Motor and sensory integration[87] |
| Pretectal nucleus | Behavioral response to visual stimuli[88] |
| Mammillary body | Recollective memory[89] |
| Somatosensory cortex | Detection of touch, texture, pain, and temperature[90] |
| Caudate putamen | Movement, learning, memory, reward, and motivation[82] |
| Amygdala | Emotional processing[70] |
| Ventral tegmental area (VTA) | Regulating appetitive and reward behavior[81] |
| Lateral septum | Reward and fear processing and memory[91] |

| | |
|---|---|
| Bed nucleus of the stria terminalis (BNST) | Fear, anxiety, and stress processing and social behavioral response[92] |

**Table 2. Functions of brain regions in mice**

**Stability of WildR Microbiome**

Given the clinical relevance of WildR-colonized mice to human phenotypes and newly discovered behavior and brain activity changes, we performed genomic analyses to ensure stability of the microbiome. In the first WildR study, the WildR microbiome remained stable in mice bred and maintained in gnotobiotic isolators[18]. Though this housing method is effective in preventing contamination, it is space inefficient and costly to continue long-term. In this study, we housed mice in autoclaved sterile cages with sterile food and water bottles in normal housing racks, and replenished the breeders for the colony by colonizing GF mice with cecal contents from the existing WildR mice. SPF and WildR gut microbiomes were surveyed through 16S ribosomal RNA (rRNA) gene sequencing of fecal pellets collected three times over 18 months. We performed a beta diversity analysis to measure dissimilarity of the SPF and WildR gut microbiomes over time[93]. A principal coordinate analysis (PCoA) plot displaying the unweighted UniFrac distance metric shows the differences in beta diversity between SPF and WildR colonies (Figure 18). Equal shifts in the third time point of SPF and WildR samples are likely due to low read depth of the sequencing run (~6,000 reads versus ~50,000 reads).

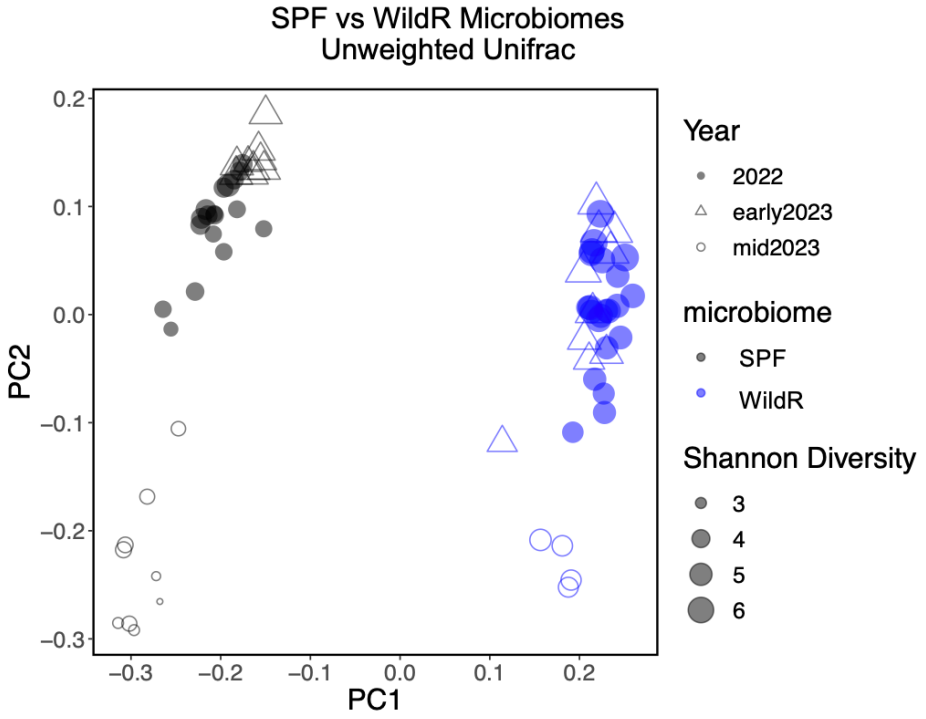


**Figure 18. The WildR microbiome differs significantly from that of conventional SPF laboratory mice.** 16S rRNA genetic data of SPF and WildR fecal pellets shown on unweighted unifrac PCoA. Data plotted by microbiome, time point, and Shannon diversity metric.

We surveyed changes to bacteria members through relative abundance of individual Operational Taxonomic Units (OTUs). OTUs are sequences that are binned into clusters by sequence similarity and are used to assign taxonomy. We performed a longitudinal analysis of OTUs detected in fecal samples from SPF and WildR mice ordered from JAX and Taconic, and in fecal samples from mice in the following three colonization rounds. We found that the bacteria that we observed in the original source fecal material remained present in fecal samples from the following colonization rounds, and we did not find growth of bacteria that weren't detected in the original source material (Figure 19).

This indicates that the WildR and SPF microbiomes are stable, and our husbandry techniques are sufficient to prevent contamination. We searched for taxa identified as differentially abundant in WildR and SPF mice and compared them to studies on microbes with known functional effects on mice in health and disease. One particular bacteria of interest, *Akkermansia muciniphila*, is not present in the WildR microbiome. *A. muciniphila* is commonly present in the gut microbiome of lab SPF mice, and has been implicated in several mouse models of diseases such as epilepsy, multiple sclerosis, obesity, diabetes, and cancer[94–98]. The absence of this microbe in the WildR microbiome and the many wild mice caught in the Rosshart et. al. 2017 study suggest it is not natural member of the community, and therefore may not be biologically relevant to mice. Given this information, it would be worthwhile to perform follow-up studies in the stated disease models with the WildR microbiome to investigate changes in health and to screen for other microbes that impact disease outcomes.

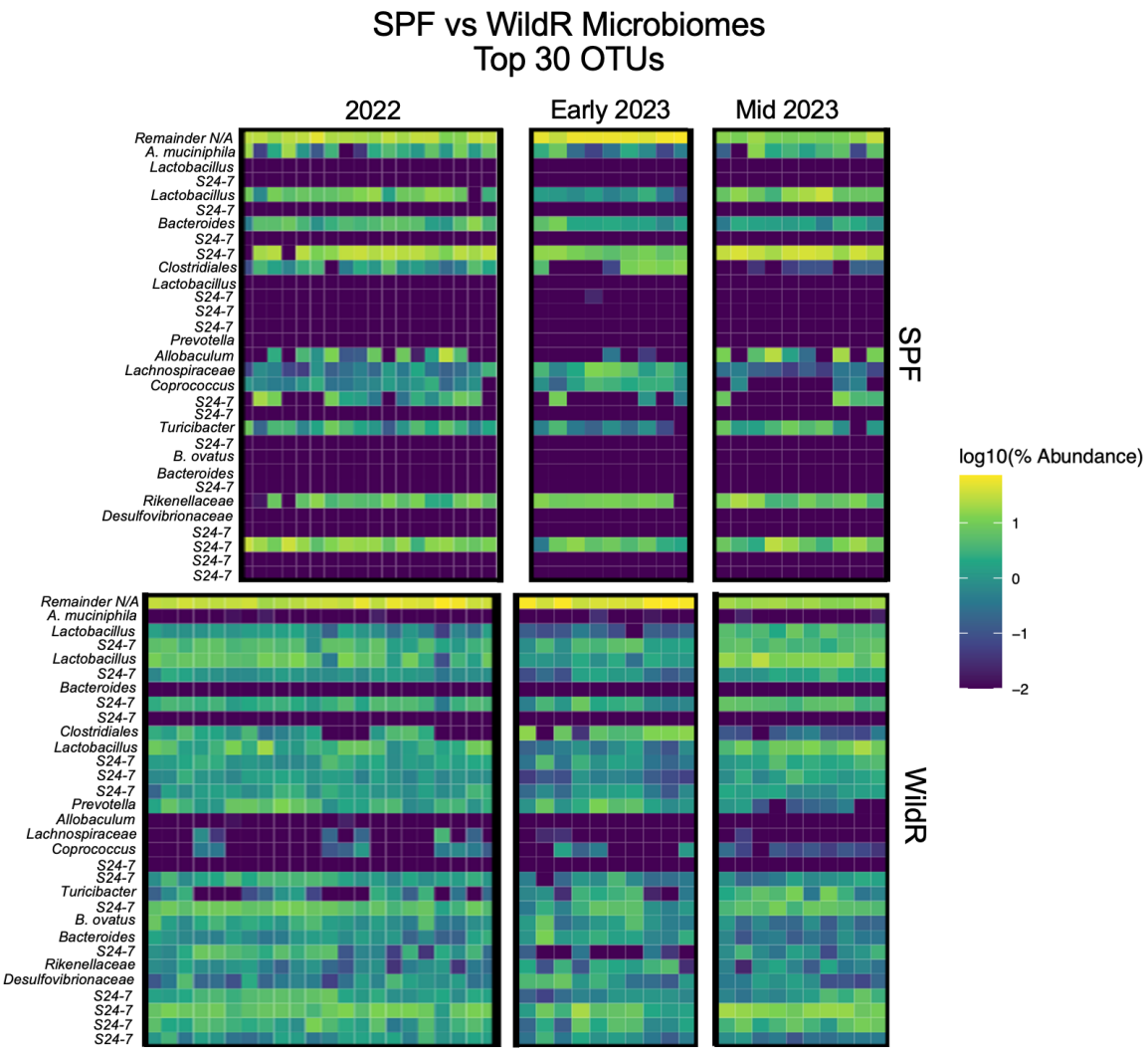


**Figure 19. Relative abundance of individual OTUs in SPF and WildR fecal samples**

Though 16S rRNA sequencing is a useful approach to survey the broad composition of the gut microbiome, it has limitations. Often bacteria can only be identified to the genus level since many species have high similarity in the 16S rRNA gene, rendering them indistinguishable. To achieve species-level information about known neuroactive microbes, we performed qPCR on DNA extracted from fecal pellets. *Lactobacillus reuteri* was a clear candidate, since it stimulates the release of the hormone oxytocin,

reduces stress-induced release of corticosterone, and alters GABA receptor expression in the brain[99–101]. Behaviorally, *L. reuteri* has been shown to decrease anxiety-like behaviors and ameliorate social deficits in mouse models of autism spectrum disorder (ASD)[102–105]. Our results show that *L. reuteri* was relatively less abundant in WildR mice than SPF mice, and so was not driving the observed behavioral phenotypes (Figure 20).

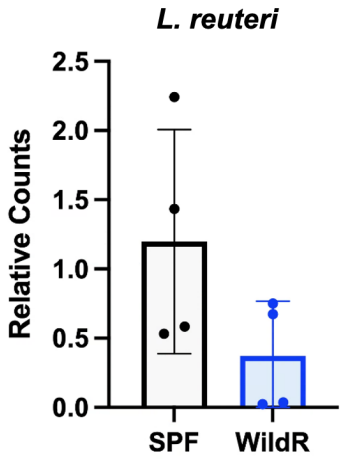


**Figure 20. Relative abundance of *L. reuteri* in SPF and WildR microbiomes**

## DISCUSSION

The "hygiene hypothesis" postulates that excessive cleanliness can impact our health negatively, based on correlational data that countries with decreasing infectious disease burden have increasing incidences of autoimmune diseases and allergies[106,107]. Furthermore, research has shown that patients diagnosed with IBD, and several other conditions, have decreased microbiome diversity[35,108]. Wild mouse gut microbiomes have more microbiome diversity than the SPF mice that have been used in biomedical research for half a century. As research continues to show that SPF mice have stunted immune systems and non-translatable results to clinical drug candidates, a growing number of investigators are employing "re-wilded" mice in their studies to find differences in host health outcomes.

With the knowledge that the immune system and the microbiome modulate neurological phenotypes, our study explores the impact of the WildR microbiome on the brain and behavior. In a wide array of behavioral tests, we discovered that WildR-colonized male mice are more sociable than SPF-colonized male mice. The microbiome specifically affected this phenotype, and did not alter social behavior with female mice, anxiety-like behavior nor cognitive behaviors. Given the diversity in neural circuits involved in social behavior, we performed experiments aimed at identifying the underlying pathway. We did not observe differences in exploration, olfaction, the HPA axis, oxytocin, or aggression. The results of the tube test showed that WildR male mice were more dominant than SPF male mice. Additionally, we found differences in quantity of activated neurons in the hippocampus and amygdala between the two groups following social exposure. A

radiolabeled-tracer uptake experiment showed variations in brain activity between WildR and SPF mice both after social exposure and at baseline. Once more, alterations in activation were observed in the hippocampus and amygdala, extending to include the nucleus accumbens, thalamus, and hypothalamus. Considering the behavioral data and brain regions involved, our current belief is that WildR mice are less fearful of novel mouse, causing them to approach and interact more.

Since this project was designed as an exploration, there are many unanswered questions left to investigate. The selection of behavioral assays used to screen the WildR and SPF animals could be expanded to test other behaviors. The radiolabeled-tracer uptake experiment showed that WildR mice have increased activity in the hippocampus and reduced activity in the somatosensory cortex, which indicates that the mice may perform differently on memory and sensory tests. Examples of these tests include Barnes' maze, fear conditioning, and hot plate sensitivity. Since the animals were tested in standard conditions, future studies could test if more diverse microbiomes effect resilience to stressful conditions such as chronic restraint stress, social defeat, or social isolation.

In this study, we investigated the behavioral phenotype from a neurological approach instead of a microbiological one. From a microbiome perspective, it is unclear if there is a critical window in mouse development in which the WildR microbiota must be present to confer the neurobehavioral effects[109–111]. Studies performed on microbially-depleted mice and GF animals do not always show the same trends[112–115]. The reverse approach, colonizing GF mice with a complex microbiome in adulthood, also results in different

phenotypes from those seen in conventionally bred and raised SPF mice[116]. It would be valuable to perform both microbiota colonization and depletion experiments to study the role of development on the manifestation of the behavioral phenotype.

Additionally, it is possible that distinct microbes within the WildR microbiome modulate social behavior. Though we didn't find differences in one species that is known to influence social behavior, *L. reuteri*, there may be certain species within the WildR microbiome that do. In a future study, WildR mice should be treated with individual antibiotics that deplete different groups of bacteria to see if we can identify candidate neuroactive strains. Furthermore, even though the vast majority of the microbiome is bacteria, fungal and viral species are not to be forgotten. Both fungi and viruses modulate the immune system and influence host fitness[117–120]. It is possible that fungi and viruses may contribute to the phenotypes we have observed, and should be tested. In one approach, a consortia of species could be isolated from WildR mice and administered to SPF mice, or mice could be treated with antifungal or antiviral drugs.

This work contributes to the growing body of research investigating the impact of the microbiome on brain function and behavior. As the field advances, studies are transitioning from establishing correlations to elucidating underlying mechanisms. Our hope is that future research will determine the specific ways in which the WildR microbiome influences the brain and shapes social behaviors. At this point, the possibilities seem endless as we find more routes of gut-brain communication. For example, certain bacteria can secrete molecules that effect oligodendrocyte maturation

and anxiety-like behavior[121]. Others can signal through the vagus nerve to effect social, anxiety, and depression-like behaviors[102,122]. Bacteria that synthesize SCFAs also modulate social and anxiety-like behaviors[123,124]. It is possible that similar pathways are involved in this phenotype, or new ones entirely.

## MATERIALS & METHODS

### Mice

All mouse experiments were performed in accordance with the NIH Guide for the Care and Use of Laboratory Animals using protocols approved by the Institutional Animal Care and Use Committee at the California Institute of Technology. Mice were fed ad libitum for the entire duration of experiments. Specific pathogen free (SPF) C57BL/6 (Jackson Laboratories, Bar Harbor, ME Stock # 000664) and WildR mice (Taconic Biosciences) were used for this study.

### Cecal Microbiota Transfer

Donor SPF and WildR animals were euthanized by $CO_2$ and carcasses were transferred into an anerobic chamber. Ileocecal contents were scraped from the intestines and resuspended in PBS with 1.5% sodium bicarbonate, and spun down at 200 xg for 3 minutes. Recipient GF animals were gavaged with supernatant 3x over 1 week.

### Behavior Testing

All behavior tests were performed at 10-12 weeks of age. Mice were acclimated to the testing room for at least 45 min before all behavior tests. Tests were performed 2–3 days apart for rest between tests.

*Open-field test*

The open-field test is a standard paradigm for anxiety and locomotion. The open-field apparatus is a square open arena (50 × 50 cm) bordered by opaque white plastic walls. Each mouse was placed into the arena in the center and behavior was recorded for 10

min. The center zone (17 × 17 cm) was defined as the middle of the open-field chamber. Behavior in the open field was recorded by a video camera mounted over the arena. Ethovision (Noldus Information Technology) was used to analyze the number of entries to, and the duration in, the center zone. Open-field chambers were disinfected using Rescue disinfectant (Virox technologies) and then allowed to dry.

*Elevated plus maze (EPM)*

This test is similar to EZM, but is performed in a plus-shaped maze with two closed arms and two open arms. The test was recorded using an overhead camera, and tracked and analyzed using the EthoVision XT 10 software package (Noldus Information Technology). Mice were introduced to the center region of the arena and allowed to explore for 5 min while being tracked. The number of entries into and the time spent in open and closed arms were analyzed. Before and in between testing, the maze was disinfected using Rescue disinfectant (Virox technologies) and then allowed to dry.

*Light-dark box*

The light-dark box test is another assessment for anxiety. It was performed in a $50 \times 30\ cm^2$ arena with a $30 \times 30\ cm^2$ open section and a black, lidded section sized $20 \times 30\ cm^2$ with an open doorway for alternation between light and dark areas. Before testing, the arena was disinfected using Rescue disinfectant (Virox technologies), and dried. Mice were placed into the dark box and the lid was closed, and the mice were then recorded using an overhead camera, and tracked and analyzed using the EthoVision XT 10 software package (Noldus Information Technology). Entry and duration in the light chamber was analyzed over a 10 min period. The chambers were disinfected using Rescue disinfectant (Virox technologies) and then allowed to dry.

*Novel object recognition*

The novel object recognition test evaluates cognition and memory. In the training phase, a mouse was introduced to a square open arena (50 × 50 cm) bordered by opaque white plastic walls with two of the same objects in the middle of the arena for 5 minutes. Mice were then returned to their home cage for 7 hours. Then mice were reintroduced to the arena with one familiar and one novel object and tested for 10 minutes. Time spent at each object during the training and test were scored using the EthoVision XT 10 software package (Noldus Information Technology). The chambers and objects were disinfected using Rescue disinfectant (Virox technologies) and then allowed to dry.

*Y-maze*

The Y-maze alternations test is an assay for exploration and cognitive function. It was performed in a white Y maze (Maze Engineers), video-taped from above. Entries into each arm and number of repetitive, spontaneous alterations were scored using the EthoVision XT 10 software package (Noldus Information Technology). The maze was disinfected using Rescue disinfectant (Virox technologies) and then allowed to dry.

*Grooming*

Grooming in the open-field test is a standard test for repetitive behavior. The subject was acclimated to a novel cage with no bedding and lid for 10 minutes before testing. The following 10 minutes were recorded from the side for self-grooming behavior. Grooming was manually analyzed using BORIS software.

*Direct social interaction*

DSI is a test of socialization with a novel animal. The subject mouse was acclimated to a novel cage with clean bedding for 10 minutes before testing. A same-sex, sexually naïve,

age-matched novel B6 mouse (Jackson Laboratories, Bar Harbor, ME Stock #000664) was introduced into the cage. All interactions between the two mice were video recorded for five minutes. Aggressive behaviors were only observed in 1% of interactions. Social behaviors included anogenital sniffing, nose-nose sniffing, and active approach. All interactions initiated by the subject mouse were manually analyzed using BORIS software.

*Three-chamber test*

This test was performed in a 40 (width) × 60 (length) × 20 (height)-cm Plexiglass box divided equally into three chambers by transparent walls made of Plexiglas with open doors (10 cm width × 7 cm height). The procedure consists of two consecutive phases: habituation and sociability. In the habituation phase, test mice were placed in the center of the social chamber for 10 min and allowed to freely explore each compartment. In the sociability phase, test mice were enclosed in the center compartment with the doors closed. Two inverted steel wire cups were placed in each of the two side chambers. An unfamiliar, strain-, age-, and sex- matched mouse was placed in one of the inverted wire cups. The other inverted wire cup represented a novel object. After setting up, doors were opened simultaneously, and the test mouse was allowed to investigate the chamber for 10 min. The behavior was recorded with a video camera mounted above the apparatus. EthoVision XT 10 (Noldus Information Technology) was used to analyze the time spent by the mouse in each chamber, frequency of entry into each chamber, and distance travelled in each phase. The chambers were disinfected using Rescue disinfectant (Virox technologies) and then allowed to dry.

*Ultrasonic vocalization*

At the end of the previous behavioral tests, mice were single-housed and exposed to a new SPF C57BL/6J female for 10 min every day for 5 days before the test. On the sixth day, mice were habituated to an empty cage with a filter soaked with 10 µl of fresh pooled female urine for 10 min. Then, a novel female mouse was introduced to the cage and ultrasonic vocalizations were recorded using an Avisoft UltraSoundGate 116Hme microphone (Avisoft Bioacoustics) and the Avisoft Sas-lab Recorder software (Avisoft Bioacoustics). Total vocalization and vocalization counts were recorded during 3 min sessions of male–female interaction.

*Tube test*

The tube test is an assessment for social dominance. Mice were acclimated to handling for three days, and then acclimated to walk in the tube 10 times for two days. The tube used for the test was clear plastic measuring 30.5 cm length and 3.2 cm inner diameter. On the day of the test, mice of different microbiomes were inserted into either end of the tube, and released at the middle. The mouse that first left the tube with all four paws was deemed the "loser," and the mouse that remained was the "winner." Mice participated in three rounds in one day, and the result was scored manually during the test.

*Isolation-induced aggression*

To increase likelihood of aggression, the subject mouse was single housed for two weeks before testing. A same-sex, sexually naïve, age-matched novel B6 mouse (Jackson Laboratories, Bar Harbor, ME Stock #000664) was introduced into the home-cage for 20 minutes. All interactions between the two mice were video recorded. Attacks were manually analyzed using BORIS.

**Corticosterone measurement**

Mice were euthanized by decapitation and trunk blood was collected in Micro tube Z gel (41.1378.005; Sarstedt). Serum was separated by centrifuge at 10,000 xg for five minutes and stored at −80 °C until use. Corticosterone levels were detected using the Corticosterone EIA Kit (K014-H5; Arbor Assays) according to the manufacturer's protocol. Owing to the effects of circadian rhythm on corticosterone levels, we collected blood samples only between 13:00 and 15:00 on each day of the experiment. For the social measurements, blood was collected 1 hour following a 5-minute social test.

**Testosterone measurement**

Mice were euthanized by $CO_2$ and blood was collected by cardiac puncture followed by separation using Sarstedt K3 EDTA tubes. Plasma was separated by centrifugation at 10,000 xg for 10 minutes and stored at −80 °C until use. Testosterone levels were detected using the Testosterone ELISA Kit (80552; Crystal Chem) according to the manufacturer's protocol. For the baseline measurements, blood was collected between 8:00 and 9:00 on each day of the experiment. For the social measurements, blood was collected 45 minutes following a 5 minute social test between 13:00 and 15:00 on each day of the experiment.

**Brain sectioning and immunohistochemistry**

Mice were anaesthetized with Euthasol, and perfused with ice-cold PBS followed by 4% paraformaldehyde (PFA) in PBS. Brains were removed and post-fixed in 4% PFA in PBS

for 1 day, then washed overnight in PBS. The brains were embedded in 4% UltraPure low melting point agarose (ThermoFisher) and were coronally sectioned by vibratome (VT1000S; Leica) at a thickness of 50 μm.

Free-floating sections were incubated with primary antibody in blocking solution (10% horse serum, 0.1% triton X-100, and 0.02% sodium azide in PBS) overnight at room temperature. The next day, sections were washed in 0.1% PBST (0.1% triton X-100 in PBS) three times over 1 day. Sections were incubated with fluorescence-conjugated secondary antibody for 2 h at room temperature. Then sections were washed in 0.1% PBST (0.1% triton X-100 in PBS) three times over 1 day. The stained free-floating sections were then mounted onto Superfrost Plus microscope slides (Fisher Scientific) in PBS. Excess PBS from adhered sections was carefully removed. Slides were dried at room temperature for 2–5 min. ProLong Diamond anti-fade mountant without DAPI (150–200 μl; ThermoFisher Scientific) was applied to the slides before placing the coverslip. The slides were immersed in mountant overnight before imaging.

Primary antibodies and their dilutions were rabbit anti-c-Fos (1:250; 9F6; Cell Signaling Technologies) and rabbit anti-oxytocin (1:10,000; 20068; Immunostar). The fluorescence-conjugated secondary antibody was donkey anti-rabbit (1:1,000).

**Autoradiographic brain mapping**

Mapping of cerebral glucose metabolism was performed as described previously (source, source) in four groups: SPF/novel cage ($n = 11$), WildR/DSI ($n = 11$), SPF/novel cage

($n = 10$), and WildR/DSI ($n = 11$). At 9 weeks mice were habituated to handling for 5 min each day for 3 days before [$^{14}$C]-2-deoxy-D-glucose mapping. They were brought in their home cages to the experimental suite 16 h before mapping and were fasted overnight with water ad libitum. Each mouse received [$^{14}$C]-2-deoxy-D-glucose (MC355, radiochemical purity > 97%, specific activity 45–60 mCi mmol$^{-1}$, Moravek) at 0.3 μCi g$^{-1}$ bodyweight administered i.p. in 0.5 ml saline. All groups were acclimated to a novel cage for 1 hour. For the novel cage group, the mice were injected i.p. and returned to the cage for 45 minutes to allow uptake of the tracer. For the RSI group, the mice were injected i.p. and returned to the cage for 5 minutes before an age- and weight- matched novel intruder was introduced for 40 minutes. At the end of exposure, after cervical dislocation, the brains were extracted and flash-frozen in methylbutane over dry ice (around −55 °C) and later serially sectioned into 20-μm slices in a cryostat at −20 °C (Mikron HM550 OMP, Thermo Fisher Scientific). Slices were heat-dried on glass slides and exposed to Kodak Biomax MR diagnostic film (Eastman Kodak) for 3 days at room temperature. Autoradiographs were then digitized on an 8-bit grey scale using a voltage-stabilized light box (Northern Lights Illuminator, InterFocus) and a Retiga 4000R charge-coupled device monochrome camera (Qimaging).

Relative regional cerebral glucose uptake (rCGU) was measured and analyzed on a whole-brain basis using Statistical Parametric Mapping (SPM, version 5, Wellcome Centre for Neuroimaging, University College London) as previously described[125–127]. In brief, each three-dimensional (3D) brain was reconstructed from 68 digitized autoradiographs (voxel size: 40 × 140 × 40 μm) using TurboReg, an automated pixel-

based registration algorithm implemented in ImageJ (v.1.35, http://rsbweb.nih.gov/ij/). This algorithm registered each section sequentially to the previous section using a non-warping geometric model that included rotations, rigid-body transformation, and nearest-neighbor interpolation. One 'artifact free' mouse brain was selected as a reference, and all brains were spatially normalized to the reference in SPM. Spatial normalization consisted of applying a 12-parameter affine transformation followed by a nonlinear spatial normalization using 3D discrete cosine transforms. All normalized brains were then averaged to create a final mouse brain template. Each original 3D-reconstructed brain was then spatially normalized to the template. Normalized brains were smoothed with a Gaussian kernel (full width at half maximum = 3 × voxel dimension in the coronal plane). Voxels for each brain failing to reach a specified threshold in optical density (70% of the mean voxel value) were masked out to eliminate the background and ventricular spaces without masking grey or white matter. Differences in the absolute amount of radiotracer uptake in the brain were normalized in SPM for each mouse by scaling the voxel optical densities such that the whole-brain mean for each brain was the same (proportional scaling). For each condition (open-field and home cage exposure), one-tailed *t*-tests were performed voxel-by-voxel comparing SPF and WildR mice. The threshold for significance was set at $P < 0.05$ at the voxel level and an extent threshold of 200 contiguous voxels to eliminate false-positive statistically significant results. Color-coded functional overlays showing statistically significant changes in rCGU were displayed over coronal sections of the template brain in MRIcro (v.1.40, https://people.cas.sc.edu/rorden/mricro/mricro.html). This combination reflected a balanced approach to control both type I and type II errors. The minimum cluster

criterion was applied to avoid basing our results on significance at a single or small number of suprathreshold voxels. Brain regions were identified according to a mouse brain atlas (https://atlas.brain-map.org).

**Fecal Microbiome Community Analysis**

Bacterial 16S rRNA genes from extracted fecal DNA were PCR-amplified with barcoded primers targeting the V4 region. Sequencing was performed by Laragen, Inc (Culver City, CA). Amplicons were sequenced according to the Earth Microbiome Protocol. Sequences were analyzed using the QIIME2 (2019.10) software package. Demultiplexed reads were filtered for quality and denoised using the dada2 package.

***L. reuteri* abundance analysis**

Fecal pellets were collected from mice and stored at -80°C. Microbial DNA was extracted using the Zymo Quick-DNA Fecal/Soil Microbe Miniprep Kit (Zymo Research, Cat#D6010), according to the manufacturer's protocol. Extracted DNA was used as template for qPCR reactions (ThermoFisher Scientific, Cat#A25742) using universal bacterial primers (200 nM forward and reverse) against the microbial 16S rRNA (515F: 5'- GTGCCAGCMGCCGCGGTAA-3', 806R: 5'-GGACTACHVGGGTWTCTAAT-3') and 16s RNA primers for *L. reuteri* (F: 5'-GATTGACGATGGATCACCAGT-3', R: 5'-CATCCCAGAGTGATAGCCAA-3'). *L. reuteri* qPCR signal was normalized by the universal bacterial primers.

**REFERENCES**

1. Why Animals are Used in Research. *Natl. Inst. Health* (2022).

2. Hu, C. Of mice and model organisms. *Cold Spring Harb. Lab.* (2019).
3. Vandamme, T. F. Use of rodents as models of human diseases. *J. Pharm. Bioallied Sci.* **6**, 2–9 (2014).
4. Bryda, E. C. The Mighty Mouse: the impact of rodents on advances in biomedical research. *Mo. Med.* **110**, 207–211 (2013).
5. Baker, M. 1,500 scientists lift the lid on reproducibility. *Nature* **533**, 452–454 (2016).
6. Lauer, A. M., May, B. J., Hao, Z. J. & Watson, J. Analysis of environmental sound levels in modern rodent housing rooms. *Lab Anim.* **38**, 154–160 (2009).
7. Zeldovich, L. Genetic drift: the ghost in the genome. *Lab Anim.* **46**, 255–257 (2017).
8. Harrison, C. Housing and husbandry impact mouse phenotypes. *Lab Anim.* **52**, 9–9 (2023).
9. Georgiou, P. *et al.* Experimenters' sex modulates mouse behaviors and neural responses to ketamine via corticotropin releasing factor. *Nat. Neurosci.* **25**, 1191–1200 (2022).
10. Alegre, M.-L. Mouse microbiomes: overlooked culprits of experimental variability. *Genome Biol.* **20**, 108 (2019).
11. Ericsson, A. C. & Franklin, C. L. The gut microbiome of laboratory mice: considerations and best practices for translational research. *Mamm. Genome Off. J. Int. Mamm. Genome Soc.* **32**, 239–250 (2021).
12. Graham, D. M. A walk on the wild side. *Lab Anim.* **46**, 423–427 (2017).
13. Cadwell, K. *et al.* Virus-plus-susceptibility gene interaction determines Crohn's disease gene Atg16L1 phenotypes in intestine. *Cell* **141**, 1135–1145 (2010).

14. Wong, S.-Y. *et al.* B Cell Defects Observed in Nod2 Knockout Mice Are a Consequence of a Dock2 Mutation Frequently Found in Inbred Strains. *J. Immunol. Baltim. Md 1950* **201**, 1442–1451 (2018).
15. Kim, S. *et al.* Maternal gut bacteria promote neurodevelopmental abnormalities in mouse offspring. *Nature* **549**, 528–532 (2017).
16. Ivanov, I. I. *et al.* Induction of intestinal Th17 cells by segmented filamentous bacteria. *Cell* **139**, 485–498 (2009).
17. Maue, A. Segmented Filamentous Bacteria in Mice. *Taconic* (2017).
18. Rosshart, S. P. *et al.* Wild Mouse Gut Microbiota Promotes Host Fitness and Improves Disease Resistance. *Cell* **171**, 1015-1028.e13 (2017).
19. Rosshart, S. P. *et al.* Laboratory mice born to wild mice have natural microbiota and model human immune responses. *Science* **365**, (2019).
20. Dobson, G. P., Letson, H. L., Biros, E. & Morris, J. Specific pathogen-free (SPF) animal status as a variable in biomedical research: Have we come full circle? *EBioMedicine* **41**, 42–43 (2019).
21. Round, J. L. & Mazmanian, S. K. The gut microbiota shapes intestinal immune responses during health and disease. *Nat. Rev. Immunol.* **9**, 313–323 (2009).
22. Chung, H. & Kasper, D. L. Microbiota-stimulated immune mechanisms to maintain gut homeostasis. *Host Pathog. ● Immune Senescence* **22**, 455–460 (2010).
23. Mazmanian, S. K. & Lee, Y. K. Interplay between Intestinal Microbiota and Host Immune System. *jbv* **44**, 1–9 (2014).
24. Tabilas, C. *et al.* Early microbial exposure shapes adult immunity by altering CD8+ T cell development. *Proc. Natl. Acad. Sci. U. S. A.* **119**, e2212548119 (2022).

25. Huggins, M. A., Jameson, S. C. & Hamilton, S. E. Embracing microbial exposure in mouse research. *J. Leukoc. Biol.* **105**, 73–79 (2019).
26. Beura, L. K. *et al.* Normalizing the environment recapitulates adult human immune traits in laboratory mice. *Nature* **532**, 512–516 (2016).
27. Abolins, S. *et al.* The comparative immunology of wild and laboratory mice, Mus musculus domesticus. *Nat. Commun.* **8**, 14811 (2017).
28. Schultz, D. Can 'dirty mice' save animal research? *Science* (2016).
29. Kolata, G. Mice fall short as test subjects for some of humans' deadly ills. *N. Y. Times* (2013).
30. Hingorani, A. D. *et al.* Improving the odds of drug development success through human genomics: modelling study. *Sci. Rep.* **9**, 18911 (2019).
31. Oh, J. H. & Rehermann, B. Natural versus Laboratory World: Incorporating Wild-Derived Microbiota into Preclinical Rodent Models. *J. Immunol. Baltim. Md 1950* **207**, 1703–1709 (2021).
32. Sharon, G., Sampson, T. R., Geschwind, D. H. & Mazmanian, S. K. The Central Nervous System and the Gut Microbiome. *Cell* **167**, 915–932 (2016).
33. Morais, L. H., Schreiber, H. L. & Mazmanian, S. K. The gut microbiota–brain axis in behaviour and brain disorders. *Nat. Rev. Microbiol.* **19**, 241–255 (2021).
34. Cryan, J. F. *et al.* The Microbiota-Gut-Brain Axis. *Physiol. Rev.* **99**, 1877–2013 (2019).
35. Johnson, K. V.-A. Gut microbiome composition and diversity are related to human personality traits. *Hum. Microbiome J.* **15**, 100069 (2020).

36. Bibbó, S. *et al.* Gut microbiota in anxiety and depression: Pathogenesis and therapeutics. *Front. Gastroenterol.* **1**, (2022).

37. Liu, L. *et al.* Gut microbiota and its metabolites in depression: from pathogenesis to treatment. *EBioMedicine* **90**, 104527 (2023).

38. Raulo, A. *et al.* Social networks strongly predict the gut microbiota of wild mice. *ISME J.* **15**, 2601–2613 (2021).

39. Wu, W.-L. *et al.* Microbiota regulate social behaviour via stress response neurons in the brain. *Nature* **595**, 409–414 (2021).

40. Diaz Heijtz, R. *et al.* Normal gut microbiota modulates brain development and behavior. *Proc. Natl. Acad. Sci. U. S. A.* **108**, 3047–3052 (2011).

41. Luczynski, P. *et al.* Growing up in a Bubble: Using Germ-Free Animals to Assess the Influence of the Gut Microbiota on Brain and Behavior. *Int. J. Neuropsychopharmacol.* **19**, pyw020 (2016).

42. Neufeld, K. M., Kang, N., Bienenstock, J. & Foster, J. A. Reduced anxiety-like behavior and central neurochemical change in germ-free mice. *Neurogastroenterol. Motil.* **23**, 255–264, e119 (2011).

43. Jabarin, R., Netser, S. & Wagner, S. Beyond the three-chamber test: toward a multimodal and objective assessment of social behavior in rodents. *Mol. Autism* **13**, 41 (2022).

44. Ko, J. Neuroanatomical Substrates of Rodent Social Behavior: The Medial Prefrontal Cortex and Its Projection Patterns. *Front. Neural Circuits* **11**, 41 (2017).

45. Gao, S.-C., Wei, Y.-C., Wang, S.-R. & Xu, X.-H. Medial Preoptic Area Modulates Courtship Ultrasonic Vocalization in Adult Male Mice. *Neurosci. Bull.* **35**, 697–708 (2019).

46. Anderson, D. J. Circuit modules linking internal states and social behaviour in flies and mice. *Nat. Rev. Neurosci.* **17**, 692–704 (2016).

47. Chen, P. & Hong, W. Neural Circuit Mechanisms of Social Behavior. *Neuron* **98**, 16–30 (2018).

48. Báez-Mendoza, R., Vázquez, Y., Mastrobattista, E. P. & Williams, Z. M. Neuronal Circuits for Social Decision-Making and Their Clinical Implications. *Front. Neurosci.* **15**, 720294 (2021).

49. Bosch, O. J. & Young, L. J. Oxytocin and Social Relationships: From Attachment to Bond Disruption. *Curr. Top. Behav. Neurosci.* **35**, 97–117 (2018).

50. Carter, C. S. The Oxytocin-Vasopressin Pathway in the Context of Love and Fear. *Front. Endocrinol.* **8**, 356 (2017).

51. Donaldson, Z. R. & Young, L. J. Oxytocin, vasopressin, and the neurogenetics of sociality. *Science* **322**, 900–904 (2008).

52. Light, K. C., Grewen, K. M. & Amico, J. A. More frequent partner hugs and higher oxytocin levels are linked to lower blood pressure and heart rate in premenopausal women. *Biol. Psychol.* **69**, 5–21 (2005).

53. Jones, C., Barrera, I., Brothers, S., Ring, R. & Wahlestedt, C. Oxytocin and social functioning. *Dialogues Clin. Neurosci.* **19**, 193–201 (2017).

54. Resendez, S. L. *et al.* Social Stimuli Induce Activation of Oxytocin Neurons Within the Paraventricular Nucleus of the Hypothalamus to Promote Social Behavior in Male Mice. *J. Neurosci. Off. J. Soc. Neurosci.* **40**, 2282–2295 (2020).

55. Hörnberg, H. *et al.* Rescue of oxytocin response and social behaviour in a mouse model of autism. *Nature* **584**, 252–256 (2020).

56. Kitagawa, K. *et al.* Intranasal oxytocin administration ameliorates social behavioral deficits in a POGZWT/Q1038R mouse model of autism spectrum disorder. *Mol. Brain* **14**, 56 (2021).

57. Teng, B. L. *et al.* Prosocial effects of oxytocin in two mouse models of autism spectrum disorders. *Neuropharmacology* **72**, 187–196 (2013).

58. Peñagarikano, O. *et al.* Exogenous and evoked oxytocin restores social behavior in the Cntnap2 mouse model of autism. *Sci. Transl. Med.* **7**, 271ra8 (2015).

59. Hara, Y. *et al.* Oxytocin attenuates deficits in social interaction but not recognition memory in a prenatal valproic acid-induced mouse model of autism. *Horm. Behav.* **96**, 130–136 (2017).

60. Bakker, J., Leinders-Zufall, T. & Chamero, P. The Sense of Smell: Role of the Olfactory System in Social Behavior. in *Neuroscience in the 21st Century: From Basic to Clinical* (eds. Pfaff, D. W., Volkow, N. D. & Rubenstein, J.) 1–29 (Springer New York, 2020). doi:10.1007/978-1-4614-6434-1_29-4.

61. Takahashi, A. Toward Understanding the Sex Differences in the Biological Mechanism of Social Stress in Mouse Models. *Front. Psychiatry* **12**, 644161 (2021).

62. Yang, C. F. *et al.* Sexually dimorphic neurons in the ventromedial hypothalamus govern mating in both sexes and aggression in males. *Cell* **153**, 896–909 (2013).

63. Dreher, J.-C. *et al.* Testosterone causes both prosocial and antisocial status-enhancing behaviors in human males. *Proc. Natl. Acad. Sci.* **113**, 11633–11638 (2016).

64. Kelly, A. M., Gonzalez Abreu, J. A. & Thompson, R. R. Beyond sex and aggression: testosterone rapidly matches behavioural responses to social context and tries to predict the future. *Proc. Biol. Sci.* **289**, 20220453 (2022).

65. Fulenwider, H. D., Caruso, M. A. & Ryabinin, A. E. Manifestations of domination: Assessments of social dominance in rodents. *Genes Brain Behav.* **21**, e12731 (2022).

66. Rodriguez-Romaguera, J. & Stuber, G. D. Social Isolation Co-opts Fear and Aggression Circuits. *Cell* **173**, 1071–1072 (2018).

67. Zelikowsky, M. *et al.* The Neuropeptide Tac2 Controls a Distributed Brain State Induced by Chronic Social Isolation Stress. *Cell* **173**, 1265-1279.e19 (2018).

68. Hoffman, G. E., Smith, M. S. & Verbalis, J. G. c-Fos and related immediate early gene products as markers of activity in neuroendocrine systems. *Front. Neuroendocrinol.* **14**, 173–213 (1993).

69. Distel, R. J. & Spiegelman, B. M. Protooncogene c-fos as a transcription factor. *Adv. Cancer Res.* **55**, 37–55 (1990).

70. Phelps, E. A. & LeDoux, J. E. Contributions of the amygdala to emotion processing: from animal models to human behavior. *Neuron* **48**, 175–187 (2005).

71. Adolphs, R., Tranel, D., Damasio, H. & Damasio, A. R. Fear and the human amygdala. *J. Neurosci. Off. J. Soc. Neurosci.* **15**, 5879–5891 (1995).

72. Šimić, G. *et al.* Understanding Emotions: Origins and Roles of the Amygdala. *Biomolecules* **11**, (2021).

73. Andrews, D. S. *et al.* Association of Amygdala Development With Different Forms of Anxiety in Autism Spectrum Disorder. *Biol. Psychiatry* **91**, 977–987 (2022).

74. Ressler, K. J. Amygdala activity, fear, and anxiety: modulation by stress. *Biol. Psychiatry* **67**, 1117–1119 (2010).

75. Koob, G. F. Brain stress systems in the amygdala and addiction. *Brain Res.* **1293**, 61–75 (2009).

76. Hintiryan, H. *et al.* Connectivity characterization of the mouse basolateral amygdalar complex. *Nat. Commun.* **12**, 2859 (2021).

77. Hochgerner, H. *et al.* Neuronal types in the mouse amygdala and their transcriptional response to fear conditioning. *Nat. Neurosci.* **26**, 2237–2249 (2023).

78. Peters, C. *et al.* Transcriptomics reveals amygdala neuron regulation by fasting and ghrelin thereby promoting feeding. *Sci. Adv.* **9**, eadf6521.

79. Scheggia, D. *et al.* Reciprocal cortico-amygdala connections regulate prosocial and selfish choices in mice. *Nat. Neurosci.* **25**, 1505–1518 (2022).

80. Wei, J. *et al.* Amygdala neural ensemble mediates mouse social investigation behaviors. *Natl. Sci. Rev.* **10**, nwac179 (2023).

81. Cai, J. & Tong, Q. Anatomy and Function of Ventral Tegmental Area Glutamate Neurons. *Front. Neural Circuits* **16**, 867053 (2022).

82. Driscoll, M. E., Bollu, P. C. & Tadi, P. Neuroanatomy, Nucleus Caudate. in *StatPearls* (StatPearls Publishing, 2023).

83. Gale, J. T., Shields, D. C., Ishizawa, Y. & Eskandar, E. N. Reward and reinforcement activity in the nucleus accumbens during learning. *Front. Behav. Neurosci.* **8**, 114 (2014).

84. Fallon, I. P. *et al.* The role of the parafascicular thalamic nucleus in action initiation and steering. *Curr. Biol. CB* **33**, 2941-2951.e4 (2023).

85. Yip, D. W. & Lui, F. Physiology, Motor Cortical. in *StatPearls* (StatPearls Publishing, 2023).

86. Knierim, J. J. The hippocampus. *Curr. Biol.* **25**, R1116–R1121 (2015).

87. Casas-Torremocha, D., Clascá, F. & Núñez, Á. Posterior Thalamic Nucleus Modulation of Tactile Stimuli Processing in Rat Motor and Primary Somatosensory Cortices. *Front. Neural Circuits* **11**, 69 (2017).

88. Sprague, J. M., Berlucchi, G. & Rizzolatti, G. The Role of the Superior Colliculus and Pretectum in Vision and Visually Guided Behavior. in *Visual Centers in the Brain* (eds. Berlucchi, G. et al.) 27–101 (Springer Berlin Heidelberg, 1973). doi:10.1007/978-3-642-65495-4_2.

89. Peterson, D. C., Reddy, V. & Mayes, D. A. Neuroanatomy, Mammillary Bodies. in *StatPearls* (StatPearls Publishing, 2023).

90. Raju, H. & Tadi, P. Neuroanatomy, Somatosensory Cortex. in *StatPearls* (StatPearls Publishing, 2023).

91. Rizzi-Wise, C. A. & Wang, D. V. Putting Together Pieces of the Lateral Septum: Multifaceted Functions and Its Neural Pathways. *eNeuro* **8**, ENEURO.0315-21.2021 (2021).

92. Lebow, M. A. & Chen, A. Overshadowed by the amygdala: the bed nucleus of the stria terminalis emerges as key to psychiatric disorders. *Mol. Psychiatry* **21**, 450–463 (2016).

93. Lozupone, C., Lladser, M. E., Knights, D., Stombaugh, J. & Knight, R. UniFrac: an effective distance metric for microbial community comparison. *ISME J.* **5**, 169–172 (2011).

94. Everard, A. *et al.* Cross-talk between Akkermansia muciniphila and intestinal epithelium controls diet-induced obesity. *Proc. Natl. Acad. Sci.* **110**, 9066–9071 (2013).

95. Fan, S. *et al.* Akkermansia muciniphila: a potential booster to improve the effectiveness of cancer immunotherapy. *J. Cancer Res. Clin. Oncol.* **149**, 13477–13494 (2023).

96. Cekanaviciute, E. *et al.* Multiple Sclerosis-Associated Changes in the Composition and Immune Functions of Spore-Forming Bacteria. *mSystems* **3**, (2018).

97. Olson, C. A. *et al.* The Gut Microbiota Mediates the Anti-Seizure Effects of the Ketogenic Diet. *Cell* **173**, 1728-1741.e13 (2018).

98. Plovier, H. *et al.* A purified membrane protein from Akkermansia muciniphila or the pasteurized bacterium improves metabolism in obese and diabetic mice. *Nat. Med.* **23**, 107–113 (2017).

99. Danhof, H. A., Lee, J., Thapa, A., Britton, R. A. & Di Rienzi, S. C. Microbial stimulation of oxytocin release from the intestinal epithelium via secretin signaling. *Gut Microbes* **15**, 2256043 (2023).

100. Tette, F.-M., Kwofie, S. K. & Wilson, M. D. Therapeutic Anti-Depressant Potential of Microbial GABA Produced by Lactobacillus rhamnosus Strains for GABAergic Signaling Restoration and Inhibition of Addiction-Induced HPA Axis Hyperactivity. *Curr. Issues Mol. Biol.* **44**, 1434–1451 (2022).

101. Varian, B. J. *et al.* Microbial lysate upregulates host oxytocin. *Brain. Behav. Immun.* **61**, 36–49 (2017).

102. Sgritta, M. *et al.* Mechanisms Underlying Microbial-Mediated Changes in Social Behavior in Mouse Models of Autism Spectrum Disorder. *Neuron* **101**, 246-259.e6 (2019).

103. Buffington, S. A. *et al.* Microbial Reconstitution Reverses Maternal Diet-Induced Social and Synaptic Deficits in Offspring. *Cell* **165**, 1762–1775 (2016).

104. Buffington, S. A. *et al.* Dissecting the contribution of host genetics and the microbiome in complex behaviors. *Cell* **184**, 1740-1756.e16 (2021).

105. Zhang, W. *et al.* Lactobacillus reuteri normalizes altered fear memory in male Cntnap4 knockout mice. *EBioMedicine* **86**, 104323 (2022).

106. Murdaca, G., Greco, M., Borro, M. & Gangemi, S. Hygiene hypothesis and autoimmune diseases: A narrative review of clinical evidences and mechanisms. *Autoimmun. Rev.* **20**, 102845 (2021).

107. Bloomfield, S. F., Stanwell-Smith, R., Crevel, R. W. R. & Pickup, J. Too clean, or not too clean: the hygiene hypothesis and home hygiene. *Clin. Exp. Allergy J. Br. Soc. Allergy Clin. Immunol.* **36**, 402–425 (2006).

108. Shan, Y., Lee, M. & Chang, E. B. The Gut Microbiome and Inflammatory Bowel Diseases. *Annu. Rev. Med.* **73**, 455–468 (2022).

109. Lu, J. *et al.* Effects of Intestinal Microbiota on Brain Development in Humanized Gnotobiotic Mice. *Sci. Rep.* **8**, 5443 (2018).

110. Cox, L. M. *et al.* Altering the intestinal microbiota during a critical developmental window has lasting metabolic consequences. *Cell* **158**, 705–721 (2014).

111. Lynch, C. M. K. *et al.* Critical windows of early-life microbiota disruption on behaviour, neuroimmune function, and neurodevelopment. *Brain. Behav. Immun.* **108**, 309–327 (2023).

112. Bayer, F., Ascher, S., Pontarollo, G. & Reinhardt, C. Antibiotic Treatment Protocols and Germ-Free Mouse Models in Vascular Research. *Front. Immunol.* **10**, 2174 (2019).

113. Bourré, L. Germ-Free or Antibiotic-Treated Mice? Which Model for Studying the Role of the Gut Microbiota in Preclinical Studies. *Crown Biosci.* (2020).

114. Kennedy, E. A., King, K. Y. & Baldridge, M. T. Mouse Microbiota Models: Comparing Germ-Free Mice and Antibiotics Treatment as Tools for Modifying Gut Bacteria. *Front. Physiol.* **9**, 1534 (2018).

115. Johnson, K. V. A. & Burnet, P. W. J. Opposing effects of antibiotics and germ-free status on neuropeptide systems involved in social behaviour and pain regulation. *BMC Neurosci.* **21**, 32 (2020).

116. Desbonnet, L., Clarke, G., Shanahan, F., Dinan, T. G. & Cryan, J. F. Microbiota is essential for social development in the mouse. *Mol. Psychiatry* **19**, 146–148 (2014).

117. Virgin, H. W. The virome in mammalian physiology and disease. *Cell* **157**, 142–150 (2014).

118. Iliev, I. D. & Cadwell, K. Effects of Intestinal Fungi and Viruses on Immune Responses and Inflammatory Bowel Diseases. *Gastroenterology* **160**, 1050–1066 (2021).

119. Jaswal, K., Todd, O. A. & Behnsen, J. Neglected gut microbiome: interactions of the non-bacterial gut microbiota with enteric pathogens. *Gut Microbes* **15**, 2226916 (2023).

120. Huffnagle, G. B. & Noverr, M. C. The emerging world of the fungal microbiome. *Trends Microbiol.* **21**, 334–341 (2013).

121. Needham, B. D. *et al.* A gut-derived metabolite alters brain activity and anxiety behaviour in mice. *Nature* **602**, 647–653 (2022).

122. Bravo, J. A. *et al.* Ingestion of Lactobacillus strain regulates emotional behavior and central GABA receptor expression in a mouse via the vagus nerve. *Proc. Natl. Acad. Sci.* **108**, 16050–16055 (2011).

123. Wu, J.-T. *et al.* Oral short-chain fatty acids administration regulates innate anxiety in adult microbiome-depleted mice. *Neuropharmacology* **214**, 109140 (2022).

124. Osman, A. *et al.* Acetate supplementation rescues social deficits and alters transcriptional regulation in prefrontal cortex of Shank3 deficient mice. *Brain. Behav. Immun.* **114**, 311–324 (2023).

125. Holschneider, D. P., Guo, Y., Wang, Z., Vidal, M. & Scremin, O. U. Positive Allosteric Modulation of Cholinergic Receptors Improves Spatial Learning after Cortical Contusion Injury in Mice. *J. Neurotrauma* **36**, 2233–2245 (2019).

126. Wang, Z., Pang, R. D., Hernandez, M., Ocampo, M. A. & Holschneider, D. P. Anxiolytic-like effect of pregabalin on unconditioned fear in the rat: an autoradiographic brain perfusion mapping and functional connectivity study. *NeuroImage* **59**, 4168–4188 (2012).

127. Sokoloff, L. Localization of Functional Activity in the Central Nervous System by Measurement of Glucose Utilization with Radioactive Deoxyglucose. *J. Cereb. Blood Flow Metab.* **1**, 7–36 (1981).

*Chapter 5*

# THESIS CONCLUSION

"Nothing exists for itself alone, but only in relation to other forms of life."

-Charles Darwin

The information discussed in this thesis spans diverse disciplines and topics. The unifying theme across the previous chapters is the benefits of cooperation: cooperation between (1) biological systems within an organism, (2) organisms within the same species, and (3) organisms of different species.

*(1) Biological systems within an organism*

Biological systems must work in coordination to keep an organism alive. Across the many systems that exist, the immune system and nervous system are the primary focus of this thesis. These two systems are connected to the extent that the distinction between the two is unclear[1]. Complement proteins used to defend our bodies from foreign pathogens are also used for synaptic pruning during development[2]. T cells have receptors for neurotransmitters (dopamine, serotonin, and glutamate)[3]. Though these interactions occur across the body, the site of most neuroimmune interactions is the gut. There, 70-80% of the body's immune cells and 100 million neurons interact to coordinate digestion and protect the host[4]. My thesis reports novel interactions between the immune system and nervous systems. In Chapter II, one of the key findings from activation of gut neuronal subtypes ($ChAT^+$ and $TH^+$) is modulation of immune cells and processes. In Chapter III, I show that depletion of a neuronal protein (SHANK3) associated with synaptic dysfunction in the brain and behavioral changes alters gut motility and susceptibility to inflammation.

*(2) Organisms of the same species*

When comparing longevity of mammalian species, solitary species have shorter life spans than group-living species[5]. Group living provides many benefits such as protection from predators, assistance in caring for young, and improved well-being due to social bonding[6]. Both humans and rodents live in groups and depend on other members of their species for support. Recently, it has been suggested that another outcome of social networks is microbiota transmission[7]. Indeed, humans and mice share remarkable microbiome similarity with cohabitants. Further, individuals with more social contacts have more diverse microbiomes[8,9]. Surprisingly, my findings suggest that the observed phenomenon linking sociability and microbiome diversity may not solely stem from sociability, as it appears to be influenced by the reverse direction as well. The behavioral results in chapter IV show that the increased diversity of a wild mouse microbiome enhances intraspecies interactions within mice.

*(3) Organisms of different species*

The microbiome is an active modulator of the biological processes of its host, especially the immune and nervous systems. Many of the findings on the importance of the gut microbiome were discovered through the development of germ-free (GF) mouse models[10]. GF mice have many immune defects, such as T cell deficiencies, altered immunoglobulin profiles, and increased susceptibility to infection[10–12]. Additionally, GF mice have altered neurogenesis and expression of genes related to brain function as well as altered cognition, anxiety, and social behaviors[10,12,13]. As an extension of these

findings, my work in Chapter III shows that the GF condition partially ameliorates autism-related behavior changes in the *Shank3B*$^{-/-}$ mouse model.

More studies have discovered mechanisms of action of individual microbes on host physiology. Certain microbes can alter corticosterone release, oxytocin and oxytocin receptor expression, and maturation and function of supportive brain cell types[14–18]. The next stage of this field of research is to determine the differential impacts on the host of natural and complex microbiomes. Motivated by this perspective, studies have shown that wild and pet store microbiomes result in mice with immune profiles that more closely resemble those of humans[19]. Given the prolific crosstalk between biological systems, it is unlikely this is the only impact wild microbiomes have on the host. In support of this theory, my findings in Chapter IV show that a wild mouse gut microbiome alters brain activity profiles and behavior in mice.

The relationship between the gut microbiome and host is bidirectional. Diet, lifestyle, genetics, age, and immunity all impact the composition and function of the gut microbiome[20]. Since the microbiome encompasses 100 times as many genes as the human genome, alterations in composition have profound impact on function[20]. In Chapter III, I found that depletion of SHANK3 results in less diverse microbiomes and altered taxa as compared to controls. Further, engineered activation of different neuronal subtypes (ChAT$^{+}$ and TH$^{+}$) in Chapter II has robust effects on gut microbiome composition, and corresponding changes in expression of gene clusters.

*Final thoughts*

This thesis presents several novel findings on the interactions between and within life forms. Biological interactions have been evolving for 3.7 billion years, since the first microbes appeared on earth[21]. Microbes have been with us since multicellular organisms appeared 600 million years ago[22]. This time frame has provided ample opportunity to develop more immense and intricate exchanges, especially between microbes and their hosts. Understanding and embracing the complexity of these relationships is crucial to the future of biology. When biological entities are broken down into parts, with increasing levels of magnification on individual components and their function, we gain valuable insight but miss the context. The living world is interconnected because it is evolutionarily favorable[23–26]. Studying a living thing without its environment and interactions with others misses the point of its existence. As an old proverb says, we must not "lose sight of the forest for the trees."[27]

**REFERENCES**


1. Dobie, T. Neuro-immune interactions: The spectacular forest. *Neuron* 3407–2408 (2022).
2. Stephan, A. H., Barres, B. A. & Stevens, B. The complement system: an unexpected role in synaptic pruning during development and disease. *Annu. Rev. Neurosci.* **35**, 369–389 (2012).
3. Levite, M. Neurotransmitters activate T-cells and elicit crucial functions via neurotransmitter receptors. *Cancer/Immunomodulation* **8**, 460–471 (2008).
4. Yoo, B. B. & Mazmanian, S. K. The Enteric Network: Interactions between the Immune and Nervous Systems of the Gut. *Immunity* **46**, 910–926 (2017).
5. Zhu, P. *et al.* Correlated evolution of social organization and lifespan in mammals. *Nat. Commun.* **14**, 372 (2023).
6. Krause, J. & Ruxton, G. Living in Groups. in (Oxford University Press, 2002).
7. Sarkar, A. *et al.* Microbial transmission in animal social networks and the social microbiome. *Nat. Ecol. Evol.* **4**, 1020–1035 (2020).
8. Raulo, A. *et al.* Social networks strongly predict the gut microbiota of wild mice. *ISME J.* **15**, 2601–2613 (2021).
9. Johnson, K. V.-A. Gut microbiome composition and diversity are related to human personality traits. *Hum. Microbiome J.* **15**, 100069 (2020).
10. Luczynski, P. *et al.* Growing up in a Bubble: Using Germ-Free Animals to Assess the Influence of the Gut Microbiota on Brain and Behavior. *Int. J. Neuropsychopharmacol.* **19**, pyw020 (2016).

11. Round, J. L. & Mazmanian, S. K. The gut microbiota shapes intestinal immune responses during health and disease. *Nat. Rev. Immunol.* **9**, 313–323 (2009).
12. Bourré, L. Germ-Free or Antibiotic-Treated Mice? Which Model for Studying the Role of the Gut Microbiota in Preclinical Studies. *Crown Biosci.* (2020).
13. Neufeld, K. M., Kang, N., Bienenstock, J. & Foster, J. A. Reduced anxiety-like behavior and central neurochemical change in germ-free mice. *Neurogastroenterol. Motil.* **23**, 255–264, e119 (2011).
14. Needham, B. D. *et al.* A gut-derived metabolite alters brain activity and anxiety behaviour in mice. *Nature* **602**, 647–653 (2022).
15. Wu, W.-L. *et al.* Microbiota regulate social behaviour via stress response neurons in the brain. *Nature* **595**, 409–414 (2021).
16. Resendez, S. L. *et al.* Social Stimuli Induce Activation of Oxytocin Neurons Within the Paraventricular Nucleus of the Hypothalamus to Promote Social Behavior in Male Mice. *J. Neurosci. Off. J. Soc. Neurosci.* **40**, 2282–2295 (2020).
17. Sgritta, M. *et al.* Mechanisms Underlying Microbial-Mediated Changes in Social Behavior in Mouse Models of Autism Spectrum Disorder. *Neuron* **101**, 246-259.e6 (2019).
18. Buffington, S. A. *et al.* Dissecting the contribution of host genetics and the microbiome in complex behaviors. *Cell* **184**, 1740-1756.e16 (2021).
19. Rosshart, S. P. *et al.* Laboratory mice born to wild mice have natural microbiota and model human immune responses. *Science* **365**, (2019).
20. Gilbert, J. A. *et al.* Current understanding of the human microbiome. *Nat. Med.* **24**, 392–400 (2018).

21. RICARDO, A. & SZOSTAK, J. W. ORIGIN OF LIFE ON EARTH. *Sci. Am.* **301**, 54–61 (2009).
22. Brodsky, V. Ya. Direct cell-cell communications and social behavior of cells in mammals, protists, and bacteria. Possible causes of multicellularity. *Russ. J. Dev. Biol.* **40**, 69–82 (2009).
23. Margulis, L. SYMBIOSIS AND EVOLUTION. *Sci. Am.* **225**, 48–61 (1971).
24. Dimijian, G. G. Evolving together: the biology of symbiosis, part 1. *Proc. Bayl. Univ. Med. Cent.* **13**, 217–226 (2000).
25. Leung, T. & Poulin, R. PARASITISM, COMMENSALISM, AND MUTUALISM: EXPLORING THE MANY SHADES OF SYMBIOSES. *Vie Milieu - Life Environ.* **58**, 107–115 (2008).
26. Martin Mark O. "It's a Microbial World; We Just Live in It": Microbial Symbionts Profiled Masterfully by Yong. *J. Microbiol. Biol. Educ.* **17**, 496–498 (2016).
27. Heywood, J. *The Proverbs of John Heywood*. (1546).